A DISSERTATION
FOR THE DEGREE OF DOCTOR OF PHILOSOPHY

Immunomodulation by extracellular vesicles from deferoxamine preconditioned canine adipose tissue derived mesenchymal stem cells in experimental autoimmune encephalomyelitis mouse model

자가 면역 뇌척수염 마우스 모델에서 **deferoxamine**을 전처리한 개의 지방유래 중간엽줄기세포로부터 유래한 세포외소포체의 면역 조절 효과

2023년 2월

Major in Veterinary Clinical Science
(Veterinary Internal Medicine)
College of Veterinary Medicine
Graduate School of Seoul National University

Su-Min Park

자가 면역 뇌척수염 마우스 모델에서 **deferoxamine**을 전처리한 개의 지방유래 중간엽줄기세포로부터 유래한 세포외소포체의 면역 조절 효과

지도교수 윤 화 영
이 논문을 수의학박사 학위논문으로 제출함
2022년 11월

서울대학교 대학원
수의과대학 임상수의학 **(**수의내과학**)** 전공
박 수 민

박수민의 박사 학위 논문을 인준함
2022년 12월

위 원 장 채 준 석 (인)

부 위 원 장 윤 화 영 (인)

위 원 서 경 원 (인)

위 원 송 우 진 (인)

위 원 안 주 현 (인)

Immunomodulation by extracellular vesicles from deferoxamine preconditioned canine adipose tissue derived mesenchymal stem cells in experimental autoimmune encephalomyelitis mouse model

Su-Min Park

(Supervised by Prof. Hwa-Young Youn, DVM, PhD)

Major in Veterinary Clinical Science

(Veterinary Internal Medicine)

College of Veterinary Medicine

Graduate School of Seoul National University

Abstract

Mesenchymal stem/stromal cells (MSCs) are effective therapeutic agents that ameliorate inflammation through paracrine effect. In particular, several studies have been tried to apply MSC to autoimmune neurological diseases such as multiple sclerosis. Multiple sclerosis is a disease in which nerve damage occurs when inflammatory cells infiltrate nerve tissue due to loosing self-regulated immune system. Also in dogs, there is a similar disease, which is a meningoencephalitis of unknown etiology (MUE). The cause of

MUE is not yet clear, but it is assumed to be caused by immune problem, and in this regard, main treatment is administrating non-specific immunosuppressants. Although about 25% of dogs which has neurological disease struggle with MUE, treatment has not been developed significantly. Non-specific immunosuppressants, including steroids, has several problems such as gastrointestinal disorders and hormonal secretion disorders, on the other hand, immunosuppressants treatment effect is not guaranteed, one of the difficulties in treating MUE.

In this respect, extracellular vesicles (EVs) derived from MSCs have been investigated as a treatment option for autoimmune diseases. However, further study is needed on clinical efficacy of EV. To improve the secretion of anti-inflammatory factors from MSCs, preconditioning with hypoxia or hypoxia-mimetic agents has been attempted. Moreover, the molecular changes in preconditioned MSC-derived EVs have been explored and its clinical efficacy has not been proven. This study aimed to evaluate the therapeutic effect of EVs derived from deferoxamine (DFO)-preconditioned canine adipose tissue-derived (cAT)-MSCs (EV^{DFO}) in an experimental autoimmune encephalomyelitis (EAE) mouse model and explore the mechanism underlying immunomodulation function of EV.

This dissertation is composed of three parts. The first part of dissertation revealed that cAT-MSCs preconditioned with DFO (MSC^{DFO}) can more effectively direct and reprogram macrophage polarization into the M2 anti-inflammation state by paracrine effect. MSC^{DFO} exhibited enhanced

secretion of anti-inflammatory factors such as prostaglandin E2 and tumor necrosis factor-α-stimulated gene-6. To evaluate the interaction between MSC^{DFO} and macrophages, RAW 264.7 cells were co-cultured with cAT-MSCs using the transwell system, and changes in the expression of factors related to macrophage polarization were analyzed using the quantitative real-time PCR and western blot assays. When RAW 264.7 cells were co-cultured with MSC^{DFO}, the expression of M1 and M2 markers decreased (iNOS, 1.32 fold, $p<0.01$; IL-6, 3.46 fold, $p<0.05$) and increased (CD206, 2.61 fold, $p<0.001$; Ym1, 4.92 fold, $p<0.01$), respectively, compared to co-culturing with non-preconditioned cAT-MSCs. Thus, cAT-MSCs preconditioned with DFO can more effectively direct and reprogram macrophage polarization into the M2 phase, an anti-inflammatory state.

The second part of dissertation is designed to evaluate that EV^{DFO} regulated macrophage through activating signal transducer and transcription3 (STAT3) phosphorylation. In MSC^{DFO}, Hypoxia-inducible factor 1-alpha was found to accumulate and expression of Cyclooxygenase-2 (COX-2) was increased (16.77 fold, $p<0.001$). Changes in expression of COX-2 were reflected in the derived EVs as well. The canine macrophage cell line, DH82, was treated with EV^{non} and EV^{DFO} after lipopolysaccharide stimulation and polarization changes were evaluated with quantitative real-time PCR and immunofluorescence analyses. When DH82 was treated with EV^{DFO}, the expression of M1 marker was reduced (IL-1β, 2.45 fold, $p<0.001$; IL-6, 17.26 fold, $p<0.001$) while that of M2 surface marker was enhanced (CD206, 7.24

fold, $p<0.001$) compared to that when DH82 was treated with EV^{non}. Further, phosphorylation of STAT3 expression was increased more when DH82 cells were treated with EV^{DFO} (1.79 fold, $p<0.001$). EV derived from cAT-MSC treated with si-COX2 showed similar effect with EV and the effect of immunomodulation was decreased than EV^{DFO} (IL-1β, 2.21 fold, $p<0.001$; IL-6, 1.43 fold, $p<0.001$; CD206, 2.27 fold, $p<0.001$). Thus, COX-2 in EV may be one of key factor to regulate STAT3 and modulate macrophage.

The last part of dissertation demonstrates that EV^{DFO} treatment has a relatively higher efficacy in reducing inflammation than non-preconditioned EV treatment and could modulate immune system through regulating STAT3 in EAE model. EAE mice were divided into different groups based on intranasal administration of EVs or EV^{DFO} (C57BL/6, male, control=6, EAE=8, EAE+EV=8, EAE+EV^{DFO}=8, 10 μg/day;14 injections). On day 25 post-EAE induction, the mice were euthanized, and the spleen, brain, and spinal cord were analyzed into histopathologic and expression of RNA and protein level. Histologically, in the EV and EV^{DFO} groups, the infiltration of inflammatory cells decreased significantly (EV, 1.38 fold, $p<0.01$; EV^{DFO}, 1.72 fold, $p<0.01$), and demyelination was alleviated (EV, 2.96 fold, $p<0.05$; EV^{DFO}, 5.28 fold, $p<0.05$). Immunofluorescence staining showed that the expression of CD206 and Foxp3, markers of M2 macrophages and regulatory T (Treg) cells, respectively, increased significantly in the EV^{DFO} group compared to the EAE and EAE+EV group. In the EAE group, the number of CD4+CD25+Foxp3+ Treg cells in the spleen decreased significantly

compared with the naïve group (2.74 fold, $p<0.001$). In contrast, the number of Treg cells showed a greater increase in the EAE+EV^{DFO} group than in the EAE+EV group (1.55 fold, $p<0.05$). The protein expression of STAT3 and pSTAT3 increased in the spleen in the EAE groups compared to the naïve group (STAT3, 2.02 fold, $p<0.001$; pSTAT3, 2.14 fold, $p<0.001$). However, following EV treatment, STAT3 expression decreased compared to the EAE group (1.32 fold, $p<0.001$), especially reduction of STAT3 was evident in EV^{DFO} compared to EV group (1.90 fold, $p<0.001$). Therefore, EV could regulate STAT3 expression and EV^{DFO} has more effect than EV.

In conclusion, that preconditioned with DFO in cAT-MSC is an effective method to improve immunomodulation effect of EVs. Also, EV^{DFO} is potential therapeutic option for multiple sclerosis through regulating STAT3 pathway and modulating immune system. These findings suggest a new approach to cell free therapy with preconditioned EV in other autoimmune diseases as well as multiple sclerosis. Furthermore, this study is a major basis that EV^{DFO} can be applied as a new treatment for MUE in dogs and the cornerstone to the development of autoimmune disease treatment in veterinary medicine.

Keyword: Multiple sclerosis / Mesenchymal stem cell / Deferoxamine / Extracellular vesicle / Anti-inflammation

Student Number: 2018-24679

CONTENTS

Chapter II. Extracellular vesicles derived from DFO-preconditioned canine AT-MSCs reprogram macrophages into M2 phase

Chapter III. Deferoxamine preconditioned cAT-MSC derived EV alleviate inflammation in EAE mouse model through regulating STAT3

LIST OF TABLES

LIST OF FIGURES

ABBREVIATIONS

MSC	Mesenchymal stem cell
HIF-1α	Hypoxia inducible factor 1-alpha
DFO	Deferoxamine
cAT	Canine adipose tissue
cAT-MSC	Canine adipose tissue-derived mesenchymal stem cell
DMEM	Dulbecco's modified Eagle medium
CCK-8	Cell counting kit-8
qRT-PCR	Quantitative real-time polymerase chain reaction
TSG-6	TNF-α-stimulated gene 6
PGE2	Prostaglandin E2
iNOS	Inducible nitric oxide synthase
EVs	Extracellular vesicles
COX-2	Cyclooxygenase-2
STAT3	Signal transducer and activator of transcription 3
FBS	Fetal bovine serum
PS	Penicillin-streptomycin
GAPDH	Glyceraldehyde 3-phosphate dehydrogenase
LPS	Lipopolysaccharides
EAE	Experimental autoimmune encephalomyelitis
MS	Multiple sclerosis
CNS	Central nervous system
MOG_{35-55}	Myelin oligodendrocyte $glycoprotein_{35-55}$
STAT3	Signal transducer and activator of transcription 3
Treg cells	Regulatory T cells

LITERATURE REVIEW

1. Generalities of preconditioned mesenchymal stem cell (MSCs)

Mesenchymal stem cells (MSCs) have two main functions, the ability of differentiate to other cell lineages and the ability of self-renew (Potten and Loeffler 1990). Especially adult mesenchymal stem cells can be obtained easily without ethical concerns and also have multipotency, which makes MSCs to an interesting option for clinical applications (Ding et al., 2011).

MSCs has potential to modulating immune system by paracrine effect (Ankrum et al., 2014, Samadi et al., 2020). However, because of impaired paracrine ability and poor survival rate in body, MSC has limited clinical efficacy (Zheng et al., 2014, Wilson et al., 2015). To overcome the limitation, there are some approaches for improving the function of MSCs. One of the strategies is improving MSC survival or function by preconditioning with toxic or lethal agents (Silva et al., 2018).

Preconditioning methods to MSCs are mainly for improving MSC survival in harsh environment. One of the preconditioning methods is hypoxic culture. When culture under hypoxia, MSCs highly express hypoxia-inducible factor (HIF)-1α, which is associated with energy metabolism and blocking oxidative phosphorylation (Hu et al., 2008). Also, HIF-1α

upregulates antioxidant and antiapoptotic factors, as a result, MSCs have potency to withstanding under oxidative stress (Sart et al., 2014, Han et al., 2016). Recently, MCSs under hypoxic culture also has potency to improving anti-inflammatory expression (Chang et al., 2019, Dong et al., 2021).

Another strategy of preconditioned MSCs is treating with inflammatory milieu. As MSCs sense the pro-inflammatory mediators, such as interferon (IFN)-ɣ, Tumor necrosis factor (TNF)-a or chemokines, NF-κB pathway is activated and the expression of immunomodulatory factors are increased (Bustos et al., 2013, Ryan et al., 2016). The preconditioning in stem cell therapy is still a new area, but over the past few years show that preconditioned methods in MSCs is an attractive clinical option.

2. Properties of extracellular vesicles (EVs) derived from MSCs

Extracellular vesicles (EVs) are lipid bilayer particles which are secreted by a variety of mammalian cell types. Recently, EVs have been researched as playing important role in cell communication (Katsuda et al., 2013).

There are many reports that EVs derived from cells contains the functional molecules and these can activate biological changes through delivery system (Ratajczak et al., 2006). The molecules in EVs, including proteins, microRNAs, and mRNAs, are depending on the origin cell which secreted

EVs (Théry et al., 2002). Through this characteristic, EVs are researched as biomarker or new treatment option.

The therapeutic potential of MSCs has been revealed that it depends on secretory function rather than differentiation (Madrigal et al., 2014). In liver disease, undifferentiated MSCs showed the therapeutic capacity by paracrine effect including interleukin (IL)-1RA, IL-6, IL-8, granulocyte-colony stimulating factor, granulocyte macrophage, monocyte chemotactic protein-1, nerve growth factor, and hepatocyte growth factor (Banas et al., 2008). In CNS disease, MSCs alleviated demyelination and infiltration of inflammatory cell to CNS through the secretory capacity (Zappia et al., 2005, Gerdoni et al., 2007). Considering these findings, secretory from MSCs plays a more important role in tissue repair.

The fact that EVs can reflect the origin cells suggests that the therapeutic paracrine effect of MSC is associated with MSCs derived EVs. As MSC showed therapeutic effect in various disease, MSCs derived EVs also has potential to clinical applicability to various disorders. Furthermore, MSCs has limitation in systemic clinical approach because of lung barrier, however, EVs has advantage to avoid barrier (Fischer et al., 2009).

3. Immunomodulation function of EVs derived from MSCs

MSCs are revealed that able to suppress the function of immune effector cells and regulate immune system (Bartholomew et al., 2002, Le

Blanc et al., 2003). Through producing the immunomodulatory cytokines, MSCs can modulate both innate and adaptive immune cells (Uccelli et al., 2008). Recently several studies have suggested that among the soluble factors, EVs derived from MSCs are involved in immune-modulatory action (Bruno and Camussi 2013).

Human embryonic stem cell derived MSC-EVs activated THP1, human macrophage cell line, as expressing IL-10, which indicate that EVs modulate macrophage into M2 like phenotype known as promoting tissue repair and alleviating injury (Zhang et al., 2014). Moreover, MSC-EV treatment improved kidney function in AKI mouse models by modulating macrophage (Bruno et al., 2012, He et al., 2012). When examined macrophage infiltration in ischemic injured kidney, MSC-EVs inhibited the recruitment of macrophage (Shen et al., 2016). As reducing macrophage infiltration, pro-inflammatory cytokines were reduced and anti-inflammatory cytokines were increased respectively (Koch et al., 2015, Lin et al., 2016). Also, in bronchopulmonary dysplasia (BPD) model, MSC-EVs ameliorated pulmonary fibrosis by reducing inflammation. MSC-EVs alleviate inflammatory cytokines from M1 macrophages, such as CCL5, TNF-α, and IL-6, while improving Arginase 1 (Arg1), an immunomodulatory factor from M2 macrophages (Willis et al., 2018). These results suggest that MSC-EVs can modulate macrophage into M2 anti-inflammatory phase and inhibit M1 inflammatory phase.

Mokarizadeh et al. revealed for the first time that EVs derived from

murine MSCs acts as a mediator for several MSC-specific molecules, such as programmed death ligand-1 (PDL-1), galectin-1 (Gal-1) and TGF-β (Mokarizadeh et al., 2012). In experimental autoimmune encephalomyelitis (EAE) mouse model, MSC-EVs inhibited the activation of auto-immune lymphocytes through inducing apoptosis of auto-reactive T cells and activating secretion of T reg (Mokarizadeh et al., 2012). Moreover, in islet transplantation or liver injury model, MSC-EVs induced differentiation of regulatory T cell (Tamura et al., 2016, Wen et al., 2016). However, there are some opinions for limitation of MSC-EVs in clinical approach. The immunomodulatory effects of MSC-EVs on T cells were lower compared to MSCs (Conforti et al., 2014, Gouveia de Andrade et al., 2015).

Thus, enhancing the function of MSC-EVs is needed to increase for clinical applicability. Considering that preconditioned MSCs enhanced the anti-inflammatory cytokines and controlled immune cells more effectively compared to MSCs (Lee and Kang 2020), preconditioned MSC-EVs has potency to improved therapeutic effect.

4. Preclinical and clinical application of MSC derived EVs in immune disorders

Autoimmune diseases have been described as over 80 different disease and the prevalence in human is estimated around 5-8%. Despite various efforts, non-specific immune-suppressant drugs are still first choice

in autoimmune disorder treatment. Unfortunately, the effects of these immune-suppressants are not perfectly optimal for treating autoimmune diseases, and long-term use is often associated with several side effects, such as susceptibility to infections (Fugger et al., 2020). Because of these limitation in auto-immune therapy, MSC-EVs are suggested as new treatment option. MSC-EVs are safer and more effective than MSCs while exhibiting similar treatment characteristics and functions (Choi et al., 2008, Jang et al., 2016, Volarevic et al., 2017). Therapeutic potential of MSC-EVs has been reported by various animal models, especially immune disorders.

Inflammatory bowel disease (IBD) is one of chronic gastrointestinal inflammatory disorder by a dysregulated immune response including autoimmune mechanism (Jurjus et al., 2004). Conventional treatments including immunosuppressive medications and antitumor necrosis factor are applied for the treatment in IBD patients (Domènech et al., 2014). However, as immunosuppressive medications has various adverse effects, development of new treatment is needed and MSC treatment is one of primitive option (Dave et al., 2015). In IBD model, rat bone marrow derived MSC-EVs improved the histological index of colitis and clinical signs, such as body weight and disease activity index. Also, the filtration of immune cell in colon was reduced (Yang et al., 2015). In dextran sulfate sodium (DSS) induced colitis model, one of IBD model, human umbilical cord derived MSC-EVs alleviated symptoms through regulation macrophage (Mao et al., 2017). To improve the effectiveness of EVs, An et al. primed MSC with TNF-α and

INF-γ and primed EVs showed improving clinical effect compared to non-primed EV in DSS colitis mouse model (An et al., 2020).

Type-1 diabetes mellitus (T1DM) is one of autoimmune disorder and , which is occurred by deficiency of insulin secretion as autoimmune destruction insulin producing beta cell (Association 2010). In streptozotocin induced T1DM, adipose tissue derived MSC-EVs reduced clinical signs and reduced glycemia. Moreover, when analyzing splenocyte of T1DM mouse, expression of inflammatory cytokines, IL-17 and IFN-γ, were reduced, otherwise, anti-inflammatory cytokines were increased with elevation of T reg cell population (Nojehdehi et al., 2018). Favaro et al. reported that MSC-EVs showed immunomodulatory functions by inhibiting inflammatory T cell in pancreatic islet tissues (Favaro et al., 2016).

Rheumatoid arthritis (RA) is chronic inflammatory disorder characterized by progressive joint destruction (Di et al., 2020). The pathogenesis of RA is known as loss of immune tolerance caused by genetic susceptibility and environmental factors, however the underlying mechanism of RA is complex and has not been precisely revealed (Smolen et al., 2007). As conventional treatment, including glucocorticoid and immunosuppressants, has several adverse effect, new treatment options such as MSC injection have been suggested (Hwang et al., 2021). Stella et al. revealed for the first as the role of MSC-EVs in RA models. MSC-EV alleviated clinical symptoms of RA through inhibiting T and B lymphocyte proliferation. Moreover, T reg and IL-10 expressing B cell was activated by

MSC-EVs (Cosenza et al., 2018). The immunomodulation of MSC-EVs on macrophage also reported in osteoarthritis model. Another report revealed that MSC-EVs improved RA by transferring IL-1ra and reducing pro-inflammatory cytokines (Tsujimaru et al., 2020). Considering these results, MSC-EVs alleviated RA by modulating immune system and transferring cytokines

Multiple sclerosis (MS) is one of autoimmune disease characterized demyelination of central nerve system (Dobson and Giovannoni 2019). The experimental autoimmune encephalomyelitis (EAE) mouse model is representative animal model of MS, which has similar pathological feature with MS (Constantinescu et al., 2011). Several reports revealed that MSC-EV ameliorate clinical sign of EAE mouse model (Clark et al., 2019, Jafarinia et al., 2020, Ahmadvand Koohsari et al., 2021). MSC-EV showed therapeutic effect in EAE model as reduction neuroinflammation. MSC-EV reduced infiltration of macrophage and T cells in spinal cord and increased population of CD4+CD25+FOXP3+ regulatory T cells (Riazifar et al., 2019). To alleviate neuroinflammation, a method of injecting MSC-EV through intranasal has been devised as the effective way to pass through BBB (Herman et al., 2021). However, since how much of MSC-EV should be injected through this method for treatment has not yet been established. Also, the amount that can be injected with intranasal is limited, methods to increase the effectiveness of MSC-EV has been researched to achieve the maximum effect with the minimum amount. To administrate MSC-EV in

neuroinflammatory disease dogs such as meningoencephalitis of unknown origin, it is necessary to design a stable EV delivery method and effective amount.

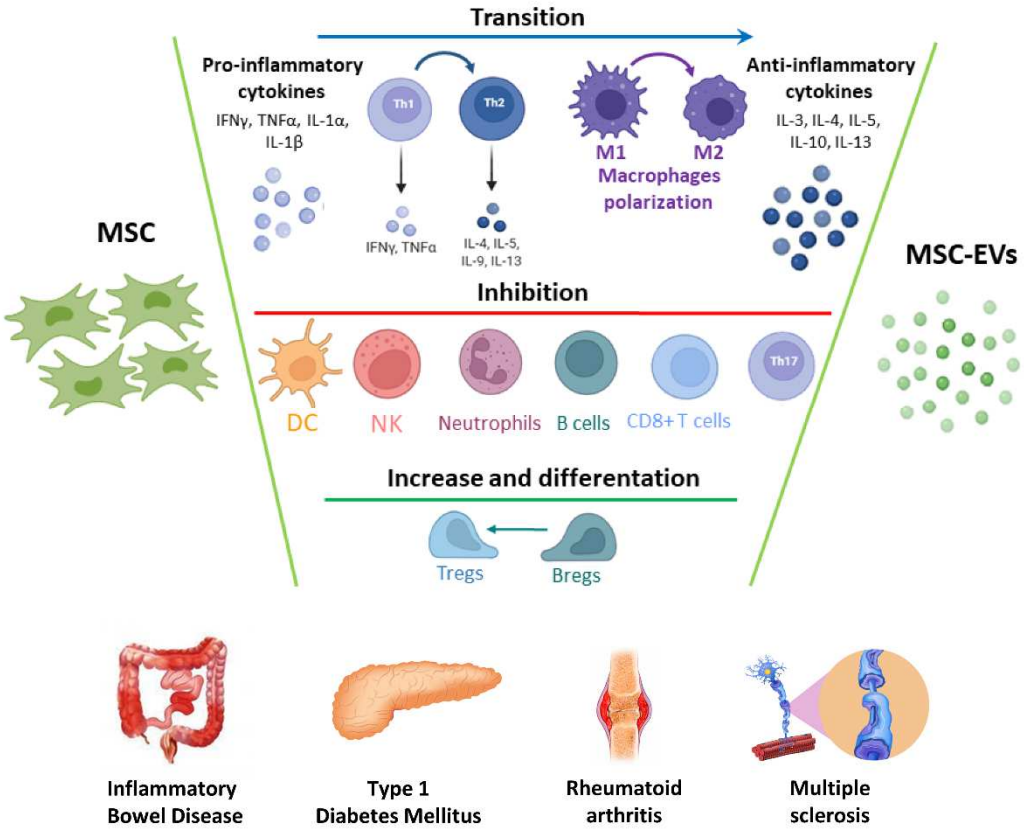

Figure 1. Preclinical and clinical application of MSC derived EVs in immune disorders. Through producing the immunomodulatory cytokines, MSCs can modulate both innate and adaptive immune cells (Uccelli et al., 2008). Recently several studies have suggested that among the soluble factors, EVs derived from MSCs are involved in immune-modulatory action (Bruno and Camussi, 2013). Mokarizadeh et al. revealed for the first time that EVs derived from murine MSCs acts as a mediator for several MSC-specific molecules, such as programmed death ligand-1 (PDL-1), galectin-1 (Gal-1) and TGF-β (Mokarizadeh et al., 2012). Using the immunomodulatory functin

of MSC-EV, MSC-EVs are suggested as new treatment option for auto-immune disease. MSC-EVs are safer and more effective than MSCs while exhibiting similar treatment characteristics and functions (Choi et al., 2008, Jang et al., 2016, Volarevic et al., 2017). Therapeutic potential of MSC-EVs has been reported by various animal models, especially immune disorders such as inflammatory bowel disease, type 1 diabetes mellitus, rheumatoid arthritis or multiple sclerosis. Enhancing the function of MSC-EVs is needed to increase for clinical applicability. Considering that preconditioned MSCs enhanced the anti-inflammatory cytokines and controlled immune cells more effectively compared to MSCs (Lee and Kang, 2020), preconditioned MSC-EVs has potency to improved therapeutic effect. MSC, mesenchymal stem cell; EV, extracellular vesicle.

Chapter I.

Preconditioning of canine adipose tissue-derived mesenchymal stem cells with deferoxamine potentiates anti-inflammatory effects by directing/reprogramming M2 macrophage polarization

1. Introduction

Stem cell therapy involves two mechanisms: one is post-attachment differentiation to the target organ(s), and the other is a paracrine effect. Hypoxia preconditioning of mesenchymal stem cells (MSCs) has been found to induce a secretory modification (Madrigal et al., 2014) and enhance several cell biology aspects such as innate immunity, angiogenesis, metabolism, and stemness (Majmundar et al., 2010). These effects are mainly mediated by upregulating hypoxia inducible factor (HIF)-1α expression (Abdollahi et al., 2011). Upregulation of HIF-1α leads to increased expression of HIF-dependent tissue protective genes (e.g., CD39 and CD73 (Tak et al., 2017)) and demonstrates the potential to protect against organ damage such as acute kidney injury (Rosenberger et al., 2008), myocardial injury (Rosenberger et al., 2008), or neuronal injury (Wu et al., 2010). However, culturing under hypoxic conditions has some problems such as an unstable oxygen concentration, the need for expensive equipment, difficulty to maintain a

constant hypoxic exposure (Buravkova et al., 2014), and induction of tumors (Jokilehto and Jaakkola 2010) or fibrosis (Higgins et al., 2007). The use of hypoxia-mimetic agents can be considered as a way to overcome these problems. These agents inhibit the degradation of HIF-1α and upregulate signaling following HIF-1α translation (Guo et al., 2006).

Deferoxamine (DFO), an iron-chelating hypoxia-mimetic agent, inhibits the HIF-1α degradation process that requires iron (Shimoni et al., 1994). Moreover, DFO yields a more pronounced hypoxia response than hypoxic culturing conditions (Fujisawa et al., 2018). DFO also possesses the potential to increase the concentration of anti-inflammatory factors. For example, MSCs treated with DFO exhibit increased mRNA expression and secretion of IL-4 (Oses et al., 2017), which is a known anti-inflammatory cytokine and inducer of M2 macrophage polarization (Wang et al., 2014). Other inducers of M2 macrophage polarization are closely related with MSC secretion factors (Eggenhofer and Hoogduijn 2012) and may be associated with HIF-1α. Thus, we postulated that DFO-preconditioned MSCs (MSC^{DFO}) could more effectively secrete anti-inflammatory factors and demonstrate the potential to reprogram and direct macrophage polarization into an anti-inflammatory state.

2. Material and methods

2.1. Isolation and characterization of canine adipose tissue-derived (cAT)-MSCs

cATs were obtained using a protocol approved by the Institutional Animal Care and Use Committee of Seoul National University (SNU; protocol no. SNU-180621-27). Canine adipose tissue was obtained from near the uterine fat during ovariohysterectomy surgery. Adipose tissues were washed four times in PBS containing 1% penicillin-streptomycin (PS; PAN biotech, Germany), then cut into small pieces. These pieces were digested with 0.1% collagen type IA (1 mg/mL; Sigma-Aldrich, MO) in PBS and incubated for 1 h at 37˚C. After digestion, Dulbecco's modified Eagle medium containing 10% FBS (PAN Biotech, Germany) was added and the mixture was centrifuged at 1200 ×*g* for 5 min. The supernatant was removed and the pellet was re-suspended in Dulbecco's modified Eagle medium with 10% FBS (PAN Biotech, Germany) and 1% PS (PAN biotech, Germany).

Before the experiments, cAT-MSCs were characterized by immunophenotyping and multilineage differentiation. To characterize cAT-MSCs, cells were evaluated by flow cytometry using fluorescent stem cell marker antibodies. The antibodies used were against CD29 (fluorescein isothiocyanate; FITC), CD34 (phycoerythrin; PE), and CD73 (PE) (BD Biosciences, NJ), and CD45 (FITC) (eBiosciences, CA). Flow cytometry was performed with a FACS Aria II system (BD Life Sciences, San Jose, CA) and analyzed using FlowJo software (Tree Star, OR). Cells were plated in 24-well

plates and cultured to 80–90% confluency. The medium was then changed to differentiation medium (PRIME-XV Adipogenic Differentiation SFM, PRIME-XV Osteogenic Differentiation SFM, or PRIME-XV Chondrogenic Differentiation XSFM; all from Irvine Scientific, CA). Differentiated cells were stained with Oil Red O, Alizarin Red, and Alcian Blue for the three-differentiation media, respectively. After characterization, cAT-MSCs at passages 3–4 were used.

2.2. Cell culture and expansion

Cells were cultured in Dulbecco's modified Eagle medium (DMEM; PAN Biotech, Germany) with 10% FBS (PAN Biotech, Germany) and 1% PS(PAN Biotech, Germany) at 37°C in a 5% CO_2 atmosphere. The culture medium was changed every 2–3 days, and cells were sub-cultured at 70–80% confluency.

The RAW 264.7 murine macrophage cell line was purchased from the Korean Cell Line Bank (Korea) and cultured in DMEM with 10% FBS at 37°C in a 5% CO_2 atmosphere until they reached 70–80% confluency.

2.3. Cell viability analysis

To measure the effect of DFO (Sigma-Aldrich, MO) on cell viability, cAT-MSCs were treated at 70–80% confluency with 10, 100, 500, 1000, or 5000 μM DFO, or PBS (PAN Biotech, Germany) as a negative control. After incubation for 24, 48, and 72 h, cell viability was measured using the Cell

Counting Kit-8 (CCK-8) assay (Donginbio, Korea).

2.4. RNA extraction, cDNA synthesis, and the quantitative real-time polymerase chain reaction (qRT-PCR)

Total RNA was extracted from cAT-MSCs preconditioned with and without DFO, and RAW 264.7 cells using the Easy-Blue total RNA extraction kit (Intron Biotechnology, Korea). cDNA was synthesized using the CellScript All-in-One 5× 1st cDNA Strand Synthesis Master Mix (CellSafe, Korea). Samples were analyzed using AMPIGENE qPCR green mix Hi-Rox with SYBR green dye (Enzo Life Sciences, NY) and 400 nM forward and reverse primers in the qRT-PCR thermal cycler (Bionics, Korea). The expression level of each gene was normalized to that of glyceraldehyde 3-phosphate dehydrogenase and calculated as relative expression against the contrasting control group.

2.5. Protein extraction, cell fractionation, and western blot analysis

Total protein was extracted from preconditioned cAT-MSCs using the Pro-Prep protein extraction solution (Intron Biotechnology, Korea). The protein concentration of samples was analyzed using the DC Protein Assay Kit (Bio-Rad, CA). Nuclear and cytosolic proteins were obtained using the Cell Fractionation Kit-Standard (Abcam, MA). For the western blot assays, 20 μg of protein were loaded and separated by SDS-PAGE. Gels were transferred to polyvinylidene difluoride membranes (EMD Millipore, MA)

and blocked in 5% non-fat dry milk with Tris-buffered saline. Membranes were incubated with primary antibodies against HIF-1α (1:500; LifeSpan BioSciences, WA), cyclooxygenase (COX)-2 (1:500, Santa Cruz Biotechnology, TX), TNF-α-stimulated gene 6 (TSG-6) (1:500, Santa Cruz Biotechnology, TX), lamin A (1:500, Santa Cruz Biotechnology, TX), α-tubulin (1:500, Santa Cruz Biotechnology, TX), CD206 (1:500, Santa Cruz Biotechnology, TX), inducible nitric oxide synthase (iNOS) (1:500, Santa Cruz Biotechnology, TX), and β-actin (1:1000, Santa Cruz Biotechnology, TX) at 4°C overnight. Membranes were then incubated with the appropriate secondary antibody for 1 h. Using an enhanced chemiluminescence kit (Advansta, CA), immunoreactive bands were detected and normalized to the housekeeping protein (β-actin).

2.6. ELISA

After preconditioning the cAT-MSCs with DFO, cell culture medium was obtained and stored at -80˚C until use. The concentrations of prostaglandin E2 (PGE2) and TSG-6 were measured using commercial ELISA kits [canine PGE2 ELISA kit (Cusabio Biotech, MD) and TSG-6 ELISA kit (MyBioSource, CA)], according to the manufacturers' instructions.

2.7. Co-culture of macrophages with preconditioned cAT-MSCs

cAT-MSCs were plated at 2×10^4 or 2×10^5 cells on 0.4 μM pore-

sized Transwell inserts (SPL Life Sciences, Korea) and treated with 100 or 500 μM DFO, or PBS as control, for 48 h. After preconditioning the cAT-MSCs with DFO, the medium containing DFO was removed and the inserts were washed with PBS.

RAW264.7 cells were seeded at 1×10^6 cells/well on 6 well plates without or with 200 ng/mL lipopolysaccharide (LPS; Sigma-Aldrich, MO) for 6 h. RAW264.7 macrophages were also co-cultured with cAT-MSCs for 48 h, then collected for further experiments.

2.8. Statistical analyses

Data are shown as mean ± standard deviation. Mean values among different groups were compared by Student's *t*-test and one-way analysis of variance using GraphPad Prism v.6.01 software (GraphPad Software, CA). *p* value < 0.05 was considered statistically significant.

3. Results

3.1. Viability of DFO preconditioning in cAT-MSC

When treating cAT-MSCs with DFO for 24 h, there was no effect on proliferation except at 5 mM (Fig. 4a). After treating with 1 mM DFO for 48 h, the viability of cells was decreased significantly compared to a 24 h treatment (Fig. 4b). When treating for 72 h, the viability of all groups, except 10 μM, were decreased (Fig. 4c).

3.2. DFO induces hypoxic response in cAT-MSCs

The mRNA and protein levels of HIF-1α were evaluated in MSC^{DFO}. DFO was administered to cAT-MSCs for 48 h for conditioning. Changes in the expression of HIF-1α mRNA were dependent on the DFO concentration (Fig. 6a). However, changes in the protein level were opposite to those in mRNA levels at various DFO concentrations. HIF-1α protein was detected in the nuclear fraction, and its concentration increased depending on the DFO concentration (Fig. 6b).

3.3. DFO preconditioning increases the expression and secretion of anti-inflammatory factors

cAT-MSCs were treated with 10, 100, or 500 μM DFO for 24 and 48 h. The expression of TGF-β, TSG-6, IL-10, and COX-2 were examined in non-conditioned or DFO-preconditioned cAT-MSCs. Except for COX-2, the concentration of other factors in cells preconditioned with DFO for 24 h did not increase significantly (data not shown). However, when preconditioning was extended to 48 h, the amount of all factors in DFO preconditioned cells increased significantly. Especially with 500 μM DFO preconditioned cells, the most factors was greatly increased compared to other concentrations (Fig. 7a-d).

Considering these results, the most effective DFO concentrations was selected as 100 and 500 μM, and examined the protein levels of TSG-6 and

COX-2 in MSC^{DFO}. COX-2 and TSG-6 protein levels were increased in 500 μM DFO preconditioned cells (Fig. 8a, b). Also, the secretion of TSG-6 and PGE2 was evaluated in 100 and 500 μM DFO preconditioned media. The increase in the level of TSG-6 was dependent on the DFO concentration, while the level of PGE2 increased significantly in 100 μM DFO preconditioned media, but not in 500 μM DFO-preconditioned media (Fig. 9a, b).

3.4. MSC^{DFO} direct macrophage polarization in vitro

In the LPS-stimulated control RAW264.7 cells, the concentration of M1 markers was increased significantly compared to that in the naïve group. In contrast, in RAW264.7 cells co-cultured with non-conditioned MSC or MSC^{DFO}, the concentration of M1 markers was significantly decreased compared to that in the control group (Fig. 10a-c). Especially, the mRNA expression of iNOS was significantly decreased in RAW264.7 cells exposed to DFO 100 or 500 μM preconditioned MSCs compared to that in the non-preconditioned cells (Fig. 10a). Furthermore, the mRNA expression of IL-6 was decreased in RAW264.7 cells co-cultured with DFO 100 μM preconditioned MSCs compared to that in the non-preconditioned MSCs (Fig. 10b).

The expression of M2 marker mRNAs was not increased in RAW264.7 cells co-cultured with non-preconditioned MSCs compared to that in the control group. In contrast, the expression of M2 marker mRNAs

was generally increased in RAW264.7 cells co-cultured with MSC^{DFO} (Fig. 10d-f). Specifically, as compared to the non-preconditioned MSC group, MSC^{DFO} enhanced the expression of CD206 in macrophages (Fig. 10d). The expression of Ym1 was increased only in the DFO 100 μM preconditioned group (Fig. 10e), while the expression of Fizz1 was not significantly different between the groups (Fig. 10f).

Because iNOS and CD206 exhibited the largest changes in mRNA levels, the protein levels of these factors were examined. The concentration of iNOS, an M1 marker, was increased in LPS-stimulated macrophages. When LPS-stimulated macrophages were co-cultured with non-preconditioned cAT-MSCs, iNOS concentration did not decrease significantly. However, when co-cultured with MSC^{DFO}, the decreased in the concentration of iNOS was dependent on the concentration of DFO (Fig. 11a). The concentration of CD206, an M2 marker, was increased when RAW264.7 macrophages were co-cultured with cAT-MSCs, and this effect was enhanced with MSC^{DFO} (Fig. 11b).

4. Discussion

This study investigated the premise that macrophages could be effectively reprogrammed and directed by MSC^{DFO}. To investigate this hypothesis, changes in the level of anti-inflammatory factors were analyzed in MSC^{DFO}. Thereafter, RAW 264.7 mouse macrophage cells were co-cultured with MSC^{DFO} to evaluate their effect on reprogramming/directing

macrophage polarization.

DFO, which chelates the iron necessary for prolyl-4 hydroxylase and inhibits hydroxylation of HIF-1α, was used as a hypoxia-mimetic agent in this research. DFO also demonstrates an antioxidant function and can modify the redox state of cells (Saad et al., 2001). Recently, several studies focused on using DFO in cultured MSCs. DFO preconditioning neural-like cells exhibited improved tolerance and therapeutic effects (Lee and Wurster 1995). Indeed, DFO preconditioning improved homing effect of MSCs (Najafi and Sharifi 2013) and enhanced endothelial progenitor cell homing (Cheng et al., 2010). Some researchers compared DFO with dimethyloxaloylglycine, another commonly used hypoxia mimetic agent, in MSCs. They reported that treating cells with DFO was more effective at stabilizing HIF-1α and increasing some cytokines than dimethyloxaloylglycine (Chang et al., 2008, Yinfei et al., 2013, Duscher et al., 2017).

The concentrations of DFO that were cytotoxic to cAT-MSCs were determined to set the concentrations for the current experiments. There was no effect on MSC viability at concentrations under 500 μM with a 48-h treatment, so these were selected. Furthermore, these concentrations were similar to those reported by previous studies as exhibiting minimal cytotoxic effects (Chu et al., 2008, Oses et al., 2017).

Next, the expression of HIF-1α in of MSC^{DFO} was examined. HIF-1α is a primary marker of the hypoxic response. When cells were treated with DFO, the expression of HIF-1α mRNA was decreased. However, HIF-1α

protein expression was increased in a concentration-dependent manner. It is possible that a structural change could cause differential transcriptional regulation under hypoxic conditions (Lin et al., 2011). Furthermore, DFO inhibited the degradation of HIF-1α, so it is assumed that feedback to HIF-1α mRNA signaling was downregulated (Griffith 1968).

After confirming that HIF-1α accumulated in MSC^{DFO}, the interaction between HIF-1α and anti-inflammatory factors was investigated. Previous researchers reported that hypoxia and HIF-1α are closely intertwined with immune reactions (Hellwig-Bürgel et al., 2005). Using this characteristic, studies have reported enhanced secretory functions in MSCs following hypoxia stimulation. The production of growth factors, like hepatic growth factor (Crisostomo et al., 2008) and vascular endothelial growth factor (Berniakovich and Giorgio 2013), and anti-inflammatory factors like IL-4 (Oses et al., 2017), was increased in MSCs cultured under hypoxic conditions. Based on these reports, it is assumed that DFO could enhance the expression of anti-inflammatory factors that are transcribed under the influence of HIF-1α. TGF-β, TSG-6, IL-10, and COX-2 were selected, except for TSG-6, which are considered to be related to HIF-1α (Shih and Claffey 2001, Lukiw et al., 2003, Hams et al., 2011) and also influence macrophage polarization (Takizawa et al., 2017, Song et al., 2018). When cAT-MSCs were treated with DFO, the expression of TGF-β, TSG-6, and COX-2 mRNAs was increased significantly. TSG-6 and COX-2 were also increased at the protein level.

TSG-6 and PGE2 were also evaluated in media from MSC^{DFO}. PGE2

was selected because it is secreted in response to COX-2 signaling (Németh et al., 2009). However, the concentration of PGE2 in 500 μM MSC^{DFO} was not increased. This was the opposite result to the mRNA and protein expression of COX-2. PGE2 is consumed during the nuclear translocation of HIF-1α from the cytoplasm (Liu et al., 2002). If an excessive amount of HIF-1α was accumulated relative to the production of PGE2, it may be exhausted in the cytoplasm and no PGE2 would be available for secretion.

Usually, pro-inflammatory cytokines such as IFN-γ or TNF-α are used to stimulate NF-κB production (Crisostomo et al., 2008) and enhance the secretion of TSG-6 (Guo et al., 2015) and other anti-inflammatory cytokines by MSCs (Saparov et al., 2016). However, preconditioning of MSCs with pro-inflammatory cytokines has the disadvantage of being toxic, even at low concentrations (Ohnishi et al., 2007). In the present study, anti-inflammatory factors, including TSG-6, were increased in MSC^{DFO}, similar to preconditioning with pro-inflammatory cytokines. Thus, preconditioning with DFO is likely to be as effective as treating with pro-inflammatory cytokines but without the toxicity disadvantage. There are no previous reports that TSG-6 and hypoxia are related. Because NF-κB and HIF-1α cross-talk, it seems that TSG-6 was increased through the accumulation of HIF-1α by a DFO-stimulated NF-κB pathway.

To confirm that MSC^{DFO} increased the levels of anti-inflammatory cytokines that function to induce M2 macrophage polarization, their macrophage directing effect was focused. Macrophage polarization can be

altered in two ways. One involves downregulating reprogramming of the M1 phase, while the other directs M0 macrophages, which are unchanged, to the M2 phase through interaction with cAT-MSCs.

Macrophage polarization was examined *in vitro* with the RAW264.7 cell line. When RAW 264.7 cells were co-cultured with non-conditioned MSCs or MSC^{DFO}, macrophage polarization phase was changed. Macrophages stimulated with LPS were changed to the M1 phase as shown by significant increases in expression of the M1 markers iNOS, IL-1ß, and IL-6. Macrophages stimulated with LPS and co-cultured with cAT-MSCs exhibited reprogrammed polarization as the expression of M1 markers was decreased to levels similar to control cells. The secretion of cytokines by MSC^{DFO} was greater than non-conditioned MSCs, and preconditioned cells reprogrammed macrophages more effectively.

Finally, it was determined whether the change from the macrophage M0 to M2 phase was more prevalent when RAW264.7 cells were exposed to MSC^{DFO}. Non-treated RAW264.7 macrophages were in the M0 phase, and expressed neither M1 nor M2 markers. However, when co-cultured with non-conditioned MSCs or MSC^{DFO}, macrophages were directed into the M2 phase as M2 markers were significantly increased. Importantly, more macrophages were directed to the M2 phase with preconditioned compared to non-preconditioned cAT-MSCs. Taken together, these findings indicate that cAT-MSCs can regulate macrophages into an anti-inflammatory state. Though the levels of secretory factors were increased in a DFO-concentration dependent

manner, preconditioning with as little as 100 μM DFO was sufficient to change macrophage polarization, and there was no significant difference between preconditioning with 100 and 500 μM DFO.

Table 1. Oligonucleotide sequences of PCR primers used in preconditioning of canine adipose tissue-derived mesenchymal stem cells with deferoxamine

Target genes	Primers	Oligonucleotide sequences (5' → 3')	Product sizes	References
Canine HIF-1α	Forward	ACT GAT GAC CAA CAA CTT GAG G	122	*
	Reverse	TTT GGA GTT TCA GAA GCA GGT A		
Canine TGF-β	Forward	GGA AAA CAC CAA CAA AAT CTA TGA G	184	*
	Reverse	GCT ATA TTT CTG GTA CAG CTC CAC A		
Canine TSG6	Forward	TCC GTC TTA ATA GGA GTG AAA GAT G	101	Song, WJ et al., 2018
	Reverse	AGA TTT AAA AAT TCG CTT TGG ATC T		
Canine COX-2;1	Forward	TTC CTG CGA AAT ACA ATT ATG AAA T	149	*
	Reverse	GCC GTA GTT CAC ATT ATA AGT TGG T		
Canine IL-10	Forward	AAG CTG GAC AAC ATA CTG CTG A	126	*
	Reverse	CTG AGG GTC TTG AGC TTC TCT C		
Canine GAPDH	Forward	TTA ACT CTG GCA AAG TGG ATA TTG T	85	Song, WJ et al., 2018
	Reverse	GAA TCA TAC TGG AAC ATG TAC ACC A		
Mouse iNOS	Forward	GGC TGT CAG AGC CTC GTG GCT TTG G	165	*
	Reverse	CCC TCC CGA AGT TTC TGG CAG CAG C		
Mouse IL-6;1	Forward	CGC ACT AGG TTT GCC GAG TA	159	*
	Reverse	CCT TTC TAC CCC AAT TTC CA		
Mouse IL-1β	Forward	GTC TTT CCC GTG GAC CTT C	102	Song, WJ et al., 2017
	Reverse	TGT TCA TCT CGG AGC CTG T		
Mouse Fizz1	Forward	AAG ACT ACA ACT TGT TCC CTT CTC A	170	*
	Reverse	TGA CCT TTT TCT CCA CAA TAG ATT C		
Mouse Ym1	Forward	GTG TAC TCA CCT GAT CTA TGC CTT T	133	Song, WJ et al., 2018
	Reverse	CAG GAG AGT TTT TAG CTC AGT GTT C		
Mouse CD206	Forward	AAC GGA ATG ATT GTG TAG TTC TAG C	163	Song, WJ et al., 2018
	Reverse	TAC AGG ATC AAT AAT TTT TGG CAT T		
Mouse GAPDH	Forward	AGT ATG TCG TGG AGT CTA CTG GTG T	154	Song, WJ et al., 2018
	Reverse	AGT GAG TTG TCA TAT TTC TCG TGG T		

*Primers with asterisk in reference section were designed by own.

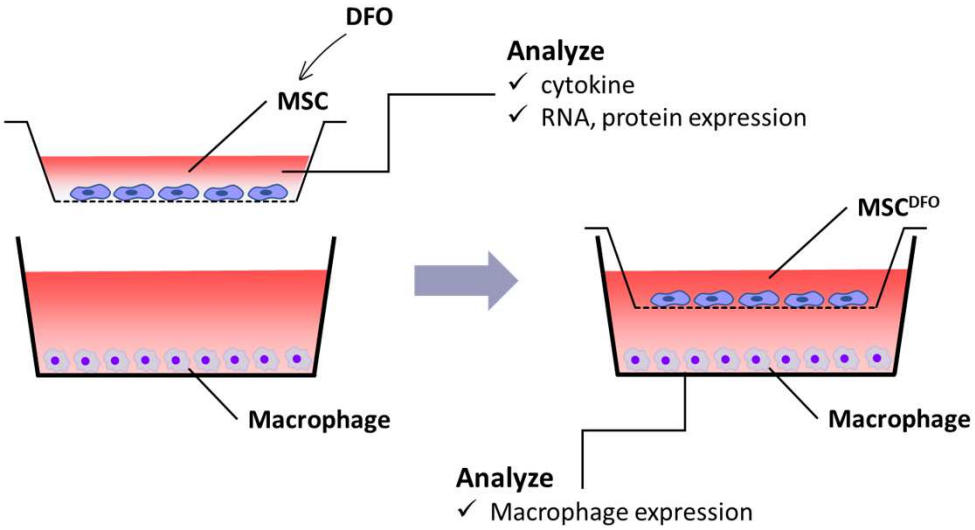

Figure 2. Schematic diagram of the in vitro co-culture experiment. cAT-MSCs were plated on Trans well inserts and treated with 100 or 500 μM DFO, or PBS as control, for 48 h. RAW264.7 cells were seeded on 6 well plates without or with 200 ng/mL LPS for 6 h. RAW264.7 macrophages were also co-cultured with preconditioned cAT-MSCs for 48 h, then collected for further experiments. MSC, mesenchymal stem cell; DFO, deferoxamine.

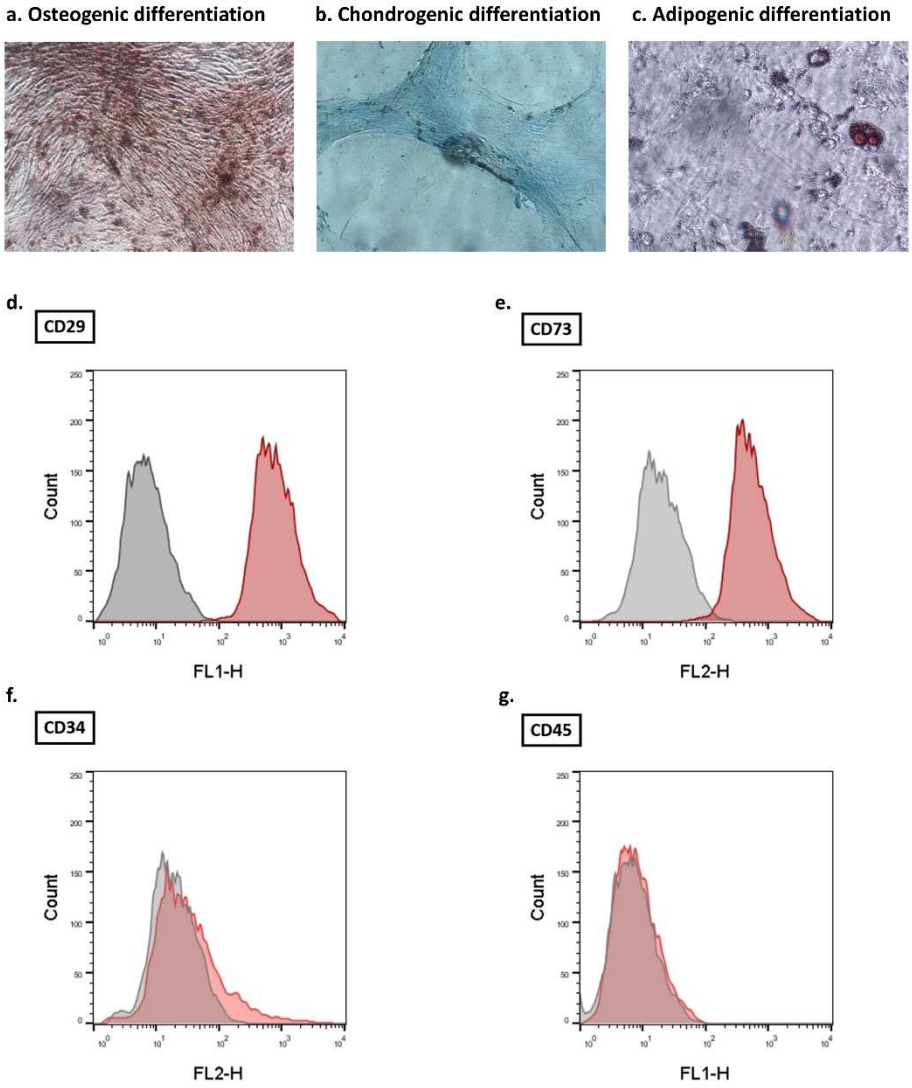

Figure 3. Characterization of canine adipose derived MSC by multilineage differentiation and immunotyping. For multilineage differentiation, cAT-MSC were differentiated into **(a)** osteocyte, **(b)** chondrocyte and **(c)** adipocyte. Differentiated cells were stained with specific dye. **(d-g)** To immunotype, the markers of cAT-MCS were analyzed with CD29, CD73 as positive and CD34, CD 45 as negative.

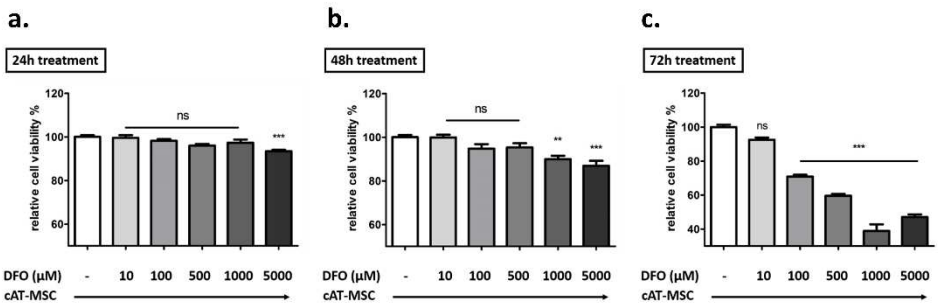

Figure 4. Viability of MSC^{DFO}. Treatment of cAT-MSCs with DFO for (**a**) 24 h, (**b)** 48 h, and (**c)** 72 h. When treating cAT-MSCs with DFO for 24 h, there was no effect on proliferation except at 5 mM. After treating with 1 mM DFO for 48 h, the viability of cells was decreased significantly compared to a 24 h treatment. When treating for 72 h, the viability of all groups, except 10 μM, were decreased. The concentration of DFO as 100 and 500 μM for 48 hours was chosen which are the highest concentrations in which did not affect cell viability. $^{**}p<0.01$, $^{***}p<0.001$; ns, not significant. cAT-MSC, canine adipose tissue derived mesenchymal stem cell; DFO, deferoxamine.

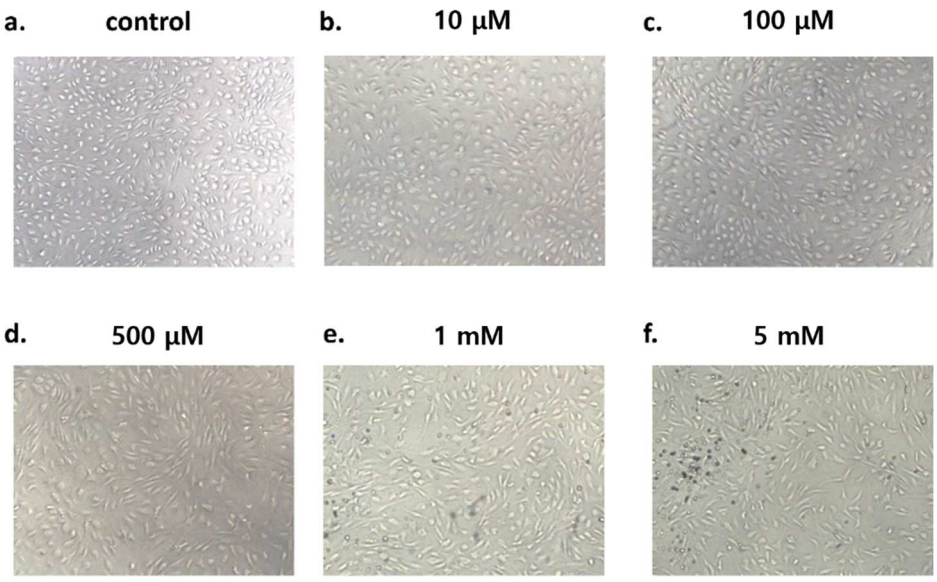

Figure 5. Morphology of MSC^{DFO}. (a-d) MSC was treated with 10, 100, or 500 µM concentration of DFO for 48 h. Cell morphology was unchanged following treatment until 500 µM; (**e, f)** Treatment with over 1 mM concentration of DFO in MSC resulted in several dead cells.

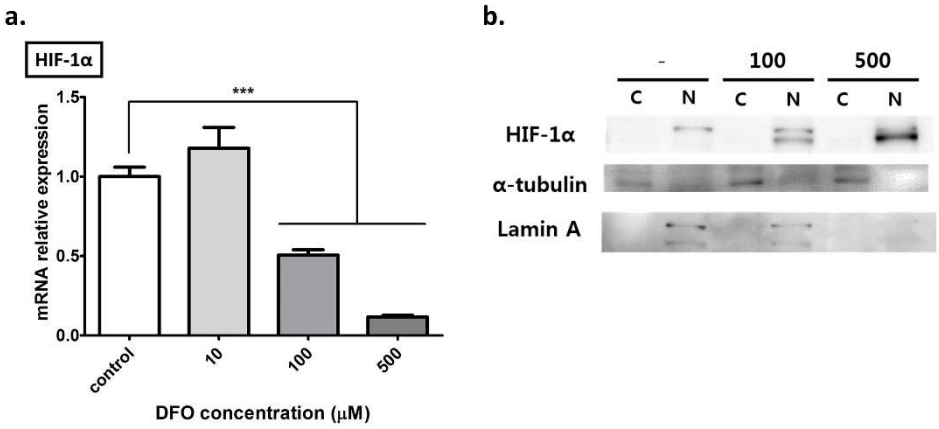

Figure 6. mRNA and protein levels of HIF-1α in MSC^{DFO}. (**a)** The mRNA level of HIF-1α is decreased in a DFO-concentration-dependent manner. (**b)** In contrast to the mRNA result, the HIF-1α protein level is increased in a DFO-concentration-dependent manner in the nuclear fraction. Results are shown as means ± standard deviation. $^{***}p<0.001$. DFO, deferoxamine.

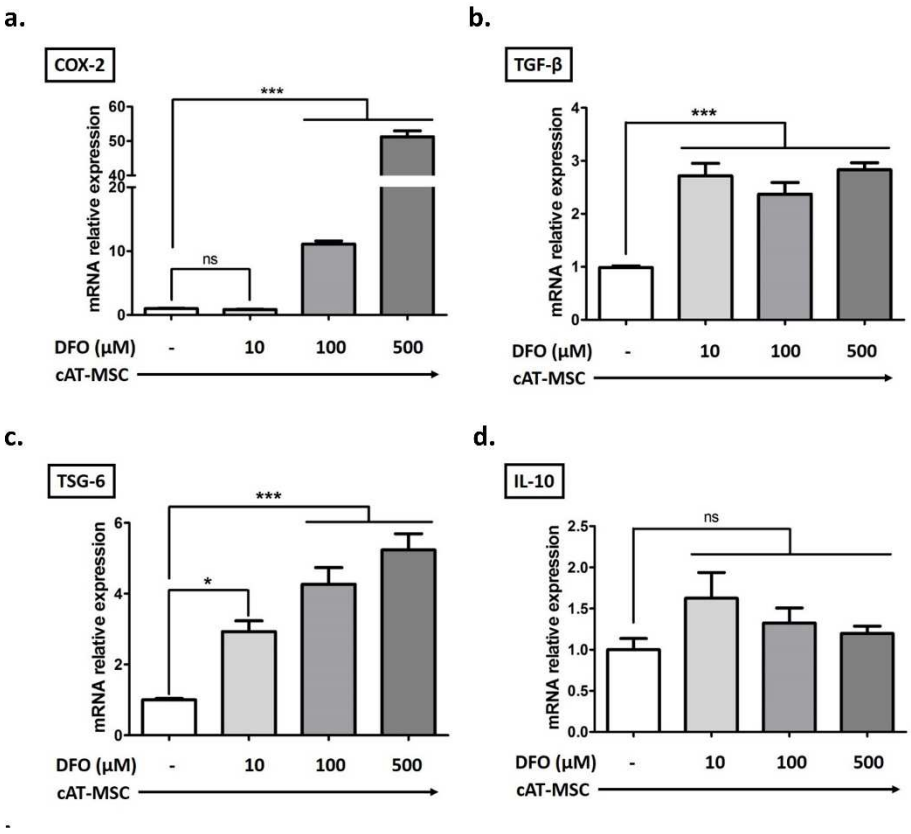

Figure 7. Anti-inflammatory factors are increased in MSC^{DFO} in RNA level. (**a)** The cyclooxygenase (COX)-2 mRNA level was increased in 100 and 500 μM DFO preconditioned cells. (**b)** TGF-β mRNA level was increased in all DFO preconditioned cells. (**c)** TNF-α-stimulated gene-6 (TSG-6) mRNA level was increased in all preconditioned cells. **(d)** IL-10 mRNA level was not significantly different in non-conditioned or DFO-preconditioned cells. Results are shown as mean ± standard deviation. $^{*}p<0.05$, $^{***}p<0.001$; ns, not significant. cAT-MSC, canine adipose tissue derived mesenchymal stem cell; DFO, deferoxamine.

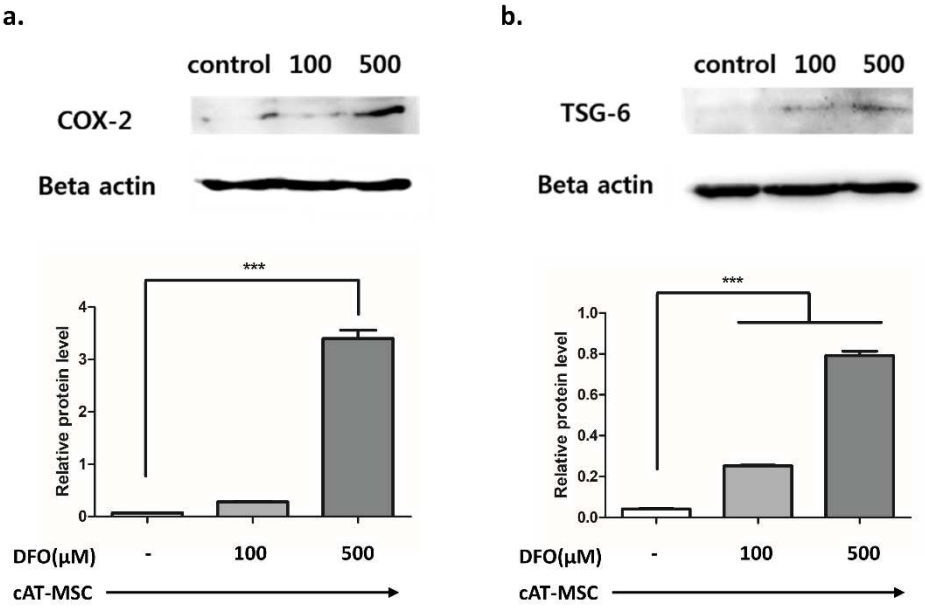

Figure 8. Anti-inflammatory factors are increased in MSC^{DFO} in protein level. (**a, b)** COX-2 and TSG-6 protein levels were increased in a DFO-concentration-dependent manner. $^{***}p<0.001$. cAT-MSC, canine adipose tissue derived mesenchymal stem cell; DFO, deferoxamine.

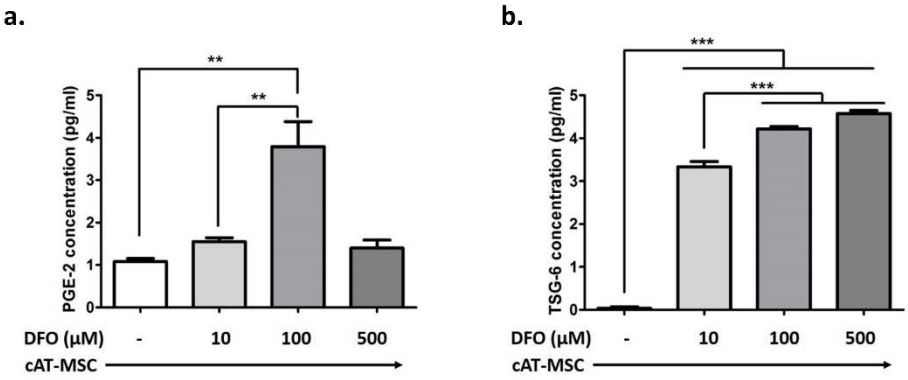

Figure 9. Anti-inflammatory factors are increased in MSC^{DFO} in cytokine level. (**a)** Secretion of prostaglandin E-2 (PGE-2), downstream of COX-2 signaling, was increased in 10 and 100 μM, but not 500 μM DFO, preconditioned cells. Cells preconditioned with 100 μM DFO exhibited a greater increase in PGE-2 levels compared to cells preconditioned with 10 μM DFO. (**b)** Secretion of TSG-6 was also increased in all DFO preconditioned cells. The increase in TSG-6 in 100 μM DFO preconditioned cells was greater than that with 10 μM DFO. Results are shown as mean ± standard deviation. $^{**}p<0.01$, $^{***}p<0.001$. cAT-MSC, canine adipose tissue derived mesenchymal stem cell; DFO, deferoxamine.

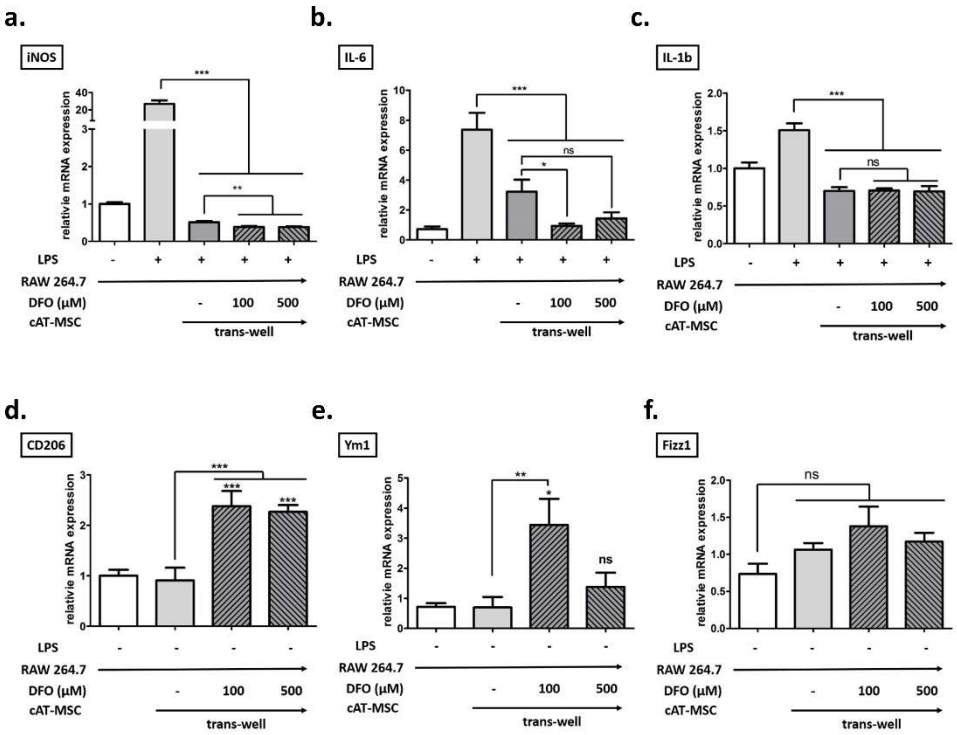

Figure 10. The polarization phase of RAW264.7 cells is changed when co-cultured with MSC^{DFO} in RNA level. (**a-c)** Lipopolysaccharide (LPS) treatment induced conversion of RAW264.7 cells to the M1 phase. Inducible nitric oxide synthase (iNOS), IL-6, and IL-1ß were selected as M1 phase markers. The mRNA levels of these markers were significantly increased in LPS-stimulated RAW 264.7 cells. When these cells were co-cultured with non-conditioned MSCs or MSC^{DFO}, the concentration of these M1 markers significantly decreased. MSC^{DFO} more effectively reduced the concentration of M1 markers than non-preconditioned cells. (**d-f)** The polarization phase of non-stimulated RAW264.7 macrophages was considered to be M0 because these cells did not express either M1 or M2 phase markers. CD206, Ym1, and Fizz1 were selected as M2 markers. When RAW264.7 cells were co-cultured

with MSC^{DFO}, the levels of M2 marker mRNAs were increased. Non-preconditioned MSCs did not change the polarization phase of non-stimulated RAW264.7 cells. $^{*}p<0.05$, $^{**}p<0.01$, $^{***}p<0.001$; ns, not significant. cAT-MSC, canine adipose tissue derived mesenchymal stem cell'; DFO, deferoxamine.

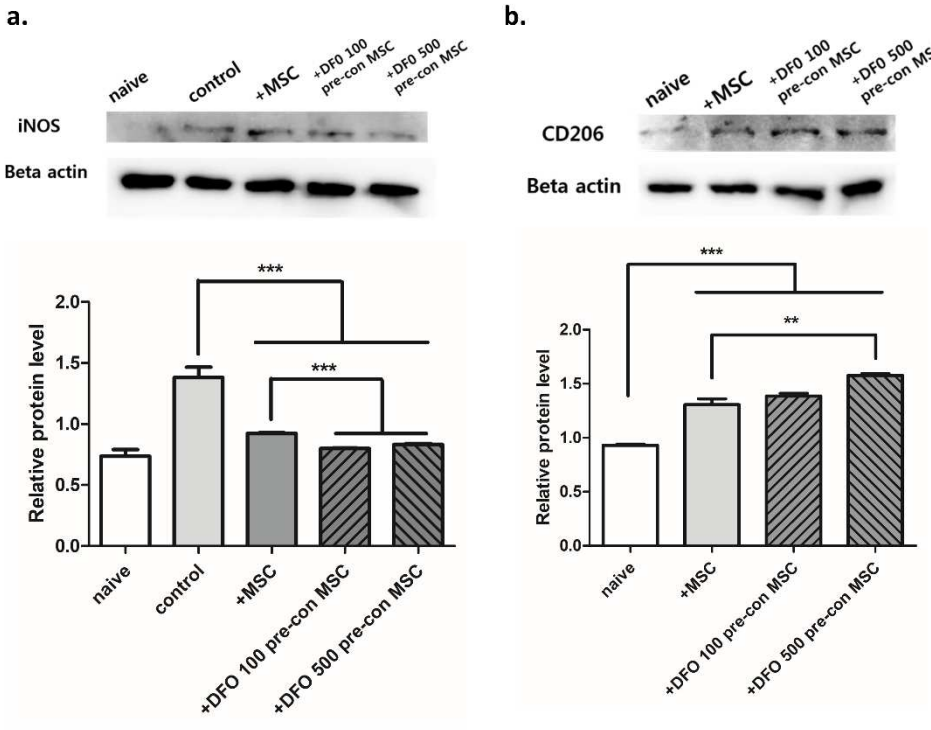

Figure 11. The polarization phase of RAW264.7 cells is changed in protein level when co-cultured with MSC^{DFO}. (**a)** MSC^{DFO} significantly reduced the protein expression of iNOS when co-cultured with RAW264.7 cells. (**b)** MSC^{DFO} significantly enhanced expression of the CD206 protein in co-cultured RAW264.7 cells. $^{**}p<0.01$, $^{***}p<0.001$. MSC, mesenchymal stem cell; DFO, deferoxamine.

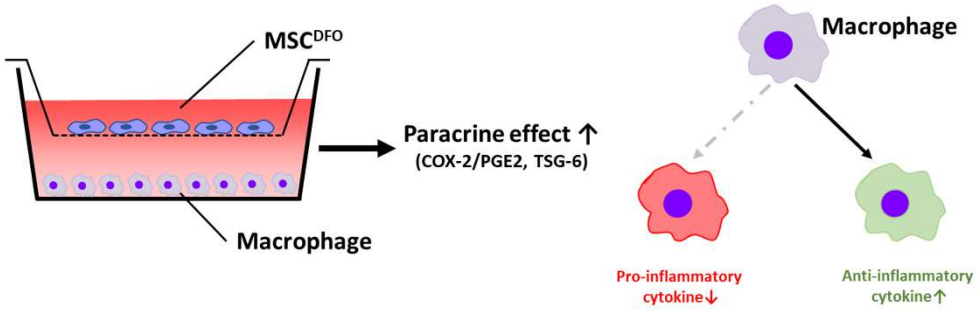

Figure 12. Schematic diagram of the effect of DFO preconditioned MSC to macrophage. The secretion of cytokines by MSC^{DFO} was greater than non-conditioned MSCs, and preconditioned cells reprogrammed macrophages more effectively. Though secretory factors from MSC^{DFO}, macrophage were regulated into an anti-inflammatory state. MSC^{DFO}, deferoxamine preconditioned mesenchymal stem cell.

Chapter II.

Extracellular vesicles derived from DFO-preconditioned canine AT-MSCs reprogram macrophages into M2 phase

1. Introduction

Among the secretomes of mesenchymal stem/stromal cells (MSCs), extracellular vesicles (EVs) have been studied frequently for playing an important role in transmitting signals across cells (Lai et al., 2015). EVs are small membrane vesicles that are 40–100 nm in diameter. They are released from cell membrane after fusion with multivesicular endosome and cell membrane, and contain proteins, metabolites, and nucleic acids (Hessvik and Llorente 2018). Studies have shown the cells to be modified via transmission of mRNA, RNA, and protein via EVs (Phinney and Pittenger 2017, Sterzenbach et al., 2017).

Further studies are being conducted on how to increase the productivity and efficacy of EVs (Hong et al., 2019). Some studies have been conducted using hypoxia-preconditioned methods to improve anti-inflammatory effect of MSC-derived EVs (Cui et al., 2018). Several studies have shown deferoxamine (DFO), a hypoxia mimetic agent, to be usable in hypoxia preconditioning (Fujisawa et al., 2018) and improve angiogenesis effect of MSC-derived EVs (Ding et al., 2019). DFO inhibits hydroxylation of hypoxia-inducible factor-1 alpha (HIF-1α) and chelates the iron necessary

for prolyl-4 hydroxylase, owing to which, HIF-1α is accumulated in the cell nucleus similar to that in hypoxic condition (Wang and Semenza 1993). Although some previous papers had reported the modification of stem cells in hypoxic culture (Basciano et al., 2011, Pezzi et al., 2017), there have not been many studies reporting the changes in MSC-derived EVs when treated with DFO.

Hypoxic stimulation induces HIF-1α accumulation in the nucleus, and control various signal pathways, such as inflammation, energy deprivation, or proliferation (Zagórska and Dulak 2004). the activation of cyclooxygenase-2 (COX-2)/prostaglandin E2 (PGE 2) synthase axis (Lee et al., 2010) by HIF-1α was focused on, since the former has anti-inflammatory function in stem cells (Yang et al., 2018). Moreover, COX-2 and signal transducer and activator of transcription 3 (STAT3) are linked to macrophages polarization (Han et al., 2019), which is the main signal molecule in M2 polarization (Nakamura et al., 2015, Roberts et al., 2019).

Therefore, in this study, it was investigated that a hypoxic culture method using DFO in order to increase the anti-inflammatory efficacy of MSC-derived EVs. Moreover, the association of HIF-1α/COX-2 anti-inflammatory pathway in MSC^{DFO} was investigated. Further, the molecular changes of MSCs to be reflected on the derived EVs was revealed, the latter then transferring the molecules to macrophages and reprogramming them into M2 phase.

2. Materials and methods

2.1. Cell preparation and culture

cAT was obtained using a protocol approved by the Institutional Animal Care and Use Committee of Seoul National University (SNU; protocol no. SNU-180621-27). Briefly, Canine adipose tissue was obtained from a healthy dog < 1 year old during routine spay surgery. The tissue was washed three times with PBS (PAN Biotech, Germany) which was contained 100 U/ml penicillin and 100 g/ml streptomycin. Then the tissues were cut into small pieces and digested for 1 h at 37°C by collagenase type IA (1 mg/ml; Sigma-Aldrich, MO). After 1 hour, the collagenase was inhibited with DMEM (PAN Biotech, Germany) with 10% FBS (PAN Biotech, Germany). To remove debris, the cell pellet was obtained after centrifugation at 1200 × *g* for 5 min and filtered through a 70-μm Falcon cell strainer (Fisher Scientific, MA). Then cells were incubated in DMEM containing 10% FBS at 37°C in a humidified atmosphere of 5% CO_2.

cAT-MSCs were characterized as described in Supporting information. Cells were differentiated into adipocytes, chondrocytes, and osteocytes to confirm their multilineage features. They were also characterized by detecting stem cell markers with flow cytometry. cAT-MSCs were characterized through immunophenotyping and multilineage differentiation. To evaluate immunophenotyping of cAT-MSCs, flow cytometry was used to detect fluorescent stem cell marker antibodies. The antibodies used were against CD29 (fluorescein isothiocyanate; FITC), CD34

(phycoerythrin; PE), and CD44 (FITC), and CD45 (FITC) (eBiosciences, CA). Flow cytometry was performed with a FACS Aria II system (BD Life Sciences, San Jose, CA) and analyzed by FlowJo software (Tree Star, OR). Cells were seeded in 24-well plates and cultured until 80–90% confluency in basal medium. The medium was then changed to differentiation medium (PRIME-XV Adipogenic Differentiation SFM, PRIME-XV Osteogenic Differentiation SFM, or PRIME-XV Chondrogenic Differentiation XSFM; all from Irvine Scientific, CA). Differentiated cells were stained with Oil Red O, Alizarin Red, and Alcian Blue respectively. After characterization, cAT-MSCs at passages 3–4 were used for subsequent experiments.

Cells were cultured in DMEM (PAN Biotech, Germany) with 10% Fetal bovine serum (FBS; PAN Biotech, Germany) and 1% penicillin-streptomycin (PS; PAN Biotech, Germany) at 37 °C in 5% CO_2 atmosphere. The culture medium was changed every 2–3 days, and cells were sub-cultured at 70–80% confluency. When cAT-MSCs were approximately 70% confluent, 100 μM DFO was added for 48 h in DMEM with 10% exosome-depleted FBS (Thermo Fischer Scientific, MA) and 1% PS (PAN Biotech, Germany).

The canine macrophage cell line DH82 was purchased from the Korean Cell Line Bank (Korea) and cultured in DMEM with 15% FBS (PAN Biotech, Germany) at 37 °C in 5% CO_2 atmosphere until they reached 70–80% confluency.

2.2. Transfection of cAT-MSCs with siRNA

When the confluency of cAT-MSC was approximately 40%, they were transfected with COX-2 siRNA or control siRNA (sc-29279 and sc-37007, respectively; Santa Cruz Biotechnology, CA) for 48 h using Lipofectamine RNAiMAX (Invitrogen, CA), following the manufacturers' instructions. COX-2 knockdown was confirmed by qRT-PCR before further experiments.

2.3. Isolation and characterization of EVs derived from cAT-MSCs

cAT-MSCs were cultured for 48 h in DMEM with 10% exosome-depleted FBS (Thermo Fischer Scientific, MA) and 1% PS (PAN Biotech, Germany). The medium from each cultured cAT-MSC sample was collected and centrifuged at 2600 × g for 20 min to remove cells and cell debris. Each supernatant was transferred to a fresh tube and appropriate volume of ExoQuick-CG (System Biosciences, CA) added. EVs were isolated according to the manufacturer's instructions.

Protein markers of isolated EVs were identified by western blotting using antibodies against CD81 (Aviva system biology, CA) and CD9 (GeneTex, CA). Morphology of the EVs was characterized using transmission electron microscopy. Briefly, 10 μl of EV suspension was placed on a 300-mesh formvar/carbon-coated electron microscopy grid with the coated side facing the suspension. Distilled water was placed on the mesh for washing and a 10-μl drop of uranyl acetate was placed on the mesh for

negative staining for 1 min, followed by observation under a transmission electron microscope (TEM; LIBRA 120, Carl Zeiss, Oberkochen, Germany) at 120 kV. Size distribution of the particles was determined using a zeta-potential and particle size analyzer (ELSZ-1000ZS, Otsuka Electronics, Osaka, Japan).

2.4. RNA extraction, cDNA synthesis, and quantitative real-time polymerase chain reaction (qRT-PCR)

Total RNA was extracted from cAT-MSCs preconditioned with DFO or from control group, and from DH82 cells using the Easy-Blue total RNA extraction kit (Intron Biotechnology, Korea). cDNA was synthesized using the CellScript All-in-One 5× first strand cDNA synthesis master mix (CellSafe, Korea). Samples were analyzed using AMPIGENE qPCR green mix Hi-ROX with SYBR Green dye (Enzo Life Sciences, NY) and 400 nM forward and reverse primers in the qRT-PCR thermal cycler (Bionics, Korea). The expression level of each gene was normalized to that of GAPDH, and relative expression calculated against the contrasting control group.

2.5. Protein extraction, cell fractionation, and western blotting

Protein was extracted from preconditioned cAT-MSC-derived exosomes and DH82 using the Pro-Prep protein extraction solution (Intron Biotechnology, Korea). Concentration of the protein samples was analyzed using the DC Protein Assay Kit (Bio-Rad, CA). Nuclear proteins were

isolated using the Cell Fractionation Kit-Standard (Abcam, MA). For western blot assays, 25 μg of proteins were loaded and separated by SDS-PAGE. Bands from SDS-PAGE were transferred to polyvinylidene difluoride membranes (EMD Millipore, Billerica, MA, USA), which were then blocked with 5% non-fat dry milk and Tris-buffered saline. Membranes were incubated with primary antibodies against HIF-1α (1:500; LifeSpan BioSciences, WA), COX-2 (1:500, Santa Cruz Biotechnology, TX), STAT3 (1:500, LifeSpan BioSciences, WA), phosphorylated (Tyr705) STAT3 (1:500, LifeSpan BioSciences, WA), lamin A (1:500, Santa Cruz Biotechnology, TX) and β-actin (1:1000, Santa Cruz Biotechnology, TX) at 4 °C overnight. The membranes were subsequently incubated with the appropriate secondary antibody for 1 h. Using an enhanced chemiluminescence detection kit (Advansta, CA), immunoreactive bands were detected and normalized to the housekeeping protein (β-actin).

2.6. Immunofluorescence analyses

DH82 cells were cultured at 2×10^5 cells in cell-culture slide (SPL, Korea), and 200 ng/ml lipopolysaccharides (LPS; Sigma-Aldrich, MO) were stimulated for 24 h. After LPS stimulation, DH82 cells were treated with EVs at concentrations of 50 μg/well for 48 h. The slide was fixed with 4% paraformaldehyde and blocked with a blocking buffer containing 5% bovine serum albumin and 0.3% Triton X-100 (both from Sigma-Aldrich, MO) for 1 h. They were then incubated overnight at 4 °C with antibodies against FITC-

conjugated CD206 (1:200; Santa Cruz Biotechnology, TX) and phycoerythrin-conjugated CD11b (1:100; Abcam, MA). After three washes, the slides were mounted in a VECTASHIELD mounting medium containing 4',6-diamidino-2-phenylindole (Vector Laboratories, CA). The samples were observed under a EVOS FL microscope (Life Technologies, Darmstadt, Germany). Immunoreactive cells were calculated with 20 random fields per group as per the ratio of DAPI/CD206-positive cells.

2.7. Statistical analyses

Data are shown as mean ± standard deviation. Mean values from the different groups were compared by Student's t-test and one-way analysis of variance using GraphPad Prism v.6.01 software (GraphPad Software, CA). *p* value < 0.05 was considered statistically significant.

3. Results

3.1. Characterization of cAT-MSC derived EVs

cAT-MSCs were characterized by flow cytometry and differentiation (Fig. 14). EVs were separated from stem cell culture media by Exo-quick^{TM}. They were round in shape, with diameter ranging from 50 nm to 100 nm, as per electron microscopic analysis (Fig. 15a). Using a particle-size analyzer, the diameter of EVs was confirmed to be approximately 100 nm (Fig. 15b). To identify the surface markers of exosomes, CD81 and CD 9 were confirmed as positive while β-actin was negative in western blotting

(Fig. 15c).

3.2. Elevation of HIF-1α/COX-2 expression in MSC^{DFO}

In CCK assay, the viability of cAT-MSCs was found to be decreased upon treatment with 1 mM DFO; therefore, DFO was used under 1 mM in further experiments (Fig. 16a). HIF-1α was accumulated in MSC^{DFO} at both 100 μM and 500 μM of DFO concentration (Fig. 16b). Considering the previous report, which found no significant difference between 100 μM and 500 μM DFO (Park et al., 2020), 100 μM DFO was chosen for the current treatment.

To evaluate the role of COX-2 in cAT-MSCs, siCOX-2 was transfected into the cells before DFO conditioning. RNA levels of COX-2 were significantly increased in cAT-MSC^{DFO} and DFO preconditioning plus control siRNA (MSC^{siRNA}) groups; the expression not being significantly different between the two. In DFO-preconditioned group, with COX-2 siRNA (MSC$^{siCOX-2}$), COX-2 expression was not increased (Fig. 17a). At protein level, COX-2 was increased in MSC^{DFO} and MSC^{siRNA}, but not in MSC$^{siCOX-2}$ (Fig. 17b).

3.3. cAT-MSC-derived EVs transport COX-2 to DH82 and activate the phosphorylation of STAT3

When expression of COX-2 protein was evaluated in EVs, it was found increased in cAT-MSC^{DFO}-derived EV (EV^{DFO}) than in non-preconditioned cAT-MSC-derived EV (EV^{non}). In cAT-MSC$^{siCOX-2}$-derived

EV ($EV^{siCOX-2}$), COX-2 was not increased, similar to that in cAT-MSCs (Fig. 18).

DH82 cells were treated with EVs to verify their anti-inflammatory effect on macrophages. They were treated with LPS before EV treatment. In the LPS-treated group, expression of p-STAT3 was increased, whereas that of STAT3 decreased compared to that in naïve group. The expression of both STAT3 and p-STAT3 increased in EV-treated groups. In the groups treated with EV^{DFO}, the expression of p-STAT3 was significantly increased than in non-preconditioned group. However, in the group treated with $EV^{siCOX-2}$, p-STAT3 was not increased compared to that in the group treated with EV^{non} (Fig. 19).

3.4. Change of polarization of DH82 when treated with preconditioned EVs

When DH82 cells were treated with LPS, the markers of M1 proinflammatory phase, namely IL-1b and IL-6, were significantly increased. However, expression of both cytokines was decreased in the groups with EV treatment. Expression of pro-inflammatory cytokines was decreased in the groups treated with EV^{DFO}, than in the groups treated with EV^{non} group. The group with $EV^{siCOX-2}$ showed no significant difference from that with EV^{non} (Fig. 20a, b).

Using immunofluorescence of CD206, which is a marker of M2 anti-inflammatory phase, the polarization phase of DH82 cells was evaluated. Red staining was against CD11b, which is a marker of macrophage. In naïve DH82

group, red staining was visibly detected and when LPS inducing in DH82, the marker was not changed. (Fig. 21a, b). In EVs treated groups, green stain of CD206 was significantly increased and the red stain was difficult to recognize (Fig. 21c-f). Especially, CD206 was significantly increased in the groups treated with EV^{DFO} (Fig. 21d). The group with $EV^{siCOX\text{-}2}$ showed slight enhancement of CD206, which was not significant compared to that in the group with EV^{DFO} (Fig. 21f, g).

4. Discussion

Mesenchymal stem cells (MSCs) have been studied for their anti-inflammatory therapeutic functions due to paracrine effect (Huang et al., 2014, Samadi et al., 2020). Since they interact with immune cells, including macrophages and T cells, MSC secretome is considered to be immunomodulatory and can regulate the anti-inflammatory phase (Kim and Hematti 2009, Sargent and Miller 2016). Previous result demonstrated that paracrine effect of cAT-MSCs can significantly reprogram macrophages from M1 pro-inflammatory phase to M2 anti-inflammatory phase (Park et al., 2020). The study proved that secretory function of MSCs plays an important role in cell interaction, especially with inflammatory cells like macrophages. Recently, EVs were reported to play an important role among secretomes, owing to their ability to communicate and deliver substances (Bruno et al., 2009, Kusuma et al., 2017, Baek et al., 2019, Riau et al., 2019). Therefore, the EVs derived from cAT-MSCs was focused. In the current study, it was

investigated whether DFO-preconditioned EVs have the potential to direct macrophages to M2 phase. To prove this hypothesis, HIF-1α/COX-2 axis was analyzed in MSC^{DFO} and EV^{DFO}. After confirming that DFO could effectively increase COX-2 expression in EVs, Canine macrophage cells, DH82, were treated with EVs to confirm the delivery function of EVs and evaluate their effect on macrophage polarization.

First, accumulation of HIF-1α in the nucleus, which is an important indicator of hypoxia, was confirmed by western blot in MSC^{DFO} (Fig. 16b). Some reports had earlier suggested that COX-2 increases significantly with hypoxic culture under HIF-1α signal pathway (Han et al., 2016) and is associated with both anti-inflammatory effect and macrophage polarization (Luo et al., 2011, Jin et al., 2019). In MSC^{DFO}, both RNA and protein expression of COX-2 was increased, implying that DFO preconditioning could increase HIF-1α accumulation, and transcription of COX-2 was activated under HIF-1α pathway (Fig. 17a, b).

Some reports have revealed that the same proteins may be detected either in MSC cytoplasm or in MSC secretomes and EVs (Selmani et al., 2008, Jansen et al., 2009, Schaeffer et al., 2009). In the current study as well, expression change of COX-2 protein in the cytosol of cAT-MSCs were also reflected in the EVs. EVs from MSC^{DFO} were enriched with COX-2 molecules (Fig. 18).

HIF-1α and COX-2/PGE2 pathway are known to be associated with STAT3 activation (Yu et al., 2018, Liu et al., 2020), which is an important

factor in macrophage M2 anti-inflammatory phase (Shiraishi et al., 2012, Hollander et al., 2016, Zhao et al., 2018). Previously published reports had suggested that macrophages are polarized into M2 phase when various molecules, such as miRNA, are delivered through EVs and stimulate STAT3 pathway in the macrophages (Haneklaus et al., 2013, Sun et al., 2013, Heo et al., 2019). Another study had revealed that not only miRNA, but proteins also can be transmitted into macrophage through EVs, and play their role (Zhao et al., 2018).

The delivery system of EVs has been reported to play an important role in the anti-inflammatory effect of stem cells, especially in relation to macrophages (Sicco et al., 2017). Reprogramming macrophages from pro-inflammatory M1 phase to anti-inflammatory M2 phase is the most important mechanism in controlling immune homeostasis (Genua et al., 2016), and EVs regulate this polarization phase by transferring substances from stem cells to macrophages (Lankford et al., 2018, Willis et al., 2018). Therefore, this study focused on the effect of COX-2 transferred by EVs to STAT3 signaling in macrophages. When the expression of pSTAT3 and STAT3 in LPS-induced DH82 were evaluated, these factors in LPS-induced DH82 treated with EV^{DFO} were increased over than with EV^{non} (Fig. 19).

The expression change of pSTAT3 in LPS-induced DH82 could be associated with macrophage phase. Thus, macrophage phase of LPS-induced DH82 with EVs treating was evaluated. In LPS-induced DH82 cells treated with EVs, which were increased with pSTAT, the marker of M1 was reduced

while that of M2 was increased (Fig. 20, 21). These changes were greater with EV^{DFO}. Considering all the results, EVs could deliver COX-2 to LPS-induced DH82, and might lead to M2 polarization by activating the phosphorylation of STAT3. Moreover, DFO preconditioning in cAT-MSCs enhance the macrophage directing effect through activating HIF-1α/COX-2 axis.

In this study, a limitation was that it was not clear whether substances such as miRNA in EVs could be stimulated to activate STAT3. Therefore, further studies would be required to analyze the changes in miRNA levels in MSC^{DFO} and EV^{DFO}. However, this study found that preconditioning with DFO could affect COX-2 in cAT-MSCs and acted as anti-inflammatory molecules. EV^{DFO} contained COX-2 protein and could effectively reprogram macrophage polarization into M2 phase via protein delivery system. The findings presented the therapeutic possibility of EV^{DFO}, which could be used in treating inflammatory diseases through macrophage reprogramming.

Table 2. Oligonucleotide sequences of PCR primers used in EVs derived from MSC^{DFO} and macrophage which was affected by EVs

Target genes	Primers	Oligonucleotide sequences (5' → 3')	Product Sizes	References
Canine HIF-1α	Forward	ACT GAT GAC CAA CAA CTT GAG G	122	*
	Reverse	TTT GGA GTT TCA GAA GCA GGT A		
Canine COX-2;2	Forward	TTC CTG CGA AAT ACA ATT ATG AAA T	149	*
	Reverse	GCC GTA GTT CAC ATT ATA AGT TGG T		
Canine GAPDH	Forward	TTA ACT CTG GCA AAG TGG ATA TTG T	85	Song, WJ et al., 2018
	Reverse	GAA TCA TAC TGG AAC ATG TAC ACC A		
Canine IL-1β	Forward	AGT TGC AAG TCT CCC ACC AG	177	*
	Reverse	TAT CCG CAT CTG TTT TGC AG		
Canine IL-6	Forward	GGC TAC TGC TTT CCC TAC CC	243	*
	Reverse	TGG AAG CAT CCA TCT TTT CC		

*Primers with asterisk in reference section were designed by own.

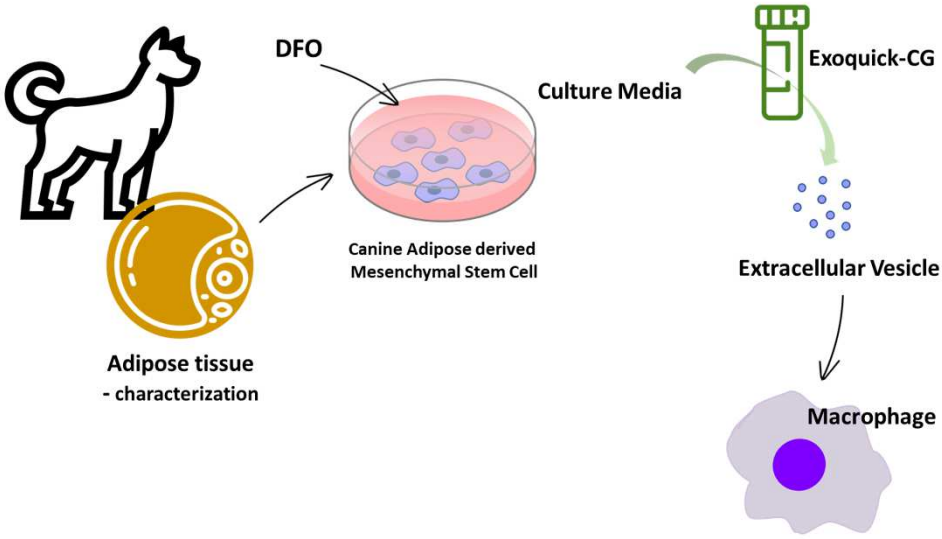

Figure 13. Schematic diagram of DFO preconditioned cAT-MSC derived EV treatment in vitro experiment. Canine adipose tissue was obtained from a healthy dog < 1 year old during routine spay surgery. Using collagenase, mesenchymal stem cell was isolated from adipose tissue. When cAT-MSCs were approximately 70% confluent, 100 μM DFO was added for 48 h in DMEM with 10% exosome-depleted FBS. The medium from each cultured cAT-MSC sample was collected and from each supernatant, EVs were isolated with of ExoQuick-CG. DH82 cells were stimulated with 200 ng/ml LPS for 24 h. After LPS stimulation, DH82 cells were treated with EVs at concentrations of 50 μg/well for 48 h. DH82 treated with EVs were analyzed by qRT-PCR, western blot and immunofluorescence. DFO, deferoxamine.s

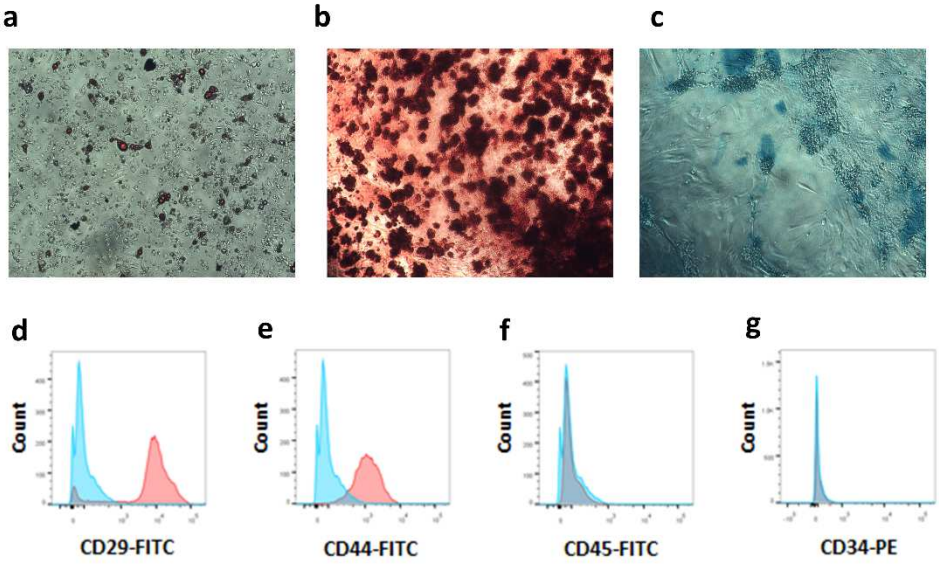

Figure 14. Characterization of canine adipose derived MSC by multilineage differentiation and immunotyping. To identify multilineage differentiation, cAT-MSC were differentiated into **(a)** adipocyte, **(b)** osteocyte and **(c)** chondrocyte. Differentiated cells were stained each specific dye. **(d-g)** To immunotype, the markers of cAT-MCS were analyzed with CD29, CD44 as positive and CD45, CD 34 as negative.

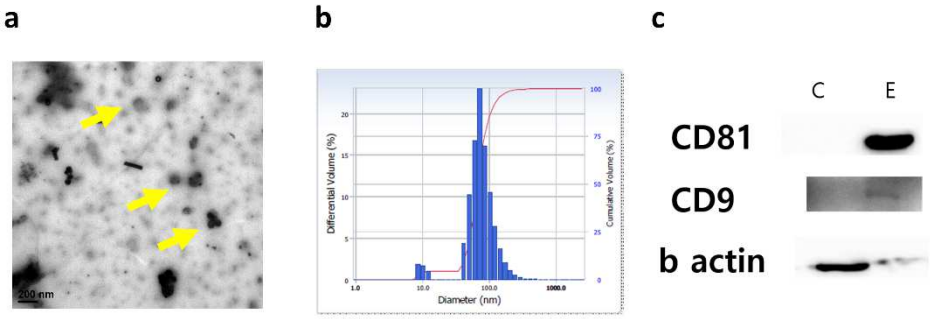

Figure 15. cAT-MSC derived EV characterization. (a) In electron microscopic analysis, EVs were measured as 50-100nm. **(b)** Through a particles-size analyzer, the diameter of EVs was confirmed as around 100nm. **(c)** CD81 and CD 9, surface marker of EV, were confirmed as positive and β-actin was confirmed as negative in western blotting.

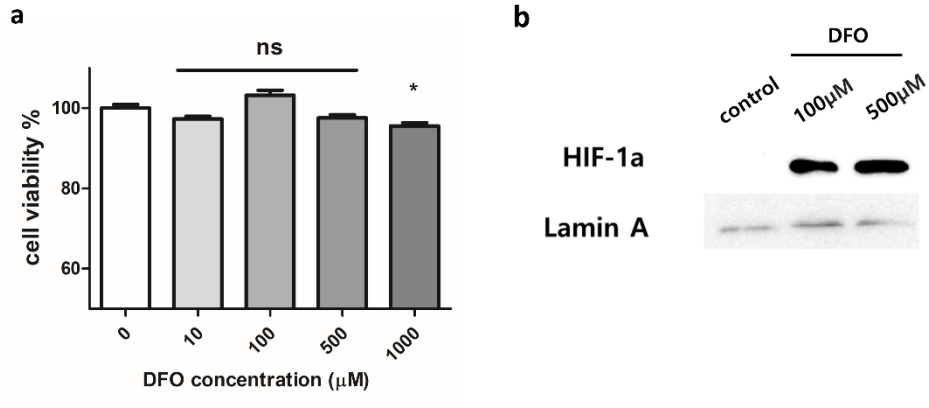

Figure 16. Viability test with DFO and the hypoxic mimicking efficacy of DFO in cAT-MSC. (a) Viability of cAT-MSCs treated with DFO and **(b)** Protein levels of HIF-1α in DFO-treated cAT-MSCs. $^{*}p<0.05$; ns, not significant. DFO, deferoxamine.

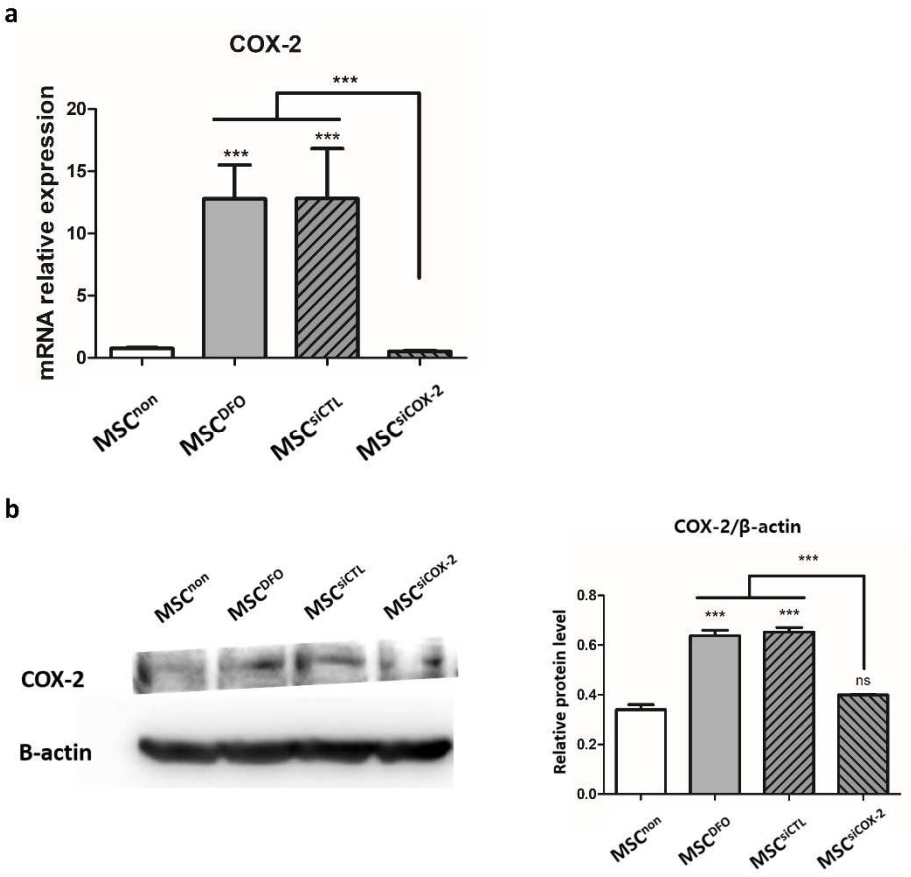

Figure 17. The RNA and protein expression levels of COX-2 in MSC^{DFO}.

(a) The mRNA level of COX-2 is increased in DFO preconditioned and treated with siCTL group. However, COX-2 is not increased in transfected with siCOX-2 group. **(b)** The protein level of COX-2 is increased in DFO preconditioned and decreased in transfected with siCOX-2 group, same as mRNA result. Results are shown as means ± standard deviation. $^{***}p<0.001$; ns, not significant. MSC^{non}, non-preconditioned MSC; MSC^{DFO}, DFO preconditioned MSC; MSC^{siCTL}, MSC treated with DFO and control siRNA; MSC$^{siCOX-2}$, MSC treated with DFO and siCOX-2.

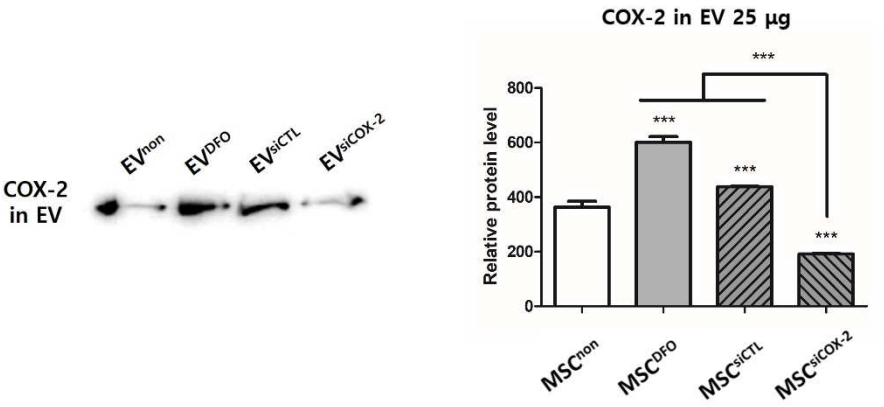

Figure 18. Protein levels of COX-2 in cAT-MSC derived EVs. COX-2 level was increased in EVs derived from MSC^{DFO} (EV^{DFO}). Otherwise, COX-2 was decreased in $EV^{siCOX-2}$. The result of COX-2 protein level in EVs was similar with cytosol COV-2 protein level in cAT-MSC. Results are shown as means ± standard deviation. $^{***}p<0.001$. EV^{non}, EV derived from non-preconditioned MSC; EV^{DFO}, EV derived from DFO preconditioned MSC; EV^{siCTL}, EV derived from MSC treated with DFO and control siRNA; $EV^{siCOX-2}$, EV derived from MSC treated with DFO and siCOX-2.

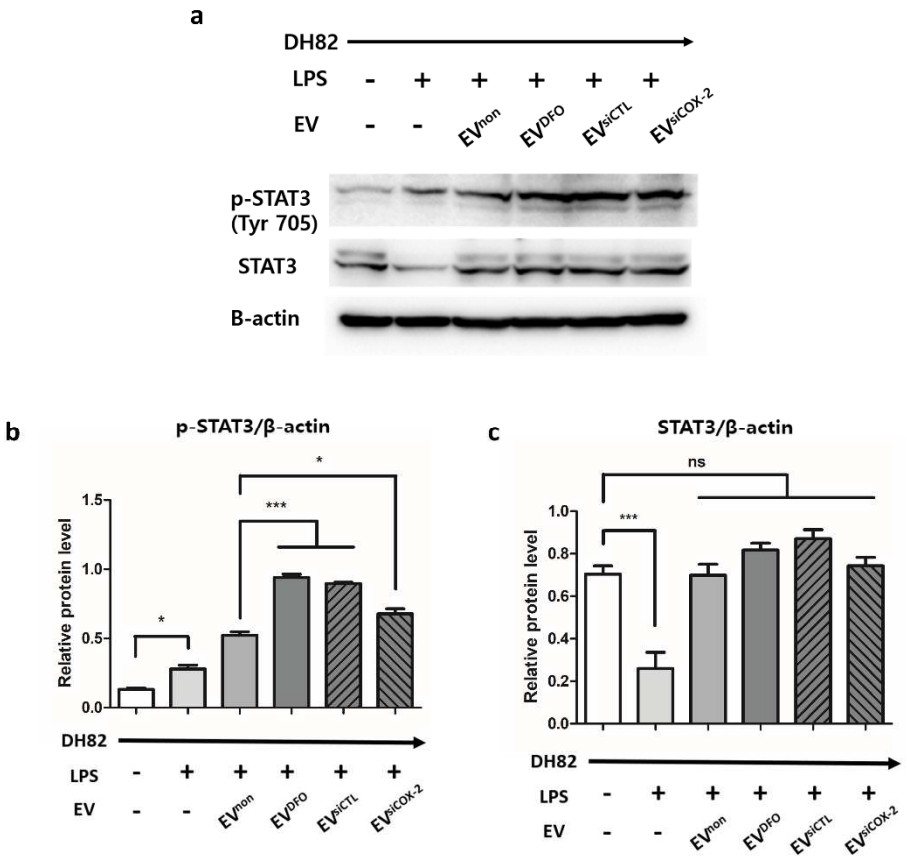

Figure 19. The effect of DFO preconditioned EV in DH82. (a-c) Protein levels of STAT3 and p-STAT3 in DH82 treated with EVs was measured by western blotting to evaluate the effect of DFO preconditioned EVs. In the all EV treated groups, p-STAT3 (Tyr 705) was increased. Compared to EV^{non} treated group, p-STAT3 is much more increased in EV^{DFO} treated group, but similar in $EV^{siCOX\text{-}2}$ treated group. Results are shown as means ± standard deviation. $^{*}p<0.05$, $^{***}p<0.001$; ns, not significant. EV^{non}, EV derived from non- preconditioned MSC; EV^{DFO}, EV derived from DFO preconditioned MSC; EV^{siCTL}, EV derived from MSC treated with DFO and control siRNA; $EV^{siCOX\text{-}2}$, EV derived from MSC treated with DFO and siCOX-2.

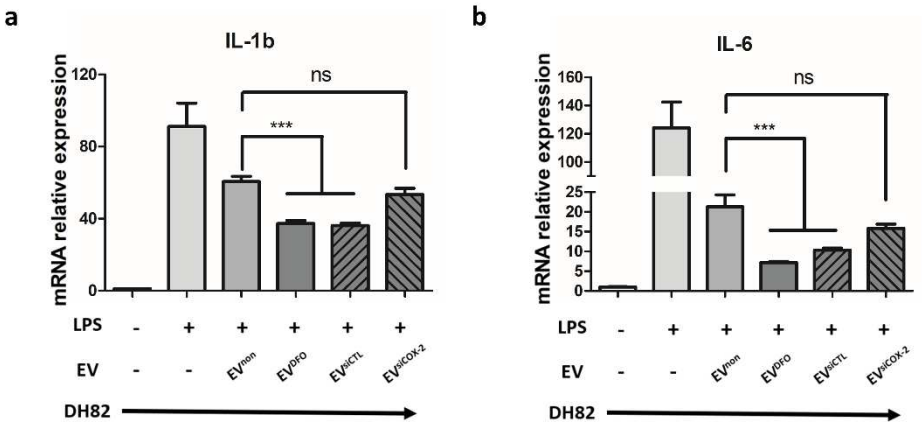

Figure 20. Analyzing RNA expression of DH82 treated with EV and EV^{DFO} by qRT-PCR. (a, b) The mRNA level of IL-1b and IL-6, which is the marker of M1 macrophage phase, was decreased in EV treated groups and significantly decreased in EV^{DFO} treated group compared to EV^{non} treated group. Conversely, the mRNA levels were similar in $EV^{siCOX\text{-}2}$ treated group and EV^{non} treated group. $^{***}p<0.001$; ns, not significant. EV^{non}, EV derived from non- preconditioned MSC; EV^{DFO}, EV derived from DFO preconditioned MSC; EV^{siCTL}, EV derived from MSC treated with DFO and control siRNA; $EV^{siCOX\text{-}2}$, EV derived from MSC treated with DFO and siCOX-2.

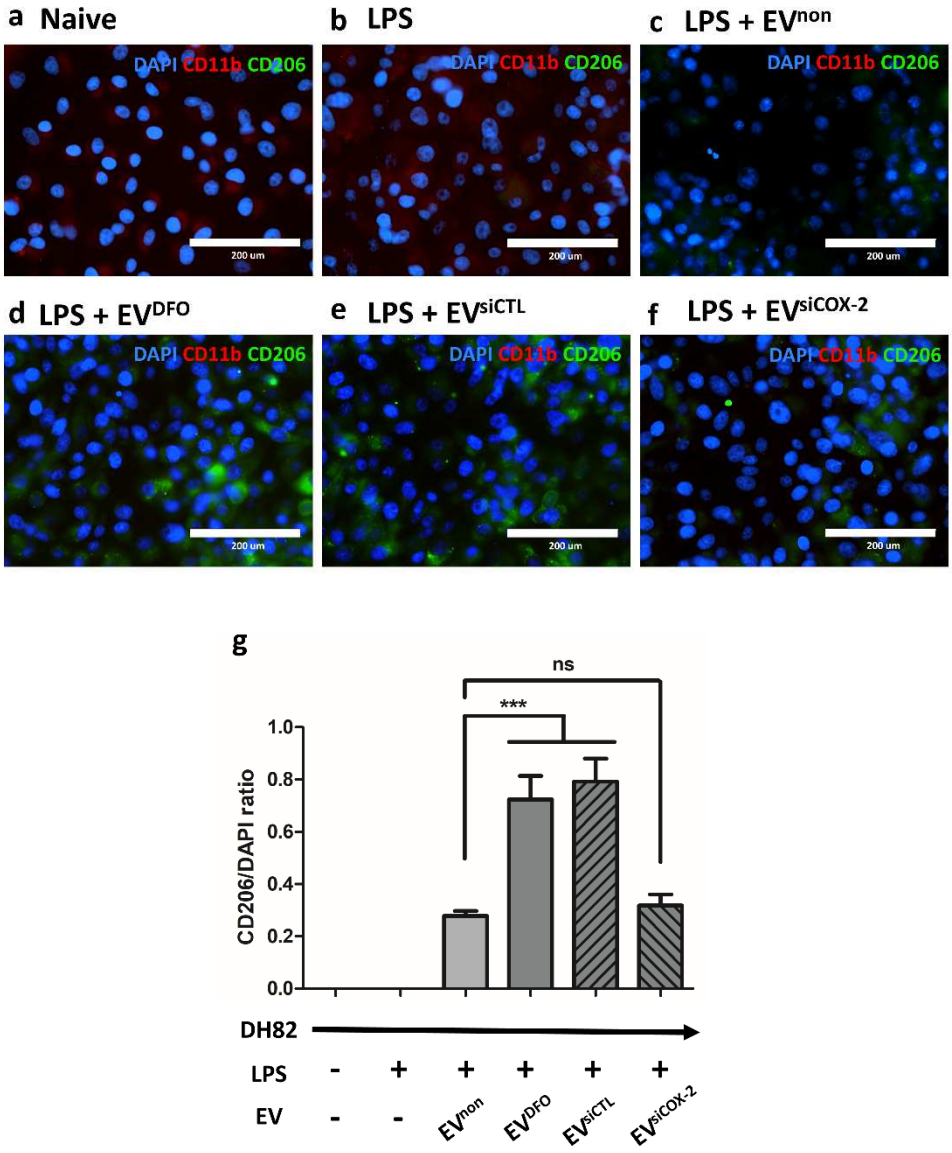

Figure 21. Analyzing protein expression of DH82 treated with EV and EV^{DFO} by immunofluorescence staining. (a-f) CD11b, which is the surface marker of macrophage, was analyzed by immunofluorescence. CD206, which is the surface marker of M2 macrophage phase, was analyzed by immunofluorescence. **(c-f)** In the EV treated groups, CD 206 with green fluorescence is increased and **(d,e)** especially more increased in EV^{DFO} group.

(f) In the $EV^{siCOX\text{-}2}$ treated group, CD206 is also increased, but not much compared to EV^{DFO} group. **(g)** The ratio of CD206/DAPI. Results are shown as means ± standard deviation. $^{***}p<0.001$; ns, not significant. EV^{non}, EV derived from non- preconditioned MSC; EV^{DFO}, EV derived from DFO preconditioned MSC; EV^{siCTL}, EV derived from MSC treated with DFO and control siRNA; $EV^{siCOX\text{-}2}$, EV derived from MSC treated with DFO and siCOX-2.

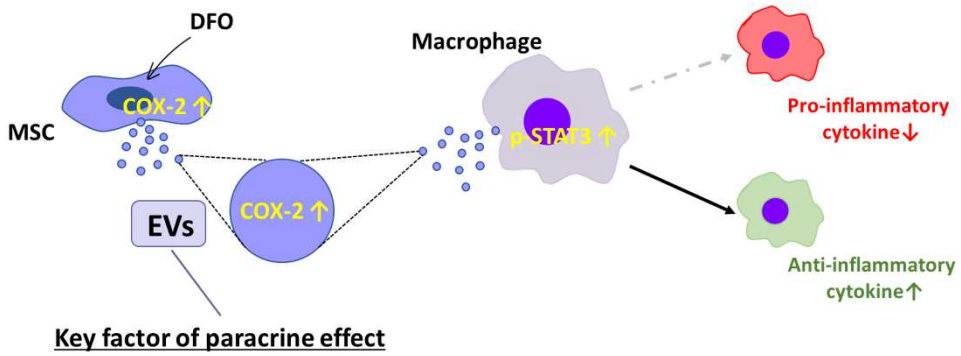

Figure 22. Schematic diagram of the effect of EV^{DFO} to macrophage and molecular changes in macrophage. Preconditioning with DFO affected COX-2 in cAT-MSCs and functioned as anti-inflammatory molecules. EV^{DFO} contained COX-2 protein reflecting changes of MSC^{DFO} and could deliver COX-2 to macrophage, and might lead to M2 polarization by activating the phosphorylation of STAT3. Through this mechanism could EV^{DFO} effectively reprogram macrophage polarization into M2 phase via protein delivery system. MSC, mesenchymal stem cell; DFO, deferoxamine; EV, extracellular vesicle.

Chapter III.

Deferoxamine-preconditioned cAT-MSC-derived Extracellular vesicles alleviate inflammation in an EAE mouse model through STAT3 regulation

1. Introduction

Multiple sclerosis (MS) is a severe autoimmune disease affecting the central nervous system (CNS) (Dobson and Giovannoni 2019). The experimental autoimmune encephalomyelitis (EAE) animal model is a representative model in MS research, and its clinical and pathological features are similar to those of patients with MS (Constantinescu et al., 2011). Although various treatments have been studied for MS and autoimmune diseases, current therapeutic strategies have limitations, and research on new strategies is needed (Hauser and Cree 2020). In the EAE model, activated T cells with the myelin oligodendrocyte glycoprotein$_{35-55}$ (MOG$_{35-55}$) peptide fragment target the CNS and trigger the infiltration of immune cells (Kurschus 2015). In the early stages of the inflammatory process, microglia/macrophages are transformed into the M1 type and release proinflammatory cytokines, which induce neuroinflammation and demyelination (Chu et al., 2018). Thus, modulating macrophages and T cells into the anti-inflammatory (M2) phenotype is the main treatment strategy in the EAE model (Loma and Heyman 2011, Vogel et al., 2013). One of the

target factors for treatment in autoimmunity is STAT3, and several studies about autoimmunity have reported that STAT3 is involved in regulating T cells (Liu et al., 2008, Yu et al., 2012, Aqel et al., 2021). In inflammatory bowel disease, STAT3 was revealed that key factor in modulating the balance of T helper 17 and regulatory T (Treg) cells. As promoting T cell proliferation, STAT3 contributed to chronic inflammation (Durant et al., 2010).

EVs in MSCs play an important role in transmitting molecules between cells (Raposo and Stahl 2019). They are released from cell membranes and contain proteins, metabolites, and nucleic acids, and several studies have shown that cells are modified by factors transmitted through EVs (Konoshenko et al., 2018). Using the transmitting function of EVs, many researchers have reported that MSC-derived EVs could be a therapeutic strategy for regulating immune cells (Robbins and Morelli 2014). MSC-derived EVs showed immunomodulation of neutrophils, macrophages, and T cells into an anti-inflammatory phenotype, alleviating clinical signs in a mouse inflammation model (Liu et al., 2015, Li et al., 2016, Lo Sicco et al., 2017).

To enhance their therapeutic effect, research is being conducted to improve the function of EVs (Lu et al., 2018). Hypoxic stimulation of MSCs is one strategy for improving the function of MSC-derived EVs (Bister et al., 2020). As hypoxic conditions are evoked in MSCs, HIF-1α accumulates in the nucleus of cells, and the cytokine levels under HIF-1α signaling are

increased (Ejtehadifar et al., 2015). These cytokines are closely related to inflammation, proliferation, and angiogenesis (Zhang et al., 2012, Madrigal et al., 2014). To stably induce hypoxic conditions, the drug DFO was used in MSCs. DFO is a hypoxia-mimetic agent that inhibits the hydroxylation of HIF-1α by chelating the iron necessary for prolyl-4 hydroxylase (Tchanque-Fossuo et al., 2017). A previous study revealed that EV^{DFO} induce macrophages into an anti-inflammatory state, which was related to the STAT3 pathway in vitro (Park et al., 2021).

In this chapter, it was assessed whether EV^{DFO} could alleviate neurological signs of the EAE model more effectively than non-preconditioned EV treatment. Also, the immunomodulation effect of EV^{DFO} through STAT3 pathway was evaluated in splenocyte. Furthermore, to determine the impact of EVs on overall immunity, this study investigated the effect of EV^{DFO} to T cells in peripheral blood mononuclear cells (PBMC) which is an important immune cell to regulate autoimmunity associated with macrophage and also revealed the effect of EV^{DFO} with STAT3 pathway in innate immune cell. The current findings suggest the EV^{DFO} has potency to regulate STAT3 pathway and could be a new therapeutic strategy for CNS autoimmune disease.

2. Material and Methods

2.1. Cell isolation and culture

Canine adipose tissue was obtained using a protocol approved by the Institutional Animal Care and Use Committee of Seoul National University (protocol no. SNU-180621-27, SNU-220818-2). Canine adipose tissue was obtained from a healthy dog during routine spaying surgery. The tissues were cut into small pieces and digested with collagenase type IA for 1 h at 37°C (1 mg/mL; Sigma-Aldrich, MO). After digestion, the cell pellet was obtained by centrifugation at 1200 × *g* for 5 min to remove debris and filtered through a 70-μm Falcon cell strainer (Fisher Scientific, MA). The cells were incubated in DMEM (Welgene, Korea) with 10% FBS (PAN Biotech, Germany) at 37°C in a humidified atmosphere containing 5% CO_2.

The cAT-MSCs were characterized by detecting stem cell markers, namely, FITC-conjugated CD29, PE-conjugated CD34, FITC-conjugated CD44, FITC-conjugated CD45, and PE-conjugated CD9, using flow cytometry on a FACS Aria II installed at the National Center for Inter-University Research Facilities at Seoul National University. The cells were differentiated into adipocytes, osteocytes, and chondrocytes to confirm their multilineage features. After characterization, cAT-MSCs at passages 3–4 were used in subsequent experiments. When cAT-MSCs were approximately 70% confluent, 100 μM DFO was added, followed by incubation for 48 h.

2.2. Isolation and characterization of EVs from cAT-MSCs

The cAT-MSCs were cultured for 48 h in DMEM (Welgene, Korea) supplemented with 10% exosome-depleted FBS (Thermo Fischer Scientific,

MA). The culture media were collected and centrifuged at 3000 × *g* for 20 min to remove cells and debris. Each supernatant was transferred to a fresh tube, and ExoQuick-CG (System Biosciences, CA) was added according to the manufacturer's instructions.

Isolated EVs were characterized using protein markers against CD63 (Novus Biologicals, CO) and CD9 (GeneTex, CA). The morphology of the EVs was identified using transmission electron microscopy. Briefly, the EV suspension (10 μL) was placed on a 300-mesh formvar/carbon-coated electron microscopy grid and stained with uranyl acetate. EVs were observed under a transmission electron microscope (LIBRA 120; Carl Zeiss, Oberkochen, Germany) at 120 kV. The size of the EV particles was measured using a zeta potential and particle size analyzer (ELSZ-1000ZS, Otsuka Electronics, Osaka, Japan).

2.3. EAE induction and therapy

Animal experimental procedures were approved by the Institutional Animal Care and Use Committee of Seoul National University, and all protocols were approved by the relevant guidelines (protocol no. SNU-220328-11). The EAE mouse model was induced in six-week-old female C57BL/6 mice, and eight mice were used in each group. Mice were immunized with 200 μg of MOG_{35-55} (Prospecbio, Israel) emulsified with 400 μg of complete Freund's adjuvant (CFA; Sigma-Aldrich, MO). The emulsification was injected into both flanks of each mouse. Subsequently, 200

ng of pertussis toxin (Sigma-Aldrich, MO) was injected intraperitoneally on days 0 and 2.

From day 9, 10 μg of EVs was intranasally injected every 24 h for 14 days. All mice were weighed daily and scored according to clinical signs of EAE. Their scores were evaluated using a scale ranging from 0 to 5, using the following system: grade 0, no obvious clinical symptoms; grade 0.5, partial tail paralysis; grade 1, tail paralysis or waddling gait; grade 1.5, partial tail paralysis and waddling gait; grade 2, tail paralysis and waddling gait; grade 2.5, partial limb paralysis; grade 3, paralysis of one limb; grade 3.5, paralysis of one limb and partial paralysis of another; grade 4, paralysis of two limbs; grade 4.5, moribund state; and grade 5, death.

2.4. Histological analysis

Hematoxylin and eosin (H&E) staining was used to evaluate the degree of accumulation of inflammatory cells, and Luxol Fast Blue (LFB) staining was used to evaluate demyelination. On day 25 post-EAE induction, the mice were euthanized by exposure to CO_2, and the spleen, brain, and spinal cord were removed from all mice. Paraffin-embedded spinal cords were prepared, and 5-μm sections of each sample were prepared and used for staining. The analysis software (CaseViewer) calculated delineated areas automatically. Cell counting was also performed with CaseViewer (Version 1.4.0.50094 and 2.0, 3DHISTECH Ltd, Hungary). Cell counting was performed with 20 x and 40 x. For semiquantitative assessment of the extent

of inflammation in the spinal cord, inflammation scores was determined as follows: 0, no inflammation; 1, cellular infiltration only in the perivascular areas and meninges; 2, mild cellular infiltration (less than one third part of the white matter is infiltrated with inflammatory cells); 3, moderate cellular infiltration (more than one third part of the white matter is infiltrated with inflammatory cells); and 4, infiltration of inflammatory cells are observed in the whole white matter referring to a scoring system described previously (Okuda et al., 2002, DaSilva and Yong 2009). The degree of demyelination was determined as a percentage of demyelinated area in comparison to total area of white matter in sections.

2.5. Immunohistochemistry analysis

Paraffin-embedded spinal cord sections were deparaffinized and rehydrated with ethyl alcohol, and antigen retrieval was performed in 10 mM citrate buffer. The sections were then washed with DPBS (Welgene, Korea) and blocked with a blocking buffer containing 1% bovine serum albumin and 0.1% Tween 20 for 30 min. After the blocking procedure, the sections were incubated overnight at 4℃ with mouse monoclonal PE-conjugated anti-CD11b (1:100; BioLegend, CA), mouse monoclonal FITC-conjugated anti-CD206 (1:100; BioLegend, CA), and mouse monoclonal FITC-conjugated anti-Foxp3 (1:100; eBioscience, CA). All samples were mounted with Vectashield mounting medium containing DAPI (Vector Laboratories, CA). Samples were observed under an EVOS FL microscope (Life Technologies,

Darmstadt, Germany).

2.6. RNA extraction, cDNA synthesis, and real-time PCR

Total RNA was extracted from cells or tissues using an Easy-Blue RNA extraction kit (iNtRON Biotechnology, Korea) according to the manufacturer's instructions. cDNA was synthesized using the Cell Script All-in-One 5X First Strand cDNA Synthesis Master Mix (Cell Safe, Korea). The samples were analyzed using AMPIGENE qPCR Green Mix Hi-ROX with SYBR Green dye (Enzo Life Sciences, NY) and 400 nM forward and reverse primers (Bionics, Korea) in a qRT-PCR thermal cycler. The expression level of each gene was normalized to that of GAPDH, and the relative expression was calculated against the contrasting control group. Primer sequences used in this study are listed in Table 3.

2.7. Protein extraction and western blotting

Protein samples were obtained from preconditioned cAT-MSC-derived EVs, mouse splenocytes, and mouse brains using a Pro-Prep protein extraction solution (Intron Biotechnology, Korea). The concentration of protein samples was analyzed using a DC Protein Assay Kit (Bio-Rad, CA). Nuclear proteins were isolated using the Cell Fractionation Kit Standard (Abcam, MA). For western blot assays, 25 μg of protein was loaded and separated using SDS-PAGE. SDS-PAGE bands were transferred to polyvinylidene difluoride membranes (EMD Millipore, MA), which were

then blocked with 5% non-fat dry milk and Tris-buffered saline. Membranes were incubated with primary antibodies against COX-2 (1:1000; Santa Cruz Biotechnology, TX), HIF-1α (1:500; LifeSpan BioSciences, WA), STAT3 (1:500, LifeSpan BioSciences, WA), pSTAT3 (Tyr705) (1:500, LifeSpan BioSciences, WA), lamin A (1:500; Santa Cruz Biotechnology, TX), and β-actin (1:1000; Santa Cruz Biotechnology, TX) at 4°C overnight. The membranes were subsequently incubated with the appropriate secondary antibody for 1 h. Using a chemiluminescence detection kit (Advansta, CA), immunoreactive bands were detected and normalized to the housekeeping protein β-actin.

2.8. Isolated splenocytes and activation

EAE mice were euthanized on day 25 after induction. Splenocytes were isolated using a 100-μm cell strainer (SPL Life Science, Korea). Red blood cells (RBCs) were eliminated using RBC lysis buffer, and splenocytes were cultured in Roswell Park Memorial Institute-1640 (RPMI-1640; Welgene, Korea) supplemented with 10% FBS (Gibco, MA), 100 units/mL penicillin G (Sigma-Aldrich, MO), and 100 μg/mL streptomycin (Sigma-Aldrich, MO). To evaluate antigen-specific reactions, splenocytes were activated using 10 μg/mL MOG_{35-55} (Prospecbio, Israel) for 48 h.

2.9. Cytokine assay

A cell culture medium was used to measure cytokine production from

activated splenocytes. The concentrations of IL-1β and IL-6 were measured using commercial ELISA kits for mouse IL-1β (Abbkine, CA) and mouse IL-6 (Invitrogen, MA) according to the manufacturer's instructions.

2.10. Flow cytometry analysis of the Treg cell population

To measure the changes in the Treg cell population after EV treatment, mouse splenocytes were stained with a Treg Detection Kit (CD4/CD25/FoxP3) (Miltenyi Biotech, Germany) according to the manufacturer's instructions, and the Treg population was analyzed using flow cytometry. Briefly, isolated splenocytes from the mice (1×10^6) were washed with staining buffer and stained with the appropriate concentration of specific monoclonal antibodies, FITC-conjugated anti-CD4 and PE-conjugated anti-CD25 antibodies, incubated with the cells at 4°C for 30 min, followed by washing steps. Cells were then fixed and permeabilized for intracellular staining of Foxp3 using an APC-conjugated anti-Foxp3 antibody. The size and granularity of the cells were analyzed via flow cytometry using the side and forward scatter signals. First, CD4+ lymphocytes were gated, among which CD25+FoxP3+ cells were selected as Treg cells. The results were analyzed using FlowJo™ 10.8.1 software.

2.11. Obtaining PBMCs and treatment with EVs

PBMCs were obtained from the debris of blood donations, which were collected into sterile CPDA packs and centrifuged to separate the red

blood cells and plasma. Separated plasma containing the buffy coat was collected and diluted with an equal volume of PBS. The diluted samples were layered over Ficoll-Paque PLUS (GE Healthcare Life Sciences, NJ) in a conical tube. After centrifugation at 400 × *g* for 30 min, the buffy coat layer was separated by pipetting. The collected buffy coat-layer sample was treated with the RBC lysis buffer and centrifuged again at 400 × *g* for 10 min. PBMCs were seeded at a density of 1×10^6 cells/well in six-well plates (SPL Life Science, Korea), resuspended in DMEM (Welgene, Korea) containing 10% FBS (PAN Biotech, Germany), 100 units/mL penicillin G (Sigma-Aldrich, MO), and 100 μg/mL streptomycin (Sigma-Aldrich, MO). Then, PBMC was stimulated with 5 μg/mL concanavalin A (Con A; Sigma-Aldrich, MO) for 6 h before further experiments. After stimulation, the medium was removed and replaced with a medium containing EVs or EV^{DFO} for 24 h.

2.12. Statistical analyses

Data are shown as the means ± standard deviation. Mean values from different groups were compared using the Mann-Whitney t-test and one-way analysis of variance using GraphPad Prism v.7.01 software (GraphPad Software, CA). Statistical significance was set at $p<0.05$.

3. Results

3.1. Characterization of cAT-MSC-derived EVs and elevation of protein levels

in MSC^{DFO}

The cAT-MSCs were characterized for surface markers using flow cytometry and differentiation (Fig. 23a, b). EVs were extracted from cAT-MSC-culture media. CD63 and CD9 were detected as positive EV markers, and β-actin was used as a negative marker in western blotting (Fig. 24a). The EVs had a round shape with diameters ranging from 100 to 200 nm, per the electron microscope analysis (Fig. 24b). Using particle-size analysis, the diameters of EVs were confirmed to be similar in size by electron microscopic analysis (Fig. 24c).

Considering previous studies,100 μM DFO was chosen to treat in cAT-MSCs (Park et al., 2020, Park et al., 2021). To confirm hypoxia preconditioning with DFO, HIF-1α was detected in MSC^{DFO} using western blotting (Fig. 25a). The protein expression of STAT3 was decreased in MSC^{DFO}; however, pSTAT3 expression was increased in MSC^{DFO} compared to non-preconditioned MSCs. The expression of COX-2 also increased in MSC^{DFO} compared to non-preconditioned MSCs (Fig. 25b). COX-2 protein expression was also measured in 25 μg of EVs and was found to be higher in EV^{DFO} than in non-preconditioned EVs (Fig. 25c).

3.2. cAT-MSC-derived EVs and EV^{DFO} alleviated clinical signs and histological changes in the EAE mouse model

Clinical signs were evaluated daily, and the onset of neurological signs occurred on day 7 and peaked on day 21 (Fig. 26). The day of onset was similar to that of the EAE control group as well as the EAE+EV and EV^{DFO} groups. In the EV and EV^{DFO} groups, clinical scores were significantly reduced compared to EAE group, and clinical signs were milder in the EV^{DFO} group. No adverse effects related to the intranasal injections were observed (Fig. 27).

On day 25 post-EAE induction, mice were euthanized, and the spinal cord was isolated with DPBS. To evaluate inflammatory cell infiltration, paraffinized spinal cord sections were stained with H&E. In the EAE group, cells with nuclei, which were suspected to be inflammatory cells, were significantly infiltrated, and in the EAE+EV^{DFO} groups, the number of infiltrated cells was lower than that in the EAE group (Fig. 28). To evaluate demyelination of the spinal cord, paraffinized sections were stained with LFB. In the EAE group, the demyelination area increased significantly; in the EAE+EV and EV^{DFO} groups, attenuated demyelination was observed compared to the EAE group (Fig. 28).

The phenotype of macrophages infiltrated in the spinal cord was evaluated using immunohistochemistry. In the EAE group, the expression of PE-CD11b increased; however, in the EAE+EV and EV^{DFO} groups, the expression of PE-CD11b decreased, and the expression of FITC-CD206 increased (Fig. 29). To evaluate the population of Treg cells infiltrating the

spinal cord, Foxp3 was detected by immunohistochemical analysis. In the EV^{DFO} group, the expression of FITC-Foxp3 increased significantly (Fig. 29).

3.3. Cytokine and protein level changes in the spinal cord and brain of EV-treated mice

The expression of cytokines was analyzed in the spinal cord and brain of all mice. The expression of CD206, which is related to the M2-type macrophages, was significantly elevated in the EAE+EV^{DFO} group; in the EAE+EV group, the expression of CD206 did not increase (Fig. 30a). The expression of iNOS, which is related to the M1-type macrophages, was significantly elevated in the EAE group but significantly lowered in the EAE+EV and EV^{DFO} groups. No significant difference was observed between the EV and EV^{DFO} groups (Fig. 30b). The expression of Foxp3, which is related to Treg cells, was significantly elevated in the EAE+EV and EV^{DFO} groups compared to that in the naïve group; however, only the expression in the EAE+EV^{DFO} group was significantly elevated compared to that in the EAE group (Fig. 30c). The levels of TNF-α, IFN-γ, and IL-1β, cytokines related to inflammation, were significantly elevated in the EAE group; however, the level of the inflammatory cytokine IL-6 did not increase. In the EAE+EV and EV^{DFO} groups, the expression of these cytokines was significantly lower compared to the EAE group; in particular, the group treated with EV^{DFO} showed a significant reduction in TNF-α and IL-6 levels

compared to the EV-treated group (Fig. 30d-g).

To evaluate the relationship between STAT3 and EV treatment, the expression of STAT3 was evaluated in mouse brain tissue. The expression of STAT3 was lower in the EAE+EV and EV^{DFO} groups than in the EAE group. pSTAT3 expression was significantly lower in the EAE group compared to the naïve group, while its expression was higher in the EAE+EV^{DFO} group than in the EAE group (Fig. 31).

3.4. EVs altered the Treg cell population in the EAE mouse model

On day 25 post-EAE induction, the spleens were dissected and isolated as splenocytes after RBC lysis. To evaluate the Treg cell population, splenocytes were bound to CD4, CD25, and Foxp3 antibodies, and CD4+CD25+Foxp3+ cells were evaluated as Treg cells. The percentage of Treg cells in the EAE group was significantly reduced. In contrast, in the EV and EV^{DFO} groups, the Treg population increased significantly, and the EV^{DFO} group showed a significant increase in the Treg population compared with the EV-treated group (Fig. 32).

3.5. Cytokine and protein level changes in the spleen in EV-treated mice

The expression levels of inflammatory cytokines were also evaluated. The expression of CD206 increased significantly in the EAE+EV and EV^{DFO} groups (Fig. 33a). The expression of TNF-α did not increase in the EAE and EAE+EV groups; however, in the EAE+EV^{DFO} group, the expression was significantly lower compared to that in the EAE group (Fig. 33c). IFN-γ expression increased significantly in the EAE group, and there was no significant difference between the EAE and EAE+EV groups. However, in the EAE+EV^{DFO} group, the expression of IFN-γ was significantly lower than that in the EAE and EAE+EV groups (Fig. 33d).

The culture media from MOG_{35-55}-activated splenocytes were obtained, and the inflammatory cytokines were evaluated. IL-1β and IL-6 levels increased significantly in the EAE group. However, in the EAE+EV and EV^{DFO} groups, levels of these cytokines were reduced compared to those in the EAE group (Fig. 34).

To evaluate the relationship between STAT3 and EV treatment, STAT3 levels was assessed in mouse splenocytes. The expression levels of STAT3 and pSTAT3 were higher in the EAE group than in the naïve group. In contrast, the expression of STAT3 and pSTAT3 decreased in the EAE+EV and EV^{DFO} groups compared to the EAE group, showing a greater decrease in the EV^{DFO} group than in the EV group (Fig. 35).

3.6. Evaluation of the effect of EVs in canine PBMCs through RNA and protein expression analyses

After stimulation of canine PBMCs with Con A, the cells were treated with EVs or EV^{DFO} for 24 h. The expression of CD4 was not significantly different between the groups (Fig. 36a). The expression of CD25 increased significantly in the Con A-stimulated groups; however, even with EV treatment, its expression did not change significantly compared to that in the Con A-stimulated group (Fig. 36b). The expression of Foxp3 increased significantly in the EV^{DFO} group compared to that in the Con A-stimulated and EV treatment groups (Fig. 36c). The expression of IL-6, TNF-α, and IFN-γ increased significantly in the Con A-stimulated group compared to that in the naïve group; however, EV^{DFO} treatment significantly decreased their expression compared to the Con A-stimulated group. In the EV group, the expression of IL-6 and IFN-γ also decreased significantly compared to that in the Con A-stimulated group; however, the expression of TNF-α did not decrease compared to the Con A-stimulated group (Fig. 36d-f).

The protein expression of pSTAT3 increased in all Con A-stimulated groups, whereas the expression of STAT3 decreased in the EV and EV^{DFO} groups. The expression of STAT3 in the EV^{DFO} group, in particular, decreased more than that in the EV group (Fig. 37).

4. Discussion

Several studies have been conducted on the immunomodulatory

function of MSCs, and their therapeutic efficacy has been actively studied in chronic inflammation and autoimmune disease (Gao et al., 2016, Li et al., 2018, Song et al., 2018). Furthermore, in previous studies, cell conditions were reflected in the contents of EVs (de Jong et al., 2012, Wen et al., 2019) and based on these results, EVs derived from MSCs have been investigated as a treatment option for inflammation (Lai et al., 2012, Katsuda et al., 2013). Pretreatment, or hypoxia treatment, is often employed to increase the therapeutic effectiveness of EVs derived from MSCs. In this study, DFO was used to induce hypoxic conditions in cAT-MSCs and identified the changes in cAT-MSC-derived EVs. Moreover, EV^{DFO} was administered by intranasally in an EAE mouse model, an autoimmune disease model used in MS research, and confirmed their therapeutic efficacy.

In this experiment, the intensity of neurological signs was significantly reduced in the EAE+EV and EAE+EV^{DFO} groups. In addition, upon histological examination, the infiltration of inflammatory cells decreased significantly, and demyelination was alleviated. Immunofluorescence staining revealed that the expression of CD206, a marker of the M2 macrophages, and Foxp3, a marker of Treg cells, increased significantly in the EV^{DFO} group compared to the EAE and EAE+EV groups. In addition, the expression of inflammatory factors, TNF-α, IFN-γ, IL-1β, and IL-6, was significantly lower in the EV^{DFO} group than that in the EAE and EAE+EV groups. Based on these results, it is assumed that EV^{DFO} modulated

macrophage into M2 type macrophages and Treg cells in the spinal cord. As immune system was modulated to anti-inflammation state, the infiltration of inflammatory cells decreased along with the expression of inflammatory factors. In a previous EAE model, demyelination was associated with inflammatory cell infiltration (Bitsch et al., 2000); therefore, demyelination also decreased as inflammatory cell infiltration was lowered by EV^{DFO} treatment in our study.

Also, the experimental changes in the spleen was evaluated in the EAE model. In the EAE group, the number of CD4+CD25+Foxp3+ Treg cells decreased significantly compared to naïve cells. In contrast, the ratio increased in the group treated with EVs or EV^{DFO}; furthermore, the increase in the number of Treg cells was relatively greater in the EAE+EV^{DFO} group than in the EAE+EV group. Thus, the EAE model showed a reduction in the number of Treg cells, which was related to the loss of immune homeostasis (Eggenhuizen et al., 2020). Otherwise, intranasally injected EVs stimulated differentiation of Treg cells; moreover, EV^{DFO} administration was more effective than EV treatment in modulating T cells. EVs also affect macrophages in spleen. The expression of CD206 increased in the EV-treated groups, and the expression of iNOS decreased in the EAE+EV^{DFO} group. Thus, EVs regulated the type of macrophage, inducing more anti-inflammatory M2 macrophages. Thus, it was confirmed that EV^{DFO} had a systemic immunomodulatory function, even though administered intranasally,

as shown in previous studies (Long et al., 2017, Guo et al., 2019).

Considering that STAT3 is an important factor in regulating immune cells in the EAE mouse model (Liu et al., 2008, Lu et al., 2020) and MSCs are closely related to the phosphorylation of the STAT3 pathway (He et al., 2018, Xia et al., 2020), the changes of STAT3 expression was confirmed in splenocyte and brain with treatment. In the spleen, the protein expression of STAT3 and pSTAT3 increased in the EAE groups compared to the naïve group. However, when treated with EVs, STAT3 expression decreased compared to the EAE group, while pSTAT3 expression was similar between the EV-treated and EAE group. STAT3 expression decreased more in the EAE+EV^{DFO} group than in the EAE+EV group. Thus, it could be estimated that EV suppressed STAT3 expression, which was related to the activation of Treg cells. Moreover, EV^{DFO} treatment was more potent than EV in suppressing STAT3 in splenocytes. In the brain, the protein expression of STAT3 in the EAE group was similar to that in the naïve group; however, STAT3 and pSTAT3 levels were lower in the EAE+EV^{DFO} group than in the EAE group.

STAT3 and pSTAT3 have important roles in neuronal inflammation. In acquired immune cells, such as T cells, suppressing the STAT3 pathway has an anti-inflammatory effect (Atreya et al., 2000, Sugimoto 2008). In brain inflammation, STAT3 suppression inhibits astrogliogenesis and promotes neurogenesis (Chen et al., 2013). Thus, EVs have the potential to regulate STAT3 in Treg cells and brain cells as well as alleviate brain inflammation.

Moreover, EV^{DFO} treatment was more efficient than EV in regulating T cells and reducing inflammation.

To confirm the effect of EVs and EV^{DFO} on T cells, PBMCs was obtained from healthy dogs and stimulated them with Con A. After treatment with EVs or EV^{DFO}, the levels of inflammatory factors were reduced compared to those in Con A-stimulated PBMCs. Inflammatory factor levels decreased more significantly in the EV^{DFO} group compared to the EV-treated group. The expression of CD4/CD25/Foxp3 was measured to examine the differentiation of T cells. Interestingly, there was no change in CD4 expression but CD25 expression increased in all groups stimulated by Con A. CD25 is not a specific marker of Treg cells, and its expression may have increased due to external stimulation (Hosono et al., 2003). As the expression of Foxp3 increased significantly, the Treg cell population increased in the EV^{DFO} group (Campbell and Koch 2011).

In PBMCs, the changes in STAT3 expression with EV and EV^{DFO} treatment were confirmed. When stimulated by Con A, expression of both STAT3 and pSTAT3 increased, but the expression of STAT3 decreased with EV and EV^{DFO} treatment, more so with EV^{DFO} treatment. Therefore, EVs may regulate T cells by suppressing STAT3, and EV^{DFO} treatment is more effective than EV treatment.

Previous studies have suggested that COX-2 and PGE2 are related to the upregulation of Foxp3+ Treg cells (Yuan et al., 2010). In the present study,

the EV^{DFO} group contained higher levels of COX-2 than the non-preconditioned EV group (Fig. 21c). Thus, COX-2 contained in the EV^{DFO} group could upregulated Foxp3+ Treg cells by affecting STAT3 expression. Another possibility is that EV^{DFO} synchronized T cells to the same state as DFO-preconditioned cAT-MSCs (Lotvall and Valadi 2007). Preconditioning with DFO in cAT-MSCs decreased the expression of STAT3; conversely, the expression of pSTAT3 increased (Fig. 21b), indicating that DFO-induced hypoxia increased STAT3 phosphorylation rather than increasing its expression (Gao et al., 2015). The expression of STAT3 and pSTAT3 in T cells treated with EV^{DFO} was similar to that in cells treated with MSC^{DFO}; therefore, EVs may perform a synchronizing function by transmitting molecules such as miRNAs.

In this study, one of limitations was that it was not clear whether other substances such as miRNA in EVs could regulate STAT3 pathway. Therefore, additional research would be required to analyze the molecules in EV and changes in EV^{DFO}. Another limitation was that since the organic relationship between macrophage and T reg with EV treatment was not analyzed in EAE mouse model, it was not revealed which cells undergo a change earlier by the influence of EV and affected to alleviate inflammation. Additional studies should be made on the relationship between innate immune and adaptive immune when affected by EV. However, this report suggests that DFO is effective in enhancing the clinical efficacy of EV and EV^{DFO} is good candidate

for cell-free therapy which has potential to alleviate CNS inflammation by intranasally. Through this study of neuroinflammatory disease mouse model, it could become a first step for EV^{DFO} as a treatment of neuroinflammatory disease in dogs or cats such as meningoencephalitis of unknown origin.

Table 3. Oligonucleotide sequences of PCR primers used when analyzing splenocyte, spinal cord and brain in EAE mouse model with EV^{DFO} treatment and analyzing PBMC with EV^{DFO} treatment

Target genes	Primers	Oligonucleotide sequences (5' → 3')	Product sizes	References
Mouse CD206	Forward	AAC GGA ATG ATT GTG TAG TTC TAG C	163	Song, WJ et al., 2018
	Reverse	TAC AGG ATC AAT AAT TTT TGG CAT T		
Mouse iNOS	Forward	GGC TGT CAG AGC CTC GTG GCT TTG G	165	*
	Reverse	CCC TCC CGA AGT TTC TGG CAG CAG C		
Mouse Foxp3	Forward	TTG GCC AGC GCC ATC TT	110	An, JH et al., 2020
	Reverse	TGC CTC CTC CAG AGA GAA GTG		
Mouse TNF-α	Forward	ACG TGG AAC TGG CAG AAG AG	100	*
	Reverse	GCC ACA AGC AGG AAT GA GA		
Mouse IFN-γ	Forward	AAC AGC TCT CCG TCC TCG TA	137	*
	Reverse	GAT CTC CCC ACT CCG GTT AT		
Mouse IL-1β	Forward	TCA CAG CAG CAC ATC AAC AA	112	*
	Reverse	TGT CCT CAT CCT GGA AGG TC		
Mouse IL-6;2	Forward	AGT TGC CTT CTT GGG ACT GA	159	*
	Reverse	TCC ACG ATT TCC CAG AGA AC		
Mouse GAPDH	Forward	AGT ATG TCG TGG AGT CTA CTG GTG T	154	Song, WJ et al., 2018
	Reverse	AGT GAG TTG TCA TAT TTC TCG TGG T		
Canine CD4	Forward	TGC TCC CAG CGG TCA CTC CT	381	An, JH et al., 2020
	Reverse	GCC CTT GCA GCA GGC GGA TA		
Canine CD25	Forward	GGC AGC TTA TCC CAC GTG CCA G	364	An, JH et al., 2020
	Reverse	ATG GGC GGC GTT TGG CTC TG		
Canine Foxp3	Forward	AGA AGC AGC GGA CAC TCA AT	199	*
	Reverse	GGC CTT TGG CTT CTC TTC TT		
Canine IL-6	Forward	GGC TAC TGC TTT CCC TAC CC	243	*
	Reverse	TGG AAG CAT CCA TCT TTT CC		
Canine TNF-α	Forward	TCA TCT TCT CGA ACC CCA AG	157	An, JH et al., 2020
	Reverse	ACC CAT CTG ACG GCA CTA TC		
Canine IFN-γ	Forward	TTC AGC TTT GCG TGA TTT TG	115	An, JH et al., 2020
	Reverse	CCG TCC GAT ACA TCT GGA TT		
Canine GAPDH	Forward	TTA ACT CTG GCA AAG TGG ATA TTG T	85	Song, WJ et al., 2018
	Reverse	GAA TCA TAC TGG AAC ATG TAC ACC A		

*Primers with asterisk in reference section were designed by own.

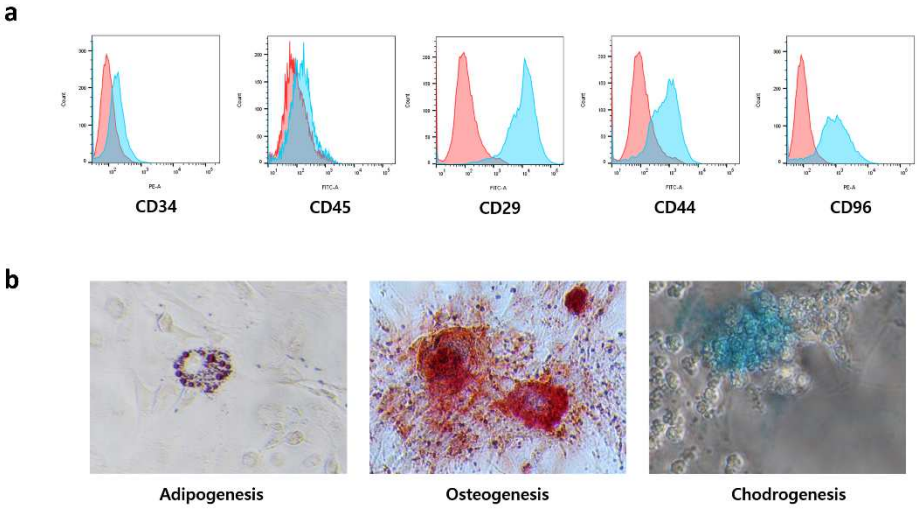

Figure 23. Characterization of canine adipose derived MSC by multilineage differentiation and immunotyping. (a) Analysis of surface markers of cAT-MSCs by flow cytometry; cAT-MSC was negative for CD34 and CD45 and positive for CD29, CD44, and CD96. **(b)** cAT-MSCs were differentiated as adipocytes, osteocytes, and chondrocytes.

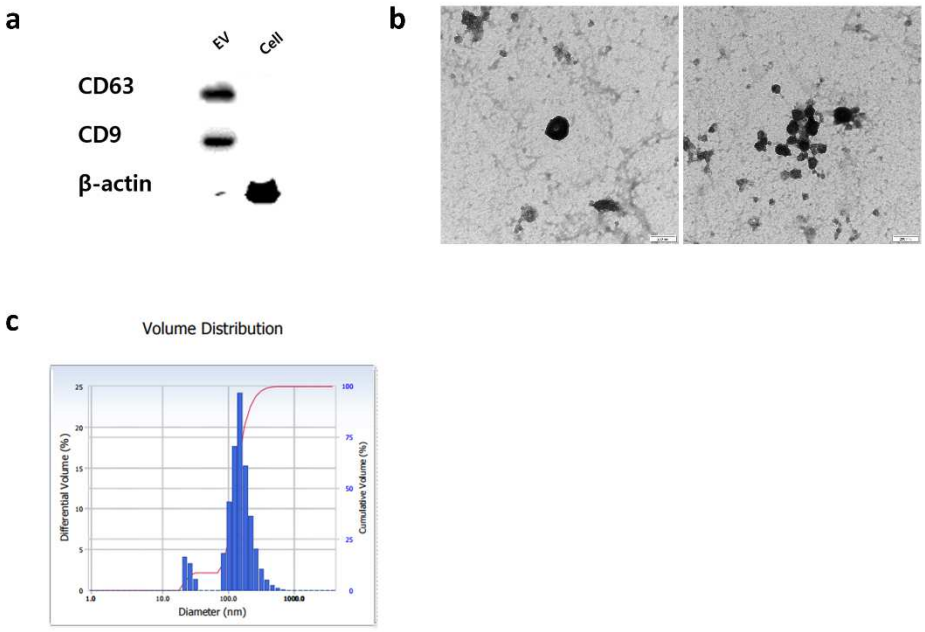

Figure 24. Characterization of EVs. (a) Analysis of EV markers by western blotting. EVs derived from cAT-MSCs were positive for CD63 and CD9 and negative for β-actin. **(b)** EVs were round in shape with diameters ranging from 100 to 200 nm in electron microscopic analysis. **(c)** The diameters of EVs were measured as 100 to 200 nm using particle-size analysis.

Figure 25. Protein expression of non-/preconditioned MSCs and EVs. (a) In MSC^{DFO}, the expression of HIF-1α was increased. **(b)** In MSC^{DF}, the expression of STAT3 decreased, while pSTAT3 (Tyr705) and COX-2 expression increased. **(c)** The expression of the COX-2 in the EV^{DFO} group as well as in the cytosols of non-/preconditioned cAT-MSCs increased compared to the EV group. MSC^{DFO}, DFO preconditioned MSC; EV^{DFO}, EV derived from DFO preconditioned MSC.

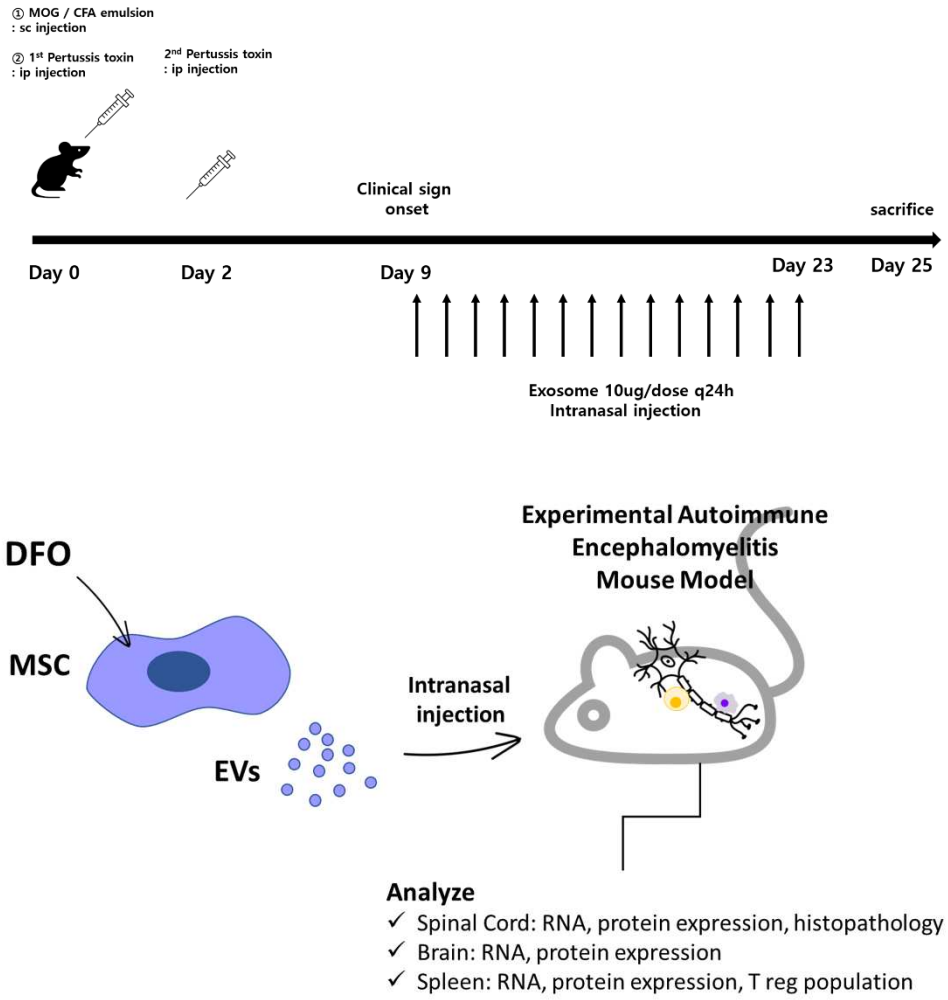

Figure 26. A schematic diagram of the in vivo experiment. The mice were immunized with 200 μg of MOG35-55 emulsified with 400 μg complete Freund's adjuvant on day 0. Subsequently, 200 ng of pertussis toxin (Sigma, USA) was injected intraperitoneally on day 0 and day 2. From day 9, 10 μg aliquot of EVs was injected intranasally every 24 h for 14 days. MSC: mesenchymal stem cell. DFO, deferoxamine; EV, extracellular vesicle.

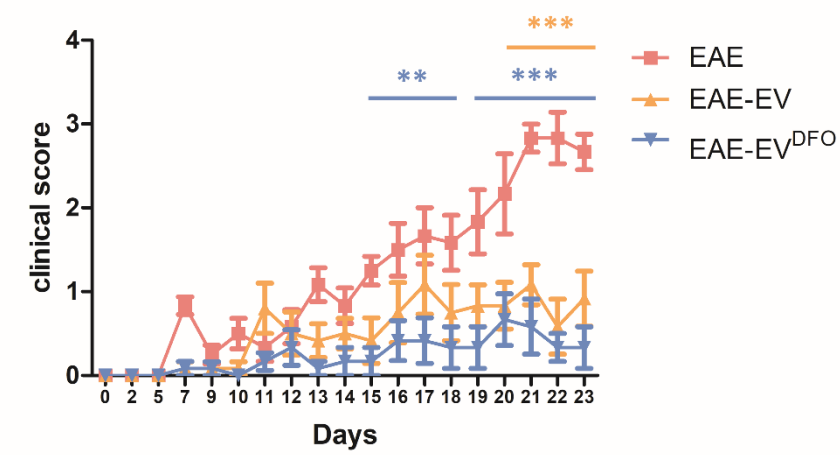

Figure 27. Clinical scores of EAE mice. The onset of neurological signs occurred on day 7 and peaked on day 21. The day of the onset in EAE mice was similar to the EAE control group and the EAE+EV and EV^{DFO} treatment groups. In mice treated with EVs and EV^{DFO}, clinical scores were significantly reduced, and the EV^{DFO}-treated group showed lower scores compared to the EV group. Additionaly, compared to the EAE group, the clinical scores of the EAE+EV group were significantly different on day 20 compared to day 23, and the clinical scores of the EAE+EV^{DFO} group were significantly different on day 15 compared to day 23. Results are shown as means ± standard deviation. $^{**}p<0.01$, $^{***}p<0.001$. EV, extracellular vesicle; EV^{DFO}, EV derived from DFO preconditioned MSC.

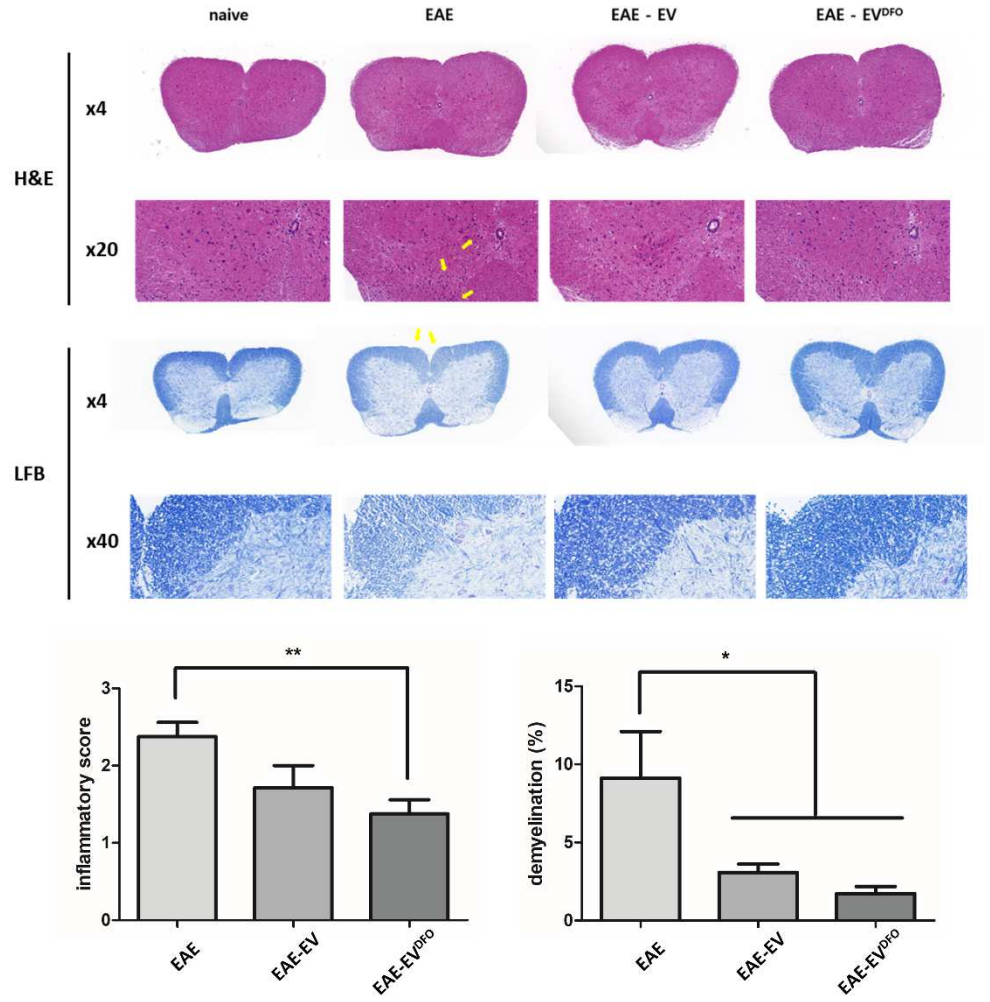

Figure 28. Histology of the spinal cord in the EAE mouse model. Infiltration of inflammatory cells was confirmed by H&E staining. Nucleated cells were significantly infiltrated in the spinal cord of the EAE mouse model (yellow arrows). In the EAE+EV^{DFO} groups, the number of infiltrated cells was reduced compared to the EAE group (upper line). LFB staining confirmed demyelination. In the EAE group, the demyelination area was significantly increased compared to the naïve group (yellow arrows). The EAE+EV and EV^{DFO} groups showed attenuated demyelination compared to

the EAE group (lower line). $^{*}p<0.05$, $^{**}p<0.01$. EV, extracellular vesicle; EV^{DFO}, EV derived from DFO preconditioned MSC.

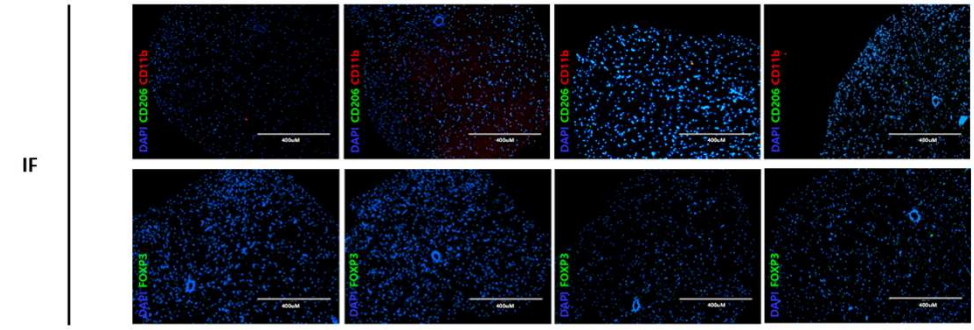

Figure 29. Immunofluorescence histology of the spinal cord in the EAE mouse model. Infiltrated cells were analyzed by immunofluorescent staining. In the EAE group, the expression of PE-CD11b increased, while FITC-CD206 expression was not observed. However, in the EAE+EV and EV^{DFO} groups, the expression of FITC-CD206 increased. Additionally, in the EV^{DFO} group, the expression of FITC-Foxp3 increased significantly compared to the EAE and EAE+EV groups.

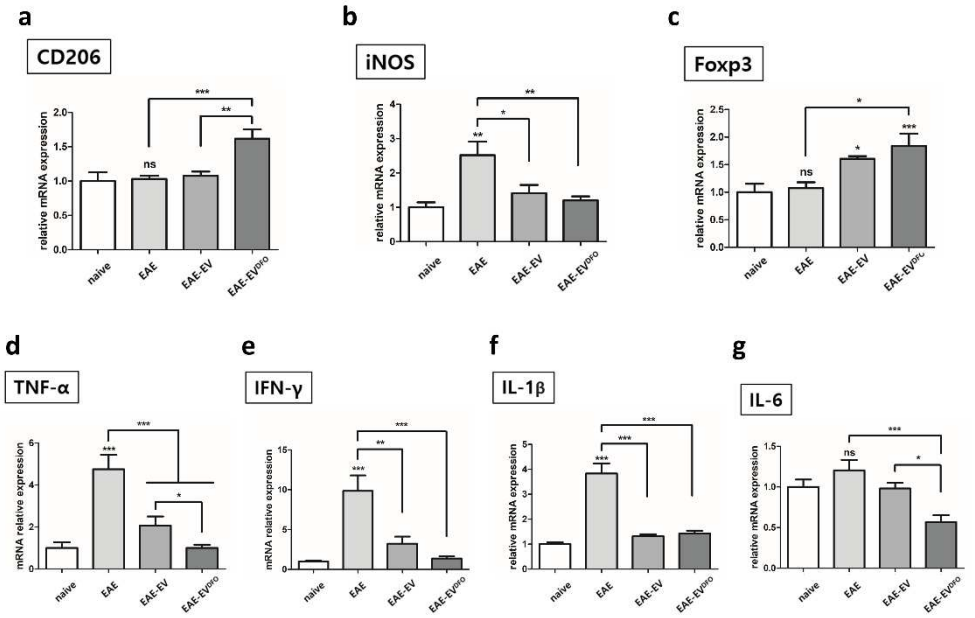

Figure 30. RNA expression of macrophage, T reg cell and proinflammatory cytokines in the spinal cord of the EAE mouse model. **(a)** The expression of CD206 increased significantly in the EAE+EV^{DFO} group compared to the EAE and EAE+EV groups. **(b)** The expression of iNOS increased significantly in the EAE group compared to the naïve group, while in the EAE+ EV and EV^{DFO} groups, the expression of iNOS decreased significantly. **(c)** The expression of Foxp3 increased significantly in the EAE+EV and EV^{DFO} groups compared to the naïve group. **(d-g)** The expression of inflammatory cytokines, TNF-α, IFN-γ, and IL-1β, increased significantly in the EAE group compared to the naïve group. In the EAE+EV and EV^{DFO} groups, the expression of TNF-α, IFN-γ, IL-1β, and IL-6 decreased significantly compared to the EAE group; the EV^{DFO}-treated group showed an especially significant reduction in TNF-α and IL-6 expression compared to the EV-treated group. Results are shown as means ± standard

deviation. $^{*}p<0.05$, $^{**}p<0.01$, $^{***}p<0.001$; ns, not significant. EV, extracellular vesicle; EV^{DFO}, EV derived from DFO preconditioned MSC.

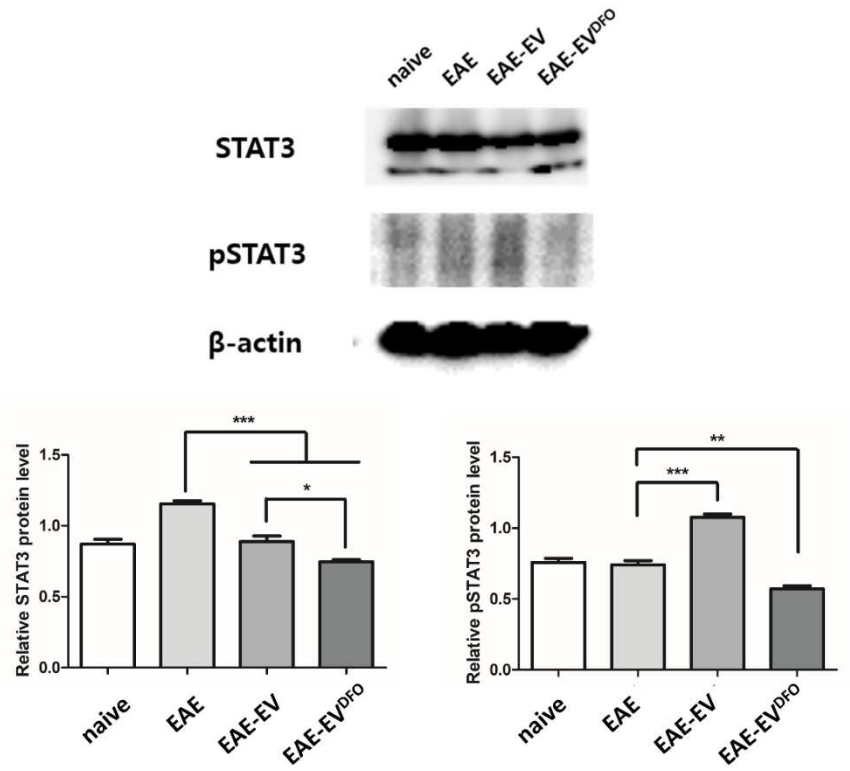

Figure 31. The expression of STAT3 decreased in the central nerve system of EAE+EV and EV^{DFO} groups compared to the EAE group. STAT3 protein expression of spinal cord and brain increased significantly in the EAE group compared to the naïve group. However, STAT3 protein expression was decreased in the EAE+EV / EV^{DFO} group compared to the EAE group. Also, in the EAE+ EV^{DFO} group, STAT3 showed more depression compared to EAE+ EV group. pSTAT3 (Tyr705) protein expression was not changed in EAE group compared to naïve. However, it was increased in EAE+EV and decreased in EAE+ EV^{DFO} group compared to EAE group. $^{*}p<0.05$, $^{**}p<0.01$, $^{***}p<0.001$. EV, extracellular vesicle; EV^{DFO}, EV derived from DFO preconditioned MSC.

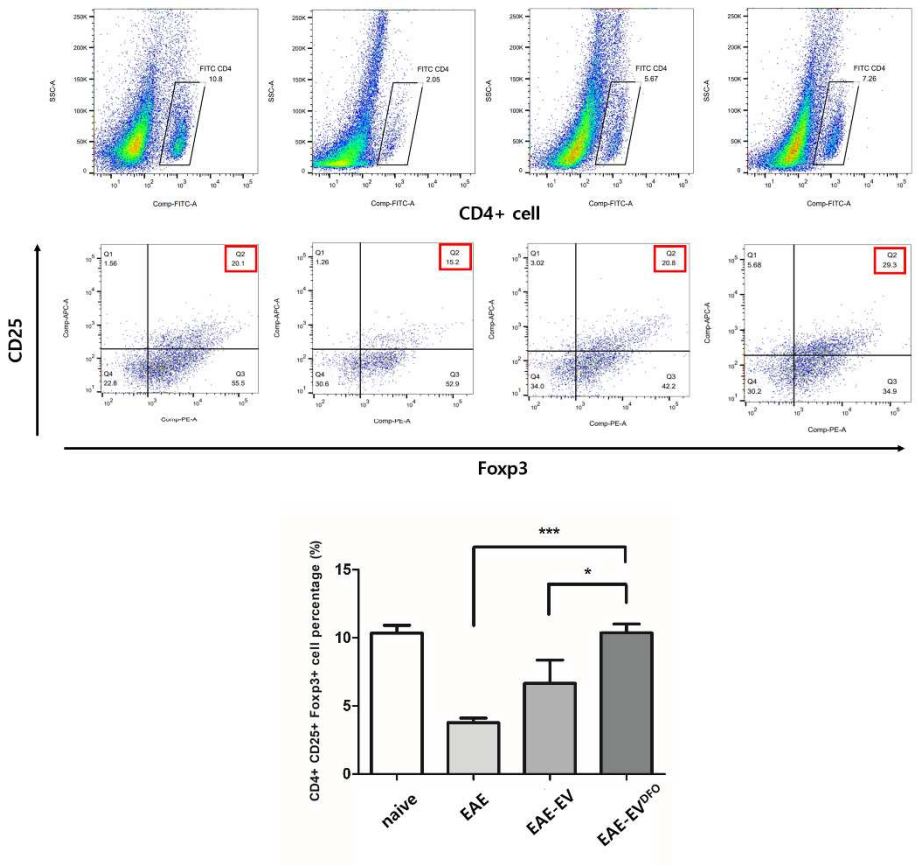

Figure 32. Analysis of CD4+CD25+Foxp3+ Treg cells in splenocytes. The numbers of CD4+ (upper line) and CD4+CD25+Foxp3+ (lower line) cells were significantly reduced in the EAE group compared to the naïve group. In the EV and EV^{DFO} groups, the Treg cell population increased significantly compared to the EAE group. Results are shown as means ± standard deviation. $^{*}p<0.05$, $^{***}p<0.001$. EV, extracellular vesicle; EV^{DFO}, EV derived from DFO preconditioned MSC.

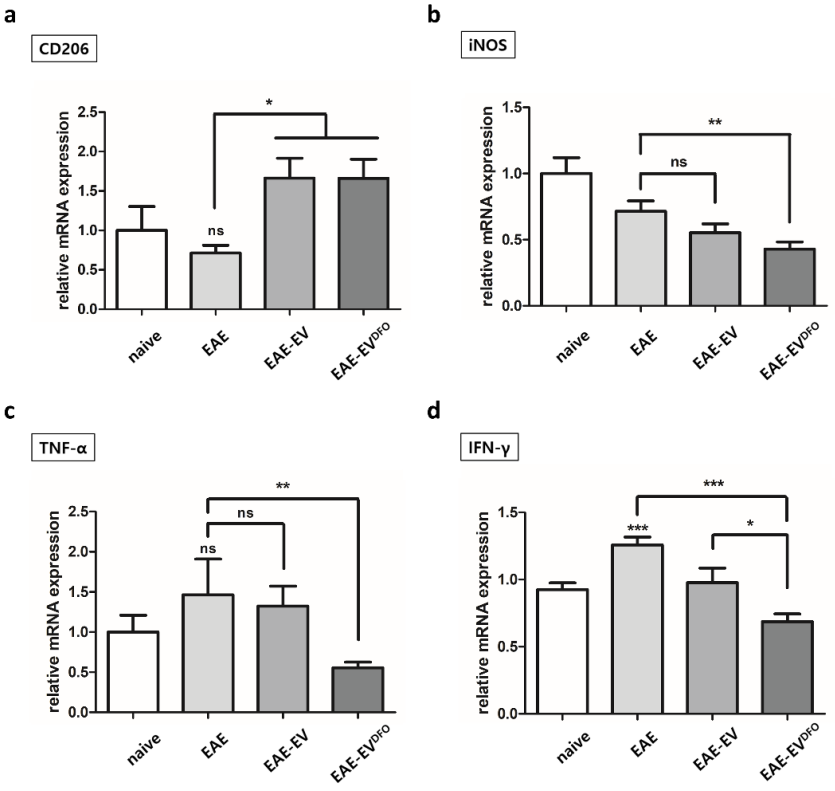

Figure 33. RNA expression of macrophage polarization and proinflammatory cytokines in splenocytes. (a) The expression of CD206 increased significantly in the EAE+EV and EV^{DFO} groups compared to the EAE group. **(b, c)** The expression levels of iNOS and TNF-α, however, were unchanged in the EAE and EAE+EV groups but decreased significantly in the $EAE+EV^{DFO}$ group. **(d)** The expression of IFN-γ increased significantly in the EAE group compared to the naïve group, while in the $EAE+EV^{DFO}$ group, its expression decreased significantly compared to the EAE and EAE+EV groups. Results are shown as means ± standard deviation. $^{*}p<0.05$, $^{**}p<0.01$, $^{***}p<0.001$; ns, not significant. EV, extracellular vesicle; EV^{DFO}, EV derived from DFO preconditioned MSC.

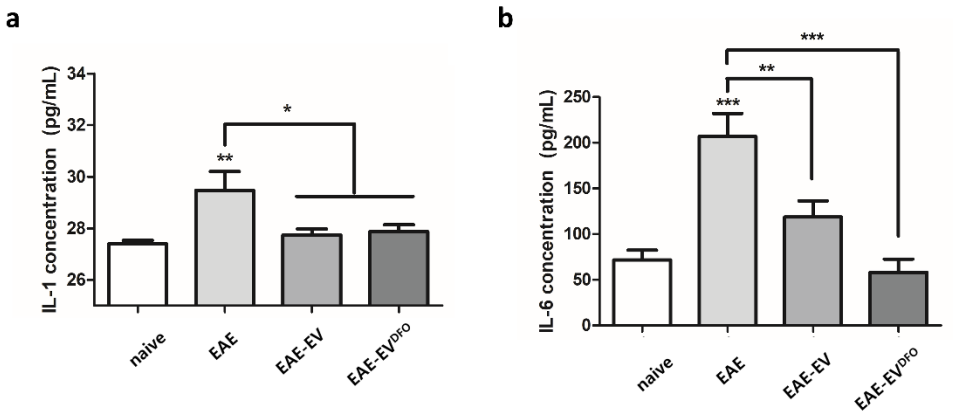

Figure 34. Proinflammatory cytokine levels in the culture media of splenocytes detached from EAE mouse model. The levels of **(a)** IL-1β and **(b)** IL-6 increased significantly in the EAE group. In the EAE+EV and EV^{DFO} groups, the levels of these cytokines were decreased compared to the EAE group; IL-6 level was especially lower in the EAE+EV^{DFO} group than that in the EAE+EV group. Results are shown as means ± standard deviation. $^{*}p<0.05$, $^{**}p<0.01$, $^{***}p<0.001$. EV, extracellular vesicle; EV^{DFO}, EV derived from DFO preconditioned MSC.

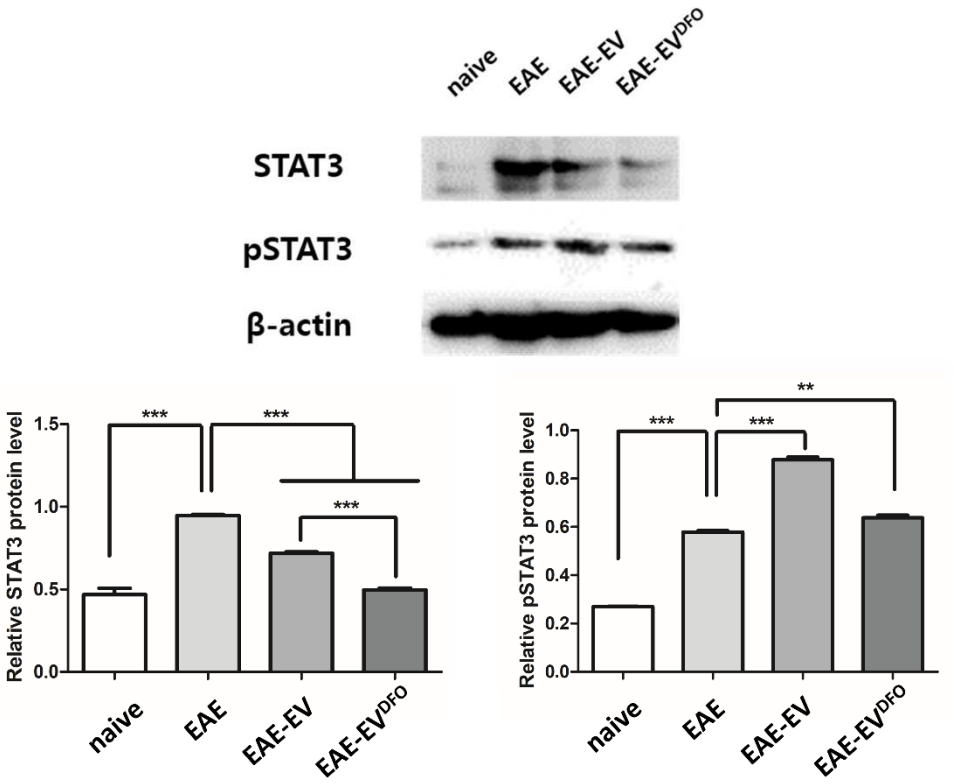

Figure 35. Protein expression of STAT3 in splenocytes detached from EAE mouse model. The protein expression of STAT3 and pSTAT3 (Tyr 705) increased in the EAE group compared to the naïve group; their expression levels were also significantly decreased in the EV^{DFO} group compared to the EAE and EAE+EV groups. $^{**}p<0.01$, $^{***}p<0.001$. EV, extracellular vesicle; EV^{DFO}, EV derived from DFO preconditioned MSC.

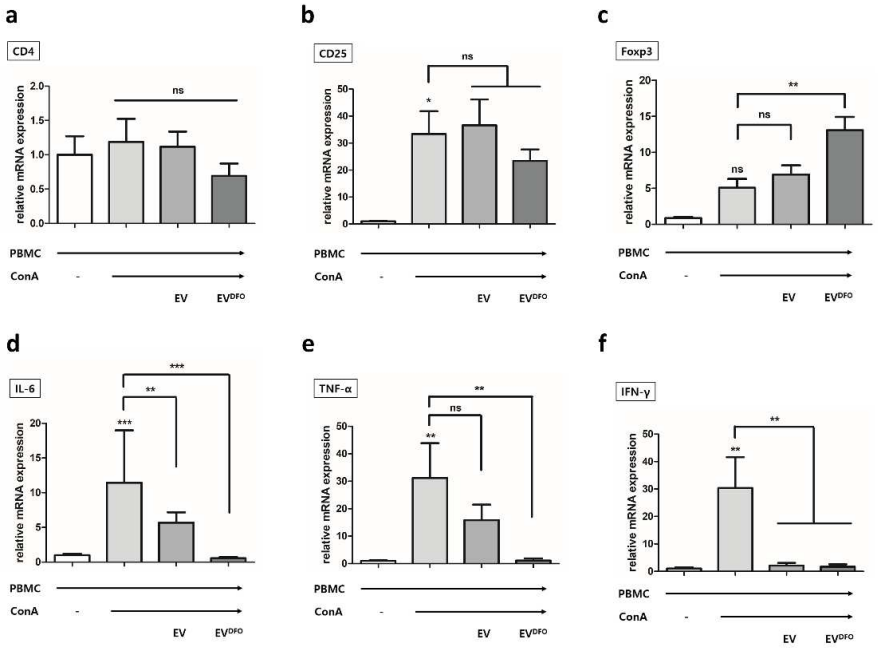

Figure 36. RNA expression of T reg and proinflammatory cytokines in EV/EV^{DFO} treated PBMCs. (a) The expression of CD4 was unchanged after stimulation with Con A and treatment with EVs. **(b)** The expression of CD25 increased significantly in the Con A-stimulated groups. EV treatment did not affect the expression of CD25 compared to the Con A-stimulated group. **(c)** The expression of Foxp3 increased significantly in the EV^{DFO} group compared to the Con A-stimulated and EV-treatment groups. **(d-f)** The expression of IL-6, TNF-α, and IFN-γ increased significantly in the Con A-stimulated group compared to the naïve group. Treatment with EV^{DFO} significantly decreased the expression of IL-6, TNF-α, and IFN-γ compared to the Con A-stimulated group. Results are shown as means ± standard deviation. $^{*}p<0.05$, $^{**}p<0.01$, $^{***}p<0.001$; ns, not significant. EV, extracellular vesicle; EV^{DFO}, EV derived from DFO preconditioned MSC.

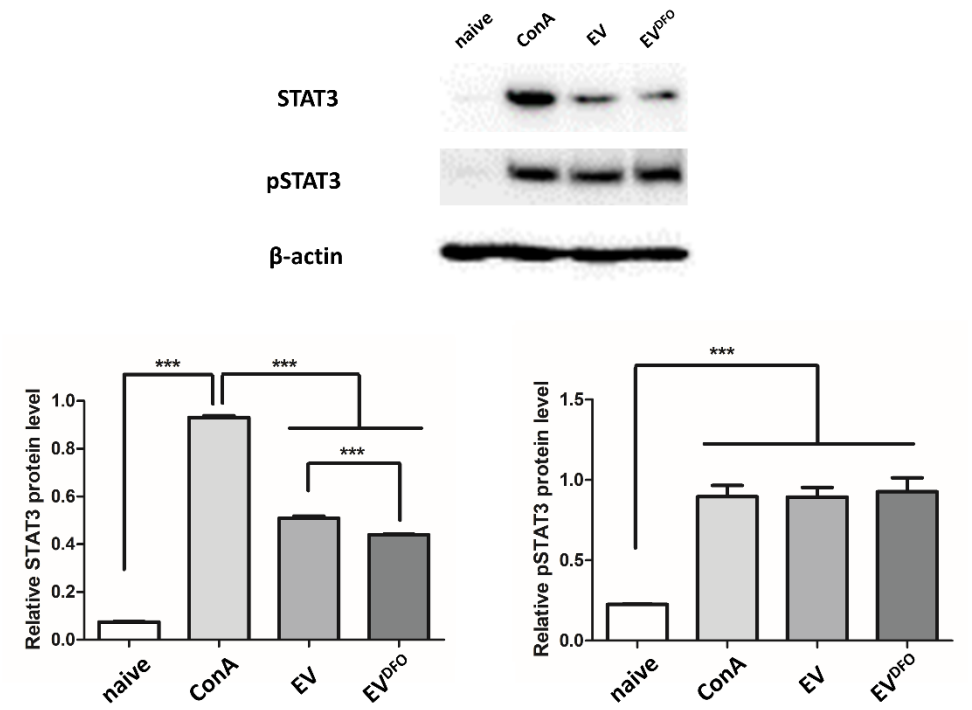

Figure 37. Protein expression of STAT3 in EV/EV^{DFO} treated PBMCs. The protein expression of pSTAT3 (Tyr 705) increased in all Con A-stimulated groups. However, the expression of STAT3 decreased in the EV and EV^{DFO} groups; the decrease in STAT3 expression in the EV^{DFO} group was greater than that in the EV group. $^{***}p<0.001$. EV, extracellular vesicle; EV^{DFO}, EV derived from DFO preconditioned MSC.

GENERAL CONCLUSION

The purpose of this study is to investigate the immunomodulation effect of DFO preconditioned cAT-MSC derived EVs in EAE mouse model. First, it was revealed that MSC^{DFO} had more effective paracrine effect and can modulate macrophage into M2 phase through paracrine effect. Secondly, EVs derived from cAT-MSC is one of key factors in paracrine effect and EV^{DFO} had more potential to modulate macrophage into anti-inflammatory phase. Finally, EV^{DFO} were treated in EAE mouse model by intranasally and alleviated the clinical symptoms. Infiltration of inflammatory cell and demyelination of spinal cord were reduced through immunomodulation effect of EV^{DFO}. Furthermore, it was investigated that EV^{DFO} modulated immune cells through regulating STAT3.

In the first experiment;

1. Hypoxic culture method with DFO preconditioning enhanced the expression of anti-inflammatory cytokines of cAT-MSCs.
2. The concentrations of PGE2 and TSG-6, which are known to play roles in immune regulation by affecting macrophages, were increased in MSC^{DFO}.
3. MSC^{DFO} induced macrophage polarization, thus directing macrophages to an anti-inflammation state by paracrine effect.

Therefore, this result support further research into this new strategy for modifying stem cell functions and confirmed the possibility of MSC^{DFO} in immunomodulation effect.

In the second experiment;

1. It was revealed that EVs is one of important factors in paracrine effect in MSCs and has immunomodulation function to macrophage.
2. DFO preconditioning increased anti-inflammatory factors, such as COX-2 in cAT-MSCs, and also increased COX-2 molecules in EVs.
3. EV^{DFO} delivered COX-2 to macrophages, which then modulated to M2 anti-inflammatory phase by activating STAT3 phosphorylation.

To the best of my knowledge, this report is the first to reveal that DFO preconditioning affects EVs and macrophage polarization via EVs. Moreover, it was investigated that EV^{DFO} modulated macrophage by transmitting COX-2 and regulating STAT3.

In the third experiment;

1. EV^{DFO} has relatively higher efficacy in reducing inflammation compare to non-preconditioned EV in EAE mouse model.
2. EV and EV^{DFO} regulated the immune system of EAE mouse model and enhance the activation of T reg cells and modulation of M2 macrophage.

3. EV^{DFO} regulated Con A stimulated PBMC more effectively compared to EV and changed STAT3 expression of PBMC.

4. It is assumed that STAT3 regulation play a major role in regulating EAE and EV^{DFO} controls the STAT3 pathway more effectively.

Our findings strongly support that preconditioned with DFO in cAT-MSC is an effective method to improve immunomodulation effect of cAT-MSC and derived EVs. Also, these results suggest that EV^{DFO} is potential therapeutic option for auto-immune disease such as EAE through regulating STAT3 pathway and modulating immune system. This report is an important data for suggesting option to increase the therapeutic efficacy of stem cell and development in cell-free therapy.

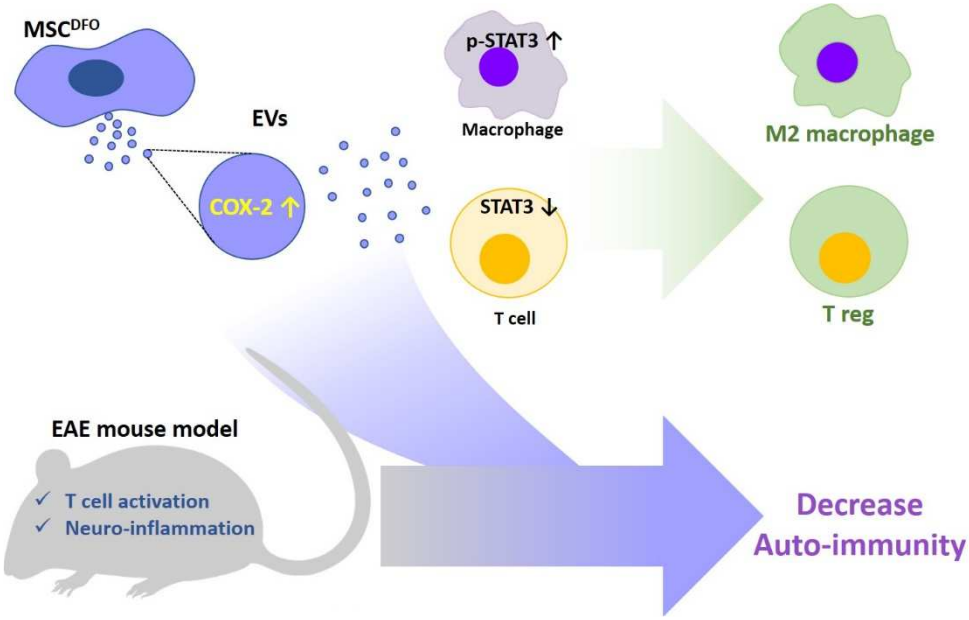

Figure 38. Schematic diagram of the effect of EV^{DFO}. DFO preconditioning method is effective to enhance the expression of anti-inflammatory cytokines in cAT-MSCs. MSC^{DFO} increased secretion of anti-inflammatory factors, such as COX-2, and also this change was reflected in EV^{DFO}. EV^{DFO} delivered COX-2 to macrophages, which then modulated to M2 anti-inflammatory phase by activating STAT3 phosphorylation. EV^{DFO} also regulated PBMC to T reg state and changed STAT3 expression of PBMC. EV^{DFO} regulated the immune system of EAE mouse model and enhance the activation of T reg cells and modulation of M2 macrophage. Through regulating immune system, EV^{DFO} has relatively higher efficacy in reducing auto-immunity in EAE mouse model. EV, extracellular vesicle; MSC^{DFO}, DFO preconditioned MSC.

REFERENCES

ABDOLLAHI, H., L. J. HARRIS, P. ZHANG, S. MCILHENNY, V. SRINIVAS, T. TULENKO and P. J. DIMUZIO (2011). The role of hypoxia in stem cell differentiation and therapeutics. *Journal of Surgical Research* 165 (1): 112-117.

AHMADVAND KOOHSARI, S., A. ABSALAN and D. AZADI (2021). Human umbilical cord mesenchymal stem cell-derived extracellular vesicles attenuate experimental autoimmune encephalomyelitis via regulating pro and anti-inflammatory cytokines. *Scientific Reports* 11 (1): 1-12.

AN, Ju Hyun, Q. LI, Dong Ha BHANG, Woo Jin SONG and Hwa Young YOUN (2020). TNF-α and INF-γ primed canine stem cell-derived extracellular vesicles alleviate experimental murine colitis. *Scientific reports* 10 (1): 1-14.

ANKRUM, J. A., J. F. ONG and J. M. KARP (2014). Mesenchymal stem cells: immune evasive, not immune privileged. *Nature biotechnology* 32 (3): 252-260.

AQEL, S. I., X. YANG, E. E. KRAUS, J. SONG, M. F. FARINAS, E. Y. ZHAO, W. PEI, A. E. LOVETT-RACKE, M. K. RACKE and C. LI (2021). A STAT3 inhibitor ameliorates CNS autoimmunity by restoring Teff: Treg balance. *JCI insight* 6 (4):e142376.

ASSOCIATION, A. D. (2010). Diagnosis and classification of diabetes mellitus. *Diabetes care* 33 (Supplement_1): S62-S69.

ATREYA, R., J. MUDTER, S. FINOTTO, J. MþLLBERG, T. JOSTOCK, S. WIRTZ, M. SCHþTZ, B. BARTSCH, M. HOLTMANN and C. BECKER (2000). Blockade of interleukin 6 trans signaling suppresses T-cell resistance against apoptosis in chronic intestinal inflammation: evidence in crohn disease and experimental colitis in vivo. *Nature medicine* 6 (5): 583-588.

BAEK, Gyuhyeon, Hojun CHOI, Youngeun KIM, Hai-Chon LEE and Chulhee CHOI (2019). Mesenchymal stem cell-derived extracellular vesicles as therapeutics and as a drug delivery platform. *Stem cells translational medicine* 8 (9): 880-886.

BANAS, A., T. TERATANI, Y. YAMAMOTO, M. TOKUHARA, F. TAKESHITA, M. OSAKI, M. KAWAMATA, T. KATO, H. OKOCHI and T. OCHIYA (2008). IFATS collection: in vivo therapeutic potential of human adipose tissue mesenchymal stem cells after transplantation into mice with liver injury. *Stem cells* 26 (10): 2705-2712.

BARTHOLOMEW, A., C. STURGEON, M. SIATSKAS, K. FERRER, K. MCINTOSH, S. PATIL, W. HARDY, S. DEVINE, D. UCKER and R. DEANS (2002). Mesenchymal stem cells suppress lymphocyte proliferation in vitro and prolong skin graft survival in vivo.

Experimental hematology 30 (1): 42-48.

BASCIANO, L., C. NEMOS, B. FOLIGUET, N. DE ISLA, M. DE CARVALHO, N. TRAN and A. DALLOUL (2011). Long term culture of mesenchymal stem cells in hypoxia promotes a genetic program maintaining their undifferentiated and multipotent status. *BMC cell biology* 12 (1): 1-12.

BERNIAKOVICH, I. and M. GIORGIO (2013). Low oxygen tension maintains multipotency, whereas normoxia increases differentiation of mouse bone marrow stromal cells. *International journal of molecular sciences* 14 (1): 2119-2134.

BISTER, N., C. PISTONO, B. HUREMAGIC, J. JOLKKONEN, R. GIUGNO and T. MALM (2020). Hypoxia and extracellular vesicles: A review on methods, vesicular cargo and functions. *Journal of extracellular vesicles* 10 (1): e12002.

BITSCH, A., J. SCHUCHARDT, S. BUNKOWSKI, T. KUHLMANN and W. BRþCK (2000). Acute axonal injury in multiple sclerosis: correlation with demyelination and inflammation. *Brain* 123 (6): 1174-1183.

BRUNO, S. and G. CAMUSSI (2013). Role of mesenchymal stem cell-derived microvesicles in tissue repair. *Pediatric nephrology* 28 (12): 2249-2254.

BRUNO, S., C. GRANGE, F. COLLINO, M. C. DEREGIBUS, V.

CANTALUPPI, L. BIANCONE, C. TETTA and G. CAMUSSI (2012). Microvesicles derived from mesenchymal stem cells enhance survival in a lethal model of acute kidney injury. *PLOS One* 7 (3): e33115.

BRUNO, S., C. GRANGE, M. C. DEREGIBUS, R. A. CALOGERO, S. SAVIOZZI, F. COLLINO, L. MORANDO, M. FALDA, B. BUSSOLATI and C. TETTA (2009). Mesenchymal stem cell-derived microvesicles protect against acute tubular injury. *Journal of the American Society of Nephrology* 20 (5): 1053-1067.

BURAVKOVA, L., E. ANDREEVA, V. GOGVADZE and B. ZHIVOTOVSKY (2014). Mesenchymal stem cells and hypoxia: where are we? *Mitochondrion* 19: 105-112.

BUSTOS, M. L., L. HULEIHEL, E. M. MEYER, A. D. DONNENBERG, V. S. DONNENBERG, J. D. SCIURBA, L. MROZ, B. J. MCVERRY, B. M. ELLIS and N. KAMINSKI (2013). Activation of human mesenchymal stem cells impacts their therapeutic abilities in lung injury by increasing interleukin (IL)-10 and IL-1RN levels. *Stem Cells Translational Medicine* 2 (11): 884-895.

CAMPBELL, D. J. and M. A. KOCH (2011). Phenotypical and functional specialization of FOXP3+ regulatory T cells. *Nature Reviews Immunology* 11 (2): 119-130.

CHANG, E. I., M. G. GALVEZ, S. EL-FTESI, E. I. CHANG, S. A. LOH and

G. C. GURTNER (2008). Novel therapy for age associated defects in neovascularization and wound healing through augmentation of HIF-1α: Stabilization with dimethyloxalylglycine and deferoxamine. *Journal of the American College of Surgeons* 207 (3): S101.

CHANG, H.-H., S.-P. HSU and C.-T. CHIEN (2019). Intrarenal transplantation of hypoxic preconditioned mesenchymal stem cells improves glomerulonephritis through anti-oxidation, anti-ER stress, anti-inflammation, anti-apoptosis, and anti-autophagy. *Antioxidants* 9 (1): 2.

CHEN, E., D. XU, X. LAN, B. JIA, L. SUN, J. C ZHENG and H. PENG (2013). A novel role of the STAT3 pathway in brain inflammation-induced human neural progenitor cell differentiation. *Current molecular medicine* 13 (9): 1474-1484.

CHENG, X. W., M. KUZUYA, W. KIM, H. SONG, L. HU, A. INOUE, K. NAKAMURA, Q. DI, T. SASAKI and M. TSUZUKI (2010). Exercise training stimulates ischemia-induced neovascularization via phosphatidylinositol 3-kinase/Akt-dependent hypoxia-induced factor-1α reactivation in mice of advanced age. *Circulation* 122 (7): 707-716.

CHOI, J., S. YOO, S. PARK, Y. KANG, W. KIM, I. OH and C. CHO (2008). Mesenchymal stem cells overexpressing interleukin-10 attenuate collagen-induced arthritis in mice. *Clinical & experimental immunology*

153 (2): 269-276.

CHU, F., M. SHI, C. ZHENG, D. SHEN, J. ZHU, X. ZHENG and L. CUI (2018). The roles of macrophages and microglia in multiple sclerosis and experimental autoimmune encephalomyelitis. *Journal of neuroimmunology* 318: 1-7.

CHU, K., Keun-Hwa JUNG, Se-Jeong KIM, Soon-Tae LEE, Juhyun KIM, Hee-Kwon PARK, Eun-Cheol SONG, Seung U. KIM, Manho KIM and Sang Kun LEE (2008). Transplantation of human neural stem cells protect against ischemia in a preventive mode via hypoxia-inducible factor-1α stabilization in the host brain. *Brain research* 1207: 182-192.

CLARK, K., S. ZHANG, S. BARTHE, P. KUMAR, C. PIVETTI, N. KREUTZBERG, C. REED, Y. WANG, Z. PAXTON and D. FARMER (2019). Placental mesenchymal stem cell-derived extracellular vesicles promote myelin regeneration in an animal model of multiple sclerosis. *Cells* 8 (12): 1497.

CONFORTI, A., M. SCARSELLA, N. STARC, E. GIORDA, S. BIAGINI, A. PROIA, R. CARSETTI, F. LOCATELLI and M. E. BERNARDO (2014). Microvescicles derived from mesenchymal stromal cells are not as effective as their cellular counterpart in the ability to modulate immune responses in vitro. *Stem cells and development* 23 (21): 2591-2599.

CONSTANTINESCU, C. S., N. FAROOQI, K. O'BRIEN and B. GRAN

(2011). Experimental autoimmune encephalomyelitis (EAE) as a model for multiple sclerosis (MS). *British journal of pharmacology* 164 (4): 1079-1106.

COSENZA, S., K. TOUPET, M. MAUMUS, P. LUZ-CRAWFORD, O. BLANC-BRUDE, C. JORGENSEN and D. NOíL (2018). Mesenchymal stem cells-derived exosomes are more immunosuppressive than microparticles in inflammatory arthritis. *Theranostics* 8 (5): 1399.

CRISOSTOMO, P. R., Y. WANG, T. A. MARKEL, M. WANG, T. LAHM and D. R. MELDRUM (2008). Human mesenchymal stem cells stimulated by TNF-α, LPS, or hypoxia produce growth factors by an NFκB-but not JNK-dependent mechanism. *American Journal of Physiology-Cell Physiology* 294 (3): C675-C682.

CUI, G. H., J. WU, F. F. MOU, W. H. XIE, F. B. WANG, Q. L. WANG, J. FANG, Y. W. XU, Y. R. DONG and J. R. LIU (2018). Exosomes derived from hypoxia-preconditioned mesenchymal stromal cells ameliorate cognitive decline by rescuing synaptic dysfunction and regulating inflammatory responses in APP/PS1 mice. *The FASEB Journal* 32 (2): 654-668.

DASILVA, A. G. and V. W. YONG (2009). Matrix metalloproteinase-12 deficiency worsens relapsing-remitting experimental autoimmune encephalomyelitis in association with cytokine and chemokine

dysregulation. *The American journal of pathology* 174 (3): 898-909.

DAVE, M., K. MEHTA, J. LUTHER, A. BARUAH, A. B. DIETZ and W. A. FAUBION JR (2015). Mesenchymal stem cell therapy for inflammatory bowel disease: a systematic review and meta-analysis. *Inflammatory bowel diseases* 21 (11): 2696-2707.

DE JONG, O. G., M. C. VERHAAR, Y. CHEN, P. VADER, H. GREMMELS, G. POSTHUMA, R. M. SCHIFFELERS, M. GUCEK and B. W. VAN BALKOM (2012). Cellular stress conditions are reflected in the protein and RNA content of endothelial cell-derived exosomes. *Journal of extracellular vesicles* 1 (1): e18396.

DI, D., L. ZHANG, X. WU and R. LENG (2020). Long-term exposure to outdoor air pollution and the risk of development of rheumatoid arthritis: a systematic review and meta-analysis. *Seminars in arthritis and rheumatism* 50: 266-275.

DING, D.-C., W.-C. SHYU and S.-Z. LIN (2011). Mesenchymal stem cells. *Cell transplantation* 20 (1): 5-14.

DING, J., X. WANG, B. CHEN, J. ZHANG and J. XU (2019). Exosomes derived from human bone marrow mesenchymal stem cells stimulated by deferoxamine accelerate cutaneous wound healing by promoting angiogenesis. *BioMed research international* 2019: e9742765.

DOBSON, R. and G. GIOVANNONI (2019). Multiple sclerosis–a review.

European journal of neurology 26 (1): 27-40.

DOMêNECH, E., M. MAóOSA and E. CABRë (2014). An overview of the natural history of inflammatory bowel diseases. *Digestive Diseases* 32 (4): 320-327.

DONG, L., Y. WANG, T. ZHENG, Y. PU, Y. MA, X. QI, W. ZHANG, F. XUE, Z. SHAN and J. LIU (2021). Hypoxic hUCMSC-derived extracellular vesicles attenuate allergic airway inflammation and airway remodeling in chronic asthma mice. *Stem Cell Research & Therapy* 12 (1): 1-14.

DURANT, L., W. T. WATFORD, H. L. RAMOS, A. LAURENCE, G. VAHEDI, L. WEI, H. TAKAHASHI, H.-W. SUN, Y. KANNO and F. POWRIE (2010). Diverse targets of the transcription factor STAT3 contribute to T cell pathogenicity and homeostasis. *Immunity* 32 (5): 605-615.

DUSCHER, D., M. JANUSZYK, Z. N. MAAN, A. J. WHITTAM, M. S. HU, G. G. WALMSLEY, Y. DONG, S. M. KHONG, M. T. LONGAKER and G. C. GURTNER (2017). Comparison of the hydroxylase inhibitor DMOG and the iron chelator deferoxamine in diabetic and aged wound healing. *Plastic and reconstructive surgery* 139 (3): e695.

EGGENHOFER, E. and M. J. HOOGDUIJN (2012). Mesenchymal stem cell-educated macrophages. *Transplantation research* 1 (1): 1-5.

EGGENHUIZEN, P. J., B. H. NG and J. D. OOI (2020). Treg enhancing

therapies to treat autoimmune diseases. *International Journal of Molecular Sciences* 21 (19): 7015.

EJTEHADIFAR, M., K. SHAMSASENJAN, A. MOVASSAGHPOUR, P. AKBARZADEHLALEH, N. DEHDILANI, P. ABBASI, Z. MOLAEIPOUR and M. SALEH (2015). The effect of hypoxia on mesenchymal stem cell biology. *Advanced pharmaceutical bulletin* 5 (2): 141.

FAVARO, E., A. CARPANETTO, C. CAORSI, M. GIOVARELLI, C. ANGELINI, P. CAVALLO-PERIN, C. TETTA, G. CAMUSSI and M. M. ZANONE (2016). Human mesenchymal stem cells and derived extracellular vesicles induce regulatory dendritic cells in type 1 diabetic patients. *Diabetologia* 59 (2): 325-333.

FISCHER, U. M., M. T. HARTING, F. JIMENEZ, W. O. MONZON-POSADAS, H. XUE, S. I. SAVITZ, G. A. LAINE and C. S. COX JR (2009). Pulmonary passage is a major obstacle for intravenous stem cell delivery: the pulmonary first-pass effect. *Stem cells and development* 18 (5): 683-692.

FUGGER, L., L. T. JENSEN and J. ROSSJOHN (2020). Challenges, progress, and prospects of developing therapies to treat autoimmune diseases. *Cell* 181 (1): 63-80.

FUJISAWA, K., T. TAKAMI, S. OKADA, K. HARA, T. MATSUMOTO, N.

YAMAMOTO, T. YAMASAKI and I. SAKAIDA (2018). Analysis of metabolomic changes in mesenchymal stem cells on treatment with desferrioxamine as a hypoxia mimetic compared with hypoxic conditions. *Stem Cells* 36 (8): 1226-1236.

GAO, F., S. M. CHIU, D. A. MOTAN, Z. ZHANG, L. CHEN, H. L. JI, H. F. TSE, Q. L. FU and Q. LIAN (2016). Mesenchymal stem cells and immunomodulation: current status and future prospects. *Cell Death Disease* 7: e2062.

GAO, W., J. MCCORMICK, M. CONNOLLY, E. BALOGH, D. J. VEALE and U. FEARON (2015). Hypoxia and STAT3 signalling interactions regulate pro-inflammatory pathways in rheumatoid arthritis. *Annals of the rheumatic diseases* 74 (6): 1275-1283.

GENUA, M., V. INGANGI, P. FONTEYNE, A. PIONTINI, A. M. YOUSIF, F. MERLINO, P. GRIECO, A. MALESCI, M. V. CARRIERO and S. DANESE (2016). Treatment with a urokinase receptor-derived cyclized peptide improves experimental colitis by preventing monocyte recruitment and macrophage polarization. *Inflammatory Bowel Diseases* 22 (10): 2390-2401.

GERDONI, E., B. GALLO, S. CASAZZA, S. MUSIO, I. BONANNI, E. PEDEMONTE, R. MANTEGAZZA, F. FRASSONI, G. MANCARDI and R. PEDOTTI (2007). Mesenchymal stem cells effectively modulate

pathogenic immune response in experimental autoimmune encephalomyelitis. *Annals of Neurology: Official Journal of the American Neurological Association and the Child Neurology Society* 61 (3): 219-227.

GOUVEIA DE ANDRADE, A. V., G. BERTOLINO, J. RIEWALDT, K. BIEBACK, J. KARBANOVã, M. ODENDAHL, M. BORNHæUSER, M. SCHMITZ, D. CORBEIL and T. TONN (2015). Extracellular vesicles secreted by bone marrow-and adipose tissue-derived mesenchymal stromal cells fail to suppress lymphocyte proliferation. *Stem cells and development* 24 (11): 1374-1376.

GRIFFITH, J. S. (1968). Mathematics of cellular control processes I. Negative feedback to one gene. *Journal of theoretical biology* 20 (2): 202-208.

GUO, M., L.-P. SONG, Y. JIANG, W. LIU, Y. YU and G.-Q. CHEN (2006). Hypoxia-mimetic agents desferrioxamine and cobalt chloride induce leukemic cell apoptosis through different hypoxia-inducible factor-1α independent mechanisms. *Apoptosis* 11 (1): 67-77.

GUO, S., N. PERETS, O. BETZER, S. BEN-SHAUL, A. SHEININ, I. MICHAELEVSKI, R. POPOVTZER, D. OFFEN and S. LEVENBERG (2019). Intranasal delivery of mesenchymal stem cell derived exosomes loaded with phosphatase and tensin homolog siRNA repairs complete

spinal cord injury. *ACS nano* 13 (9): 10015-10028.

GUO, Z.-L., B. YU, B.-T. NING, S. CHAN, Q.-B. LIN, J. C.-B. LI, J.-D. HUANG and G. C.-F. CHAN (2015). Genetically modified" obligate" anaerobic Salmonella typhimurium as a therapeutic strategy for neuroblastoma. *Journal of hematology & oncology* 8 (1): 1-12.

HAMS, E., S. P. SAUNDERS, E. P. CUMMINS, A. O'CONNOR, M. T. TAMBUWALA, W. M. GALLAGHER, A. BYRNE, A. CAMPOS-TORRES, P. M. MOYNAGH and C. JOBIN (2011). The hydroxylase inhibitor DMOG attenuates endotoxic shock via alternative activation of macrophages and IL-10 production by B-1 cells. *Shock* 36 (3): 295-302.

HAN, Kyu-Hyun, Ae-Kyeong KIM, Min-Hee KIM, Do-Hyung KIM, Ha-Ni GO and Dong-Ik KIM (2016). Enhancement of angiogenic effects by hypoxia-preconditioned human umbilical cord-derived mesenchymal stem cells in a mouse model of hindlimb ischemia. *Cell biology international* 40 (1): 27-35.

HAN, Yong-Seok, Jun Hee LEE, Yeo Min YOON, Chul Won YUN, Hyunjin NOH and Sang Hun LEE (2016). Hypoxia-induced expression of cellular prion protein improves the therapeutic potential of mesenchymal stem cells. *Cell Death & Disease* 7 (10): e2395.

HAN, Y., W. GUO, T. REN, Y. HUANG, S. WANG, K. LIU, B. ZHENG, K. YANG, H. ZHANG and X. LIANG (2019). Tumor-associated

macrophages promote lung metastasis and induce epithelial-mesenchymal transition in osteosarcoma by activating the COX-2/STAT3 axis. *Cancer letters* 440: 116-125.

HANEKLAUS, M., M. GERLIC, L. A. O'NEILL and S. MASTERS (2013). miR-223: infection, inflammation and cancer. *Journal of internal medicine* 274 (3): 215-226.

HAUSER, S. L. and B. A. CREE (2020). Treatment of multiple sclerosis: a review. *The American journal of medicine* 133 (12): 1380-1390.

HE, J., Y. WANG, S. SUN, M. YU, C. WANG, X. PEI, B. ZHU, J. WU and W. ZHAO (2012). Bone marrow stem cells-derived microvesicles protect against renal injury in the mouse remnant kidney model. *Nephrology* 17 (5): 493-500.

HE, N., Y. KONG, X. LEI, Y. LIU, J. WANG, C. XU, Y. WANG, L. DU, K. JI and Z. LI (2018). MSCs inhibit tumor progression and enhance radiosensitivity of breast cancer cells by down-regulating Stat3 signaling pathway. *Cell death & disease* 9 (10): 1-14.

HELLWIG-BþRGEL, T., D. P. STIEHL, A. E. WAGNER, E. METZEN and W. JELKMANN (2005). Hypoxia-inducible factor-1 (HIF-1): a novel transcription factor in immune reactions. *Journal of interferon & cytokine research* 25 (6): 297-310.

HEO, June Seok, Youjeong CHOI and H. O. KIM (2019). Adipose-derived

mesenchymal stem cells promote M2 macrophage phenotype through exosomes. *Stem cells international* 2019: e7921760.

HERMAN, S., I. FISHEL and D. OFFEN (2021). Intranasal delivery of mesenchymal stem cells-derived extracellular vesicles for the treatment of neurological diseases. *Stem Cells* 39 (12): 1589-1600.

HESSVIK, N. P. and A. LLORENTE (2018). Current knowledge on exosome biogenesis and release. *Cellular and Molecular Life Sciences* 75 (2): 193-208.

HIGGINS, D. F., K. KIMURA, W. M. BERNHARDT, N. SHRIMANKER, Y. AKAI, B. HOHENSTEIN, Y. SAITO, R. S. JOHNSON, M. KRETZLER and C. D. COHEN (2007). Hypoxia promotes fibrogenesis in vivo via HIF-1 stimulation of epithelial-to-mesenchymal transition. *The Journal of clinical investigation* 117 (12): 3810-3820.

HOLLANDER, L., X. GUO, H. VELAZQUEZ, J. CHANG, R. SAFIRSTEIN, H. KLUGER, C. CHA and G. V. DESIR (2016). Renalase expression by melanoma and tumor-associated macrophages promotes tumor growth through a STAT3-mediated mechanism. *Cancer research* 76 (13): 3884-3894.

HONG, P., H. YANG, Y. WU, K. LI and Z. TANG (2019). The functions and clinical application potential of exosomes derived from adipose mesenchymal stem cells: a comprehensive review. *Stem Cell Research*

& Therapy 10 (1): 242.

HOSONO, M., O. J. DE BOER, A. C. VAN DER WAL, C. M. VAN DER LOOS, P. TEELING, J. J. PIEK, M. UEDA and A. E. BECKER (2003). Increased expression of T cell activation markers (CD25, CD26, CD40L and CD69) in atherectomy specimens of patients with unstable angina and acute myocardial infarction. *Atherosclerosis* 168 (1): 73-80.

HU, X., S. P. YU, J. L. FRASER, Z. LU, M. E. OGLE, J.-A. WANG and L. WEI (2008). Transplantation of hypoxia-preconditioned mesenchymal stem cells improves infarcted heart function via enhanced survival of implanted cells and angiogenesis. *The Journal of thoracic and cardiovascular surgery* 135 (4): 799-808.

HUANG, P., N. GEBHART, E. RICHELSON, T. G. BROTT, J. F. MESCHIA and A. C. ZUBAIR (2014). Mechanism of mesenchymal stem cell–induced neuron recovery and anti-inflammation. *Cytotherapy* 16 (10): 1336-1344.

HWANG, J. Jihwan, Yeri A. RIM, Yoojun NAM and Ji Hyeon JU (2021). Recent developments in clinical applications of mesenchymal stem cells in the treatment of rheumatoid arthritis and osteoarthritis. *Frontiers in Immunology* 12 (631291): 1-15.

JAFARINIA, M., F. ALSAHEBFOSOUL, H. SALEHI, N. ESKANDARI, M. AZIMZADEH, M. MAHMOODI, S. ASGARY and M.

GANJALIKHANI HAKEMI (2020). Therapeutic effects of extracellular vesicles from human adipose-derived mesenchymal stem cells on chronic experimental autoimmune encephalomyelitis. *Journal of cellular physiology* 235 (11): 8779-8790.

JANG, Eunkyeong, Mini JEONG, Sukhyung KIM, Kiseok JANG, Bo-Kyeong KANG, Dong Yun LEE, Sang-Cheol BAE, Kyung Suk KIM and Jeehee YOUN (2016). Infusion of human bone marrow-derived mesenchymal stem cells alleviates autoimmune nephritis in a lupus model by suppressing follicular helper T-cell development. *Cell transplantation* 25 (1): 1-15.

JANSEN, F. H., J. KRIJGSVELD, A. VAN RIJSWIJK, G.-J. VAN DEN BEMD, M. S. VAN DEN BERG, W. M. VAN WEERDEN, R. WILLEMSEN, L. J. DEKKER, T. M. LUIDER and G. JENSTER (2009). Exosomal secretion of cytoplasmic prostate cancer xenograft-derived proteins. *Molecular & Cellular Proteomics* 8 (6): 1192-1205.

JIN, L., Z. DENG, J. ZHANG, C. YANG, J. LIU, W. HAN, P. YE, Y. SI and G. CHEN (2019). Mesenchymal stem cells promote type 2 macrophage polarization to ameliorate the myocardial injury caused by diabetic cardiomyopathy. *Journal of translational medicine* 17 (1): 251.

JOKILEHTO, T. and P. M. JAAKKOLA (2010). The role of HIF prolyl hydroxylases in tumour growth. *Journal of cellular and molecular*

medicine 14 (4): 758-770.

JURJUS, A. R., N. N. KHOURY and J.-M. REIMUND (2004). Animal models of inflammatory bowel disease. *Journal of pharmacological and toxicological methods* 50 (2): 81-92.

KATSUDA, T., N. KOSAKA, F. TAKESHITA and T. OCHIYA (2013). The therapeutic potential of mesenchymal stem cell-derived extracellular vesicles. *Proteomics* 13 (10-11): 1637-1653.

KIM, J. and P. HEMATTI (2009). Mesenchymal stem cell–educated macrophages: A novel type of alternatively activated macrophages. *Experimental hematology* 37 (12): 1445-1453.

KOCH, M., A. LEMKE and C. LANGE (2015). Extracellular vesicles from MSC modulate the immune response to renal allografts in a MHC disparate rat model. *Stem cells international* 2015: e486141.

KONOSHENKO, M. Y., E. A. LEKCHNOV, A. V. VLASSOV and P. P. LAKTIONOV (2018). Isolation of extracellular vesicles: general methodologies and latest trends. *BioMed research international* 2018:e8545347.

KURSCHUS, F. (2015). T cell mediated pathogenesis in EAE: molecular mechanisms. *Biomedical journal* 38 (3): 183-193.

KUSUMA, G. D., J. CARTHEW, R. LIM and J. E. FRITH (2017). Effect of the microenvironment on mesenchymal stem cell paracrine signaling:

opportunities to engineer the therapeutic effect. *Stem cells and development* 26 (9): 617-631.

LAI, R. C., S. S. TAN, B. J. TEH, S. K. SZE, F. ARSLAN, D. P. DE KLEIJN, A. CHOO and S. K. LIM (2012). Proteolytic potential of the MSC exosome proteome: implications for an exosome-mediated delivery of therapeutic proteasome. *International journal of proteomics* 2012: e971907.

LAI, R. C., R. W. Y. YEO and S. K. LIM (2015). Mesenchymal stem cell exosomes. *Seminars in cell & developmental biology* 40:82-88.

LANKFORD, K. L., E. J. ARROYO, K. NAZIMEK, K. BRYNIARSKI, P. W. ASKENASE and J. D. KOCSIS (2018). Intravenously delivered mesenchymal stem cell-derived exosomes target M2-type macrophages in the injured spinal cord. *PLOS One* 13 (1): e0190358.

LE BLANC, K., L. TAMMIK, B. SUNDBERG, S. HAYNESWORTH and O. RINGDEN (2003). Mesenchymal stem cells inhibit and stimulate mixed lymphocyte cultures and mitogenic responses independently of the major histocompatibility complex. *Scandinavian journal of immunology* 57 (1): 11-20.

LEE, B.-C. and K.-S. KANG (2020). Functional enhancement strategies for immunomodulation of mesenchymal stem cells and their therapeutic application. *Stem Cell Research & Therapy* 11 (1): 1-10.

LEE, J. J., M. NATSUIZAKA, S. OHASHI, G. S. WONG, M. TAKAOKA, C. Z. MICHAYLIRA, D. BUDO, J. W. TOBIAS, M. KANAI and Y. SHIRAKAWA (2010). Hypoxia activates the cyclooxygenase-2–prostaglandin E synthase axis. *Carcinogenesis* 31 (3): 427-434.

LEE, Y. S. and R. D. WURSTER (1995). Deferoxamine-induced cytotoxicity in human neuronal cell lines: protection by free radical scavengers. *Toxicology letters* 78 (1): 67-71.

LI, Q., Woo-Jin SONG, Min-Ok RYU, Aryung NAM, Ju-Hyun AN, Jin-Ok AHN, Dong Ha BHANG, Yun Chan JUNG and H.-Y. YOUN (2018). TSG-6 secreted by human adipose tissue-derived mesenchymal stem cells ameliorates severe acute pancreatitis via ER stress downregulation in mice. *Stem cell research & therapy* 9 (1): 1-13.

LI, X., L. LIU, J. YANG, Y. YU, J. CHAI, L. WANG, L. MA and H. YIN (2016). Exosome derived from human umbilical cord mesenchymal stem cell mediates MiR-181c attenuating burn-induced excessive inflammation. *EBioMedicine* 8: 72-82.

LIN, K.-C., H.-K. YIP, P.-L. SHAO, S.-C. WU, K.-H. CHEN, Y.-T. CHEN, C.-C. YANG, C.-K. SUN, G.-S. KAO and S.-Y. CHEN (2016). Combination of adipose-derived mesenchymal stem cells (ADMSC) and ADMSC-derived exosomes for protecting kidney from acute ischemia–reperfusion injury. *International journal of cardiology* 216: 173-185.

LIN, Q., X. CONG and Z. YUN (2011). Differential Hypoxic Regulation of Hypoxia-Inducible Factors 1α and 2αDifferential Regulation of HIF-1α and HIF-2α. *Molecular Cancer Research* 9 (6): 757-765.

LIU, Q., S. JI, T. XIA, J. LIU, Z. LIU, X. CHEN and Z.-J. ZANG (2020). MCP-1 Priming Enhanced the Therapeutic Effects of Mesenchymal Stromal Cells on Contact Hypersensitivity by Activating the COX2-PGE2/STAT3 Pathway. *Stem cells and development* 29 (16): 1073-1083.

LIU, R., X. LI, Z. ZHANG, M. ZHOU, Y. SUN, D. SU, X. FENG, X. GAO, S. SHI and W. CHEN (2015). Allogeneic mesenchymal stem cells inhibited T follicular helper cell generation in rheumatoid arthritis. *Scientific reports* 5 (1): 1-11.

LIU, X., Y. S. LEE, C.-R. YU and C. E. EGWUAGU (2008). Loss of STAT3 in CD4+ T cells prevents development of experimental autoimmune diseases. *The Journal of Immunology* 180 (9): 6070-6076.

LIU, X. H., A. KIRSCHENBAUM, M. LU, S. YAO, A. DOSORETZ, J. F. HOLLAND and A. C. LEVINE (2002). Prostaglandin E2 induces hypoxia-inducible factor-1α stabilization and nuclear localization in a human prostate cancer cell line. *Journal of Biological Chemistry* 277 (51): 50081-50086.

LO SICCO, C., D. REVERBERI, C. BALBI, V. ULIVI, E. PRINCIPI, L. PASCUCCI, P. BECHERINI, M. C. BOSCO, L. VARESIO and C.

FRANZIN (2017). Mesenchymal stem cell-derived extracellular vesicles as mediators of anti-inflammatory effects: endorsement of macrophage polarization. *Stem cells translational medicine* 6 (3): 1018-1028.

LOMA, I. and R. HEYMAN (2011). Multiple sclerosis: pathogenesis and treatment. *Curr Neuropharmacol* 9 (3): 409-416.

LONG, Q., D. UPADHYA, B. HATTIANGADY, D.-K. KIM, S. Y. AN, B. SHUAI, D. J. PROCKOP and A. K. SHETTY (2017). Intranasal MSC-derived A1-exosomes ease inflammation, and prevent abnormal neurogenesis and memory dysfunction after status epilepticus. *Proceedings of the National Academy of Sciences* 114 (17): 3536-3545.

LOTVALL, J. and H. VALADI (2007). Cell to cell signalling via exosomes through esRNA. *Cell adhesion & migration* 1 (3): 156-158.

LU, H. C., S. KIM, A. J. STEELMAN, K. TRACY, B. ZHOU, D. MICHAUD, A. E. HILLHOUSE, K. KONGANTI and J. LI (2020). STAT3 signaling in myeloid cells promotes pathogenic myelin-specific T cell differentiation and autoimmune demyelination. *Proceedings of the National Academy of Sciences* 117 (10): 5430-5441.

LU, M., H. XING, Z. XUN, T. YANG, X. ZHAO, C. CAI, D. WANG and P. DING (2018). Functionalized extracellular vesicles as advanced therapeutic nanodelivery systems. *European Journal of Pharmaceutical*

Sciences 121: 34-46.

LUKIW, W. J., A. OTTLECZ, G. LAMBROU, M. GRUENINGER, J. FINLEY, H. W. THOMPSON and N. G. BAZAN (2003). Coordinate activation of HIF-1 and NF-κB DNA binding and COX-2 and VEGF expression in retinal cells by hypoxia. *Investigative ophthalmology & visual science* 44 (10): 4163-4170.

LUO, C., E. URGARD, T. VOODER and A. METSPALU (2011). The role of COX-2 and Nrf2/ARE in anti-inflammation and antioxidative stress: Aging and anti-aging. *Medical hypotheses* 77 (2): 174-178.

MADRIGAL, M., K. S. RAO and N. H. RIORDAN (2014). A review of therapeutic effects of mesenchymal stem cell secretions and induction of secretory modification by different culture methods. *Journal of translational medicine* 12 (1): 1-14.

MAJMUNDAR, A. J., W. J. WONG and M. C. SIMON (2010). Hypoxia-inducible factors and the response to hypoxic stress. *Molecular cell* 40 (2): 294-309.

MAO, F., Y. WU, X. TANG, J. KANG, B. ZHANG, Y. YAN, H. QIAN, X. ZHANG and W. XU (2017). Exosomes derived from human umbilical cord mesenchymal stem cells relieve inflammatory bowel disease in mice. *BioMed research international* 2017: e5356760.

MOKARIZADEH, A., N. DELIREZH, A. MORSHEDI, G. MOSAYEBI, A.-

A. FARSHID and K. MARDANI (2012). Microvesicles derived from mesenchymal stem cells: potent organelles for induction of tolerogenic signaling. *Immunology letters* 147 (1-2): 47-54.

NAJAFI, R. and A. M. SHARIFI (2013). Deferoxamine preconditioning potentiates mesenchymal stem cell homing in vitro and in streptozotocin-diabetic rats. *Expert opinion on biological therapy* 13 (7): 959-972.

NAKAMURA, R., A. SENE, A. SANTEFORD, A. GDOURA, S. KUBOTA, N. ZAPATA and R. S. APTE (2015). IL10-driven STAT3 signalling in senescent macrophages promotes pathological eye angiogenesis. *Nature communications* 6 (1): 1-14.

NëMETH, K., A. LEELAHAVANICHKUL, P. S. YUEN, B. MAYER, A. PARMELEE, P. G. ROBEY, K. LEELAHAVANICHKUL, B. H. KOLLER, J. M. BROWN and X. HU (2009). Bone marrow stromal cells attenuate sepsis via prostaglandin E2–dependent reprogramming of host macrophages to increase their interleukin-10 production. *Nature medicine* 15 (1): 42-49.

NOJEHDEHI, S., S. SOUDI, A. HESAMPOUR, S. RASOULI, M. SOLEIMANI and S. M. HASHEMI (2018). Immunomodulatory effects of mesenchymal stem cell–derived exosomes on experimental type-1 autoimmune diabetes. *Journal of Cellular Biochemistry* 119 (11): 9433-

9443.

OHNISHI, S., B. YANAGAWA, K. TANAKA, Y. MIYAHARA, H. OBATA, M. KATAOKA, M. KODAMA, H. ISHIBASHI-UEDA, K. KANGAWA and S. KITAMURA (2007). Transplantation of mesenchymal stem cells attenuates myocardial injury and dysfunction in a rat model of acute myocarditis. *Journal of molecular and cellular cardiology* 42 (1): 88-97.

OKUDA, Y., M. OKUDA and C. C. BERNARD (2002). The suppression of T cell apoptosis influences the severity of disease during the chronic phase but not the recovery from the acute phase of experimental autoimmune encephalomyelitis in mice. *Journal of neuroimmunology* 131 (1-2): 115-125.

MALTINEZ-ARROYO, O., A. ORTEGA, M. J. FORNER, R. CORTES (2022). Mesenchymal Stem Cell-Derived Extracellular Vesicles as Non-Coding RNA Therapeutic Vehicles in Autoimmune Diseases *Pharmaceutics* 14 (4): 733.

OSES, C., B. OLIVARES, M. EZQUER, C. ACOSTA, P. BOSCH, M. DONOSO, P. LENIZ and F. EZQUER (2017). Preconditioning of adipose tissue-derived mesenchymal stem cells with deferoxamine increases the production of pro-angiogenic, neuroprotective and anti-inflammatory factors: Potential application in the treatment of diabetic neuropathy. *PLOS One* 12 (5): e0178011.

PARK, Su-Min, Ju-Hyun AN, Jeong-Hwa LEE, Kyung-Bo KIM, Hyung-Kyu CHAE, Ye-In OH, Woo-Jin SONG and Hwa-Young YOUN (2021). Extracellular vesicles derived from DFO-preconditioned canine AT-MSCs reprogram macrophages into M2 phase. *PLOS One* 16 (7): e0254657.

PARK, Su-Min, Q. LI, Min-Ok RYU, Aryung NAM, Ju-Hyun AN, Ji-In YANG, Sang-Min KIM, Woo-Jin SONG and Hwa-Young YOUN (2020). Preconditioning of canine adipose tissue-derived mesenchymal stem cells with deferoxamine potentiates anti-inflammatory effects by directing/reprogramming M2 macrophage polarization. *Veterinary immunology and immunopathology* 219: e109973.

PEZZI, A., B. AMORIN, Á. LAUREANO, V. VALIM, A. DAHMER, B. ZAMBONATO, F. SEHN, I. WILKE, L. BRUSCHI and M. A. L. D. SILVA (2017). Effects of hypoxia in long-term in vitro expansion of human bone marrow derived mesenchymal stem cells. *Journal of cellular biochemistry* 118 (10): 3072-3079.

PHINNEY, D. G. and M. F. PITTENGER (2017). Concise review: MSC-derived exosomes for cell-free therapy. *Stem cells* 35 (4): 851-858.

POTTEN, C. S. and M. LOEFFLER (1990). Stem cells: attributes, cycles, spirals, pitfalls and uncertainties. Lessons for and from the crypt. *Development* 110 (4): 1001-1020.

RAPOSO, G. and P. D. STAHL (2019). Extracellular vesicles: a new communication paradigm? *Nature Reviews Molecular Cell Biology* 20 (9): 509-510.

RATAJCZAK, J., K. MIEKUS, M. KUCIA, J. ZHANG, R. RECA, P. DVORAK and M. RATAJCZAK (2006). Embryonic stem cell-derived microvesicles reprogram hematopoietic progenitors: evidence for horizontal transfer of mRNA and protein delivery. *Leukemia* 20 (5): 847-856.

RIAU, A., H. S. ONG, G. H. YAM and J. MEHTA (2019). Sustained delivery system for stem cell-derived exosomes. *Frontiers in pharmacology* 10: 1368.

RIAZIFAR, M., M. R. MOHAMMADI, E. J. PONE, A. YERI, C. LASSER, A. I. SEGALINY, L. L. MCINTYRE, G. V. SHELKE, E. HUTCHINS and A. HAMAMOTO (2019). Stem cell-derived exosomes as nanotherapeutics for autoimmune and neurodegenerative disorders. *ACS nano* 13 (6): 6670-6688.

ROBBINS, P. D. and A. E. MORELLI (2014). Regulation of immune responses by extracellular vesicles. *Nature Reviews Immunology* 14 (3): 195-208.

ROBERTS, J., P. G. FALLON and E. HAMS (2019). The Pivotal Role of Macrophages in Metabolic Distress. *Macrophage Activation-Biology*

and Disease, IntechOpen: 31-50.

ROSENBERGER, C., S. ROSEN, A. SHINA, U. FREI, K.-U. ECKARDT, L. A. FLIPPIN, M. AREND, S. J. KLAUS and S. N. HEYMAN (2008). Activation of hypoxia-inducible factors ameliorates hypoxic distal tubular injury in the isolated perfused rat kidney. *Nephrology Dialysis Transplantation* 23 (11): 3472-3478.

RYAN, A., M. MURPHY and F. BARRY (2016). Mesenchymal stem/stromal cell therapy: mechanism of action and host response. *The Biology and Therapeutic Application of Mesenchymal Cells, Wiley*: 426-440.

SAAD, S. Y., T. A. NAJJAR and A. C. AL-RIKABI (2001). The preventive role of deferoxamine against acute doxorubicin-induced cardiac, renal and hepatic toxicity in rats. *Pharmacological research* 43 (3): 211-218.

SAMADI, P., S. SAKI, H. M. KHOSHINANI and M. SHEYKHHASAN (2020). Therapeutic applications of mesenchymal stem cells: A comprehensive review. *Current Stem Cell Research & Therapy* 16 (3):323-353.

SAPAROV, A., V. OGAY, T. NURGOZHIN, M. JUMABAY and W. C. CHEN (2016). Preconditioning of human mesenchymal stem cells to enhance their regulation of the immune response. *Stem cells international* 2016: e3924858.

SARGENT, A. and R. H. MILLER (2016). MSC therapeutics in chronic

inflammation. *Current stem cell reports* 2 (2): 168-173.

SART, S., T. MA and Y. LI (2014). Preconditioning stem cells for in vivo delivery. *BioResearch open access* 3 (4): 137-149.

SCHAEFFER, D., B. TSANOVA, A. BARBAS, F. P. REIS, E. G. DASTIDAR, M. SANCHEZ-ROTUNNO, C. M. ARRAIANO and A. VAN HOOF (2009). The exosome contains domains with specific endoribonuclease, exoribonuclease and cytoplasmic mRNA decay activities. *Nature structural & molecular biology* 16 (1): 56-62.

SELMANI, Z., A. NAJI, I. ZIDI, B. FAVIER, E. GAIFFE, L. OBERT, C. BORG, P. SAAS, P. TIBERGHIEN, N. ROUAS-FREISS, E. D. CAROSELLA and F. DESCHASEAUX (2008). Human leukocyte antigen-G5 secretion by human mesenchymal stem cells is required to suppress T lymphocyte and natural killer function and to induce CD4+CD25highFOXP3+ regulatory T cells. *Stem Cells* 26 (1): 212-222.

SHEN, B., J. LIU, F. ZHANG, Y. WANG, Y. QIN, Z. ZHOU, J. QIU and Y. FAN (2016). CCR2 positive exosome released by mesenchymal stem cells suppresses macrophage functions and alleviates ischemia/reperfusion-induced renal injury. *Stem cells international* 2016: e1240301.

SHIH, S. C. and K. P. CLAFFEY (2001). Role of AP-1 and HIF-1 transcription factors in TGF-β activation of VEGF expression. *Growth*

factors 19 (1): 19-34.

SHIMONI, E., R. ARMON and I. NEEMAN (1994). Antioxidant properties of deferoxamine. *Journal of the American Oil Chemists' Society* 71 (6): 641-644.

SHIRAISHI, D., Y. FUJIWARA, Y. KOMOHARA, H. MIZUTA and M. TAKEYA (2012). Glucagon-like peptide-1 (GLP-1) induces M2 polarization of human macrophages via STAT3 activation. *Biochemical and biophysical research communications* 425 (2): 304-308.

SICCO, C. L., D. REVERBERI, C. BALBI, V. ULIVI, E. PRINCIPI, L. PASCUCCI, P. BECHERINI, M. C. BOSCO, L. VARESIO and C. FRANZIN (2017). Mesenchymal stem cell-derived extracellular vesicles as mediators of anti-inflammatory effects: Endorsement of macrophage polarization. *Stem cells translational medicine* 6 (3): 1018-1028.

SILVA, L. H., M. A. ANTUNES, C. C. DOS SANTOS, D. J. WEISS, F. F. CRUZ and P. R. ROCCO (2018). Strategies to improve the therapeutic effects of mesenchymal stromal cells in respiratory diseases. *Stem Cell Research & Therapy* 9 (1): 1-9.

SMOLEN, J. S., D. ALETAHA, M. KOELLER, M. H. WEISMAN and P. EMERY (2007). New therapies for treatment of rheumatoid arthritis. *The lancet* 370 (9602): 1861-1874.

SONG, Woo-Jin, Q. LI, Min-Ok RYU, Jin-Ok AHN, Dong Ha BHANG, Yun Chan JUNG and Hwa Young YOUN (2018). TSG-6 released from intraperitoneally injected canine adipose tissue-derived mesenchymal stem cells ameliorate inflammatory bowel disease by inducing M2 macrophage switch in mice. *Stem cell research & therapy* 9 (1): 91.

STERZENBACH, U., U. PUTZ, L.-H. LOW, J. SILKE, S.-S. TAN and J. HOWITT (2017). Engineered exosomes as vehicles for biologically active proteins. *Molecular Therapy* 25 (6): 1269-1278.

SUGIMOTO, K. (2008). Role of STAT3 in inflammatory bowel disease. *World Journal of Gastroenterology* 14 (33): 5110.

SUN, Y., Q. LI, H. GUI, D.-P. XU, Y.-L. YANG, D.-F. SU and X. LIU (2013). MicroRNA-124 mediates the cholinergic anti-inflammatory action through inhibiting the production of pro-inflammatory cytokines. *Cell research* 23 (11): 1270-1283.

TAK, Eunyoung, Dong-Hwan. JUNG, Seok-Hwan KIM, Gil-Chun PARK, Dae Young JUN, Jooyoung LEE, Bo-Hyun JUNG, V. A. KIRCHNER, Shin HWANG, Gi-Won SONG and Sung-Gyu LEE (2017). Protective role of hypoxia-inducible factor-1α-dependent CD39 and CD73 in fulminant acute liver failure. *Toxicology and applied pharmacology* 314: 72-81.

TAKIZAWA, N., N. OKUBO, M. KAMO, N. CHOSA, T. MIKAMI, K.

SUZUKI, S. YOKOTA, M. IBI, M. OHTSUKA and M. TAIRA (2017). Bone marrow-derived mesenchymal stem cells propagate immunosuppressive/anti-inflammatory macrophages in cell-to-cell contact-independent and-dependent manners under hypoxic culture. *Experimental Cell Research* 358 (2): 411-420.

TAMURA, R., S. UEMOTO and Y. TABATA (2016). Immunosuppressive effect of mesenchymal stem cell-derived exosomes on a concanavalin A-induced liver injury model. *Inflammation and Regeneration* 36 (1): 1-11.

TCHANQUE-FOSSUO, C., S. DAHLE, S. BUCHMAN and R. RIVKAH ISSEROFF (2017). Deferoxamine: potential novel topical therapeutic for chronic wounds. *British Journal of Dermatology* 176: 1056-1059.

THëRY, C., L. ZITVOGEL and S. AMIGORENA (2002). Exosomes: composition, biogenesis and function. *Nature reviews immunology* 2 (8): 569-579.

TSUJIMARU, K., M. TAKANASHI, K. SUDO, A. ISHIKAWA, S. MINEO, S. UEDA, K. KUMAGAI and M. KURODA (2020). Extracellular microvesicles that originated adipose tissue derived mesenchymal stem cells have the potential ability to improve rheumatoid arthritis on mice. *Regenerative Therapy* 15: 305-311.

UCCELLI, A., L. MORETTA and V. PISTOIA (2008). Mesenchymal stem

cells in health and disease. *Nature reviews immunology* 8 (9): 726-736.

VOGEL, D., E. J. VEREYKEN, J. E. GLIM, P. D. HEIJNEN, M. MOETON, P. VAN DER VALK, S. AMOR, C. E. TEUNISSEN, J. VAN HORSSEN and C. D. DIJKSTRA (2013). Macrophages in inflammatory multiple sclerosis lesions have an intermediate activation status. *Journal of neuroinflammation* 10 (1): 1-12.

VOLAREVIC, V., M. GAZDIC, B. SIMOVIC MARKOVIC, N. JOVICIC, V. DJONOV and N. ARSENIJEVIC (2017). Mesenchymal stem cell-derived factors: Immuno-modulatory effects and therapeutic potential. *Biofactors* 43 (5): 633-644.

WANG, G. L. and G. L. SEMENZA (1993). Desferrioxamine induces erythropoietin gene expression and hypoxia-inducible factor 1 DNA-binding activity: implications for models of hypoxia signal transduction. *Blood* 82 (12): 3610-3615.

WANG, N., H. LIANG and K. ZEN (2014). Molecular mechanisms that influence the macrophage M1–M2 polarization balance. *Frontiers in immunology* 5: 614.

WEN, D., Y. PENG, D. LIU, Y. WEIZMANN and R. I. MAHATO (2016). Mesenchymal stem cell and derived exosome as small RNA carrier and Immunomodulator to improve islet transplantation. *Journal of Controlled Release* 238: 166-175.

WEN, S. W., L. G. LIMA, R. J. LOBB, E. L. NORRIS, M. L. HASTIE, S. KRUMEICH and A. MøLLER (2019). Breast cancer-derived exosomes reflect the cell-of-origin phenotype. *Proteomics* 19 (8): e1800180.

WILLIS, G. R., A. FERNANDEZ-GONZALEZ, J. ANASTAS, S. H. VITALI, X. LIU, M. ERICSSON, A. KWONG, S. A. MITSIALIS and S. KOUREMBANAS (2018). Mesenchymal stromal cell exosomes ameliorate experimental bronchopulmonary dysplasia and restore lung function through macrophage immunomodulation. *American journal of respiratory and critical care medicine* 197 (1): 104-116.

WILLIS, G. R., A. FERNANDEZ-GONZALEZ, M. REIS, S. A. MITSIALIS and S. KOUREMBANAS (2018). Macrophage immunomodulation: the gatekeeper for mesenchymal stem cell derived-exosomes in pulmonary arterial hypertension? *International journal of molecular sciences* 19 (9): 2534-2553.

WILSON, J. G., K. D. LIU, H. ZHUO, L. CABALLERO, M. MCMILLAN, X. FANG, K. COSGROVE, R. VOJNIK, C. S. CALFEE and Jae-Woo LEE, A. J. ROGERS, J. LEVITT, J. W.-KRONISH, E. K. BAJWA, A. LEAVITT, D. MCKENNA, B. T. THOMPSON, M. A. MATTHAY (2015). Mesenchymal stem (stromal) cells for treatment of ARDS: a phase 1 clinical trial. *The Lancet Respiratory Medicine* 3 (1): 24-32.

WU, Y., X. LI, W. XIE, J. JANKOVIC, W. LE and T. PAN (2010).

Neuroprotection of deferoxamine on rotenone-induced injury via accumulation of HIF-1α and induction of autophagy in SH-SY5Y cells. *Neurochemistry international* 57 (3): 198-205.

XIA, Y., X. LING, G. HU, Q. ZHU, J. ZHANG, Q. LI, B. ZHAO, Y. WANG and Z. DENG (2020). Small extracellular vesicles secreted by human iPSC-derived MSC enhance angiogenesis through inhibiting STAT3-dependent autophagy in ischemic stroke. *Stem cell research & therapy* 11 (1): 1-17.

YANG, Hye-Mi, Woo-Jin SONG, Q. LI, Su-Yeon KIM, Hyeon-Jin KIM, Min-Ok RYU, Jin-Ok AHN and Hwa-Young YOUN (2018). Canine mesenchymal stem cells treated with TNF-α and IFN-γ enhance anti-inflammatory effects through the COX-2/PGE2 pathway. *Research in veterinary science* 119: 19-26.

YANG, J., X.-X. LIU, H. FAN, Q. TANG, Z.-X. SHOU, D.-M. ZUO, Z. ZOU, M. XU, Q.-Y. CHEN and Y. PENG (2015). Extracellular vesicles derived from bone marrow mesenchymal stem cells protect against experimental colitis via attenuating colon inflammation, oxidative stress and apoptosis. *PLOS One* 10 (10): e0140551.

YINFEI, W., J. AIPING, F. CHAO, Z. YANXIN and L. XUEYUAN (2013). DFO and DMOG up-regulate the expression of CXCR4 in bone marrow mesenchymal stromal cells. *Die Pharmazie-An International Journal of*

Pharmaceutical Sciences 68 (10): 835-838.

YU, C.-R., Y. S. LEE, R. M. MAHDI, N. SURENDRAN and C. E. EGWUAGU (2012). Therapeutic targeting of STAT3 (signal transducers and activators of transcription 3) pathway inhibits experimental autoimmune uveitis. *PLOS One* 7 (1): e29742.

YU, X., Q. WAN, G. CHENG, X. CHENG, J. ZHANG, J. L. PATHAK and Z. LI (2018). CoCl2, a mimic of hypoxia, enhances bone marrow mesenchymal stem cells migration and osteogenic differentiation via STAT3 signaling pathway. *Cell biology international* 42 (10): 1321-1329.

YUAN, X.-L., L. CHEN, M.-X. LI, P. DONG, J. XUE, J. WANG, T.-T. ZHANG, X.-A. WANG, F.-M. ZHANG and H.-L. GE (2010). Elevated expression of Foxp3 in tumor-infiltrating Treg cells suppresses T-cell proliferation and contributes to gastric cancer progression in a COX-2-dependent manner. *Clinical immunology* 134 (3): 277-288.

ZAGõRSKA, A. and J. DULAK (2004). HIF-1: the knowns and unknowns of hypoxia sensing. *Acta Biochimica Polonica* 51 (3): 563-585.

ZAPPIA, E., S. CASAZZA, E. PEDEMONTE, F. BENVENUTO, I. BONANNI, E. GERDONI, D. GIUNTI, A. CERAVOLO, F. CAZZANTI and F. FRASSONI (2005). Mesenchymal stem cells ameliorate experimental autoimmune encephalomyelitis inducing T-cell

anergy. *Blood* 106 (5): 1755-1761.

ZHANG, B., Y. YIN, R. C. LAI, S. S. TAN, A. B. H. CHOO and S. K. LIM (2014). Mesenchymal stem cells secrete immunologically active exosomes. *Stem cells and development* 23 (11): 1233-1244.

ZHANG, H.-C., X.-B. LIU, S. HUANG, X.-Y. BI, H.-X. WANG, L.-X. XIE, Y.-Q. WANG, X.-F. CAO, J. LV and F.-J. XIAO (2012). Microvesicles derived from human umbilical cord mesenchymal stem cells stimulated by hypoxia promote angiogenesis both in vitro and in vivo. *Stem cells and development* 21 (18): 3289-3297.

ZHAO, H., Q. SHANG, Z. PAN, Y. BAI, Z. LI, H. ZHANG, Q. ZHANG, C. GUO, L. ZHANG and Q. WANG (2018). Exosomes from adipose-derived stem cells attenuate adipose inflammation and obesity through polarizing M2 macrophages and beiging in white adipose tissue. *Diabetes* 67 (2): 235-247.

ZHENG, G., L. HUANG, H. TONG, Q. SHU, Y. HU, M. GE, K. DENG, L. ZHANG, B. ZOU and B. CHENG (2014). Treatment of acute respiratory distress syndrome with allogeneic adipose-derived mesenchymal stem cells: a randomized, placebo-controlled pilot study. *Respiratory research* 15 (1): 1-10.

국 문 초 록

자가 면역 뇌척수염 마우스 모델에서 **deferoxamine**을 전처리한 개의 지방유래 중간엽줄기세포로부터 유래한 세포외소포체의 면역 조절 효과

박수민
(지도교수 윤화영)

서울대학교 대학원
수의과대학 임상수의학 (수의내과학) 전공

중간엽줄기세포(Mesenchymal stem cell; MSC)의 분비 능력은 염증을 개선하는데 있어서 효과적이라 보고되어, 이를 염증 치료제로 개발하기 위해 활발히 연구되고 있다. 특히나 다발성 경화증과 같이 자가면역 신경질환에서도 줄기세포 치료를 적용하려는 노력들이 이어지고 있다. 다발성 경화증은 사람의 자가면역 신경질환 중 하나로, 자기 조절 면역세포의 이상으로 인해 신경조직을 외부요인으로 오인하고 염증 세포들이 침윤되면서 신경손상이 생기는 질환이다. 개에서는

유사한 질환으로 원인 불명의 비감염성 뇌수막염이 있다. 해당 질환의 원인은 아직 명확하게 밝혀지지 않았으나 면역 이상으로 인해 생기는 것으로 추정되며, 이와 관련해 비특이적 면역억제제로 치료한다. 개의 신경질환 중 약 25%를 차지할 정도로 많은 수의 개가 해당 질환으로 투병을 하나 아직까지 치료법이 크게 발달되어 있지 않다. 스테로이드를 포함한 비특이적 면역억제제는 위장관 장애, 호르몬 분비 장애 등의 문제를 유발하는 것이 가장 큰 문제이며, 그에 반해 치료 효과가 확실하게 보장되지 않는다는 것이 뇌수막염 치료의 어려운 점이다.

자가면역 신경질환에서 비특이적 면역억제제 치료의 단점을 보완할 다른 치료 요법들에 대한 연구 개발들이 이어지고 있으며, 그중 하나가 MSC에서 유래된 세포외소포체(extracellular vesicle; EV)이다. 그러나 아직까지는 세포외소포체의 임상적 효능이 충분히 입증되지 않아 실제 임상에서 적용되지 못하고 있다. 이를 해결하기 위해 MSC의 항염증 인자 분비를 촉진시키는 방법들이 고안되었고, 그중 한 가지 방법이 저산소 배양 혹은 저산소증 모방제를 사용한 전처리 방법이다. 전처리한 MSC에서 유래한 세포외소포체 내의 분자 변화를 분석하는 연구들이 진행되고 있으나, 아직까지 이것의 임상적 효능이 충분히 밝혀지지 않아 추가적인 전임상 및 임상 적용 연구가 필요하다. 본 연구는 실험적 자가면역성 뇌척수염(experimental autoimmune encephalomyelitis; EAE) 마우스 모델에서 deferoxamine (DFO)로 전처리한 개 지방조직유래(canine adipose tissue derived; cAT)-MSCs에서 유래된 세포외소포체(EV^{DFO})의 치료 효과를 확인하고

세포외소포체의 면역조절기능의 작용원리를 탐색하였다.

첫 번째, DFO가 전처리된 cAT-MSC (MSC^{DFO})가 분비 효과를 통해 대식세포를 더 효과적으로 M2 항염증 상태로 유도할 수 있음을 밝혔다. MSC^{DFO}와 대식세포의 상호작용을 평가하기 위해 공배양 시스템을 이용하여 RAW 264.7 세포와 MSC^{DFO}를 같이 배양하였으며, 중합효소 연쇄반응 기법과 western blot 분석 기법을 이용하여 대식세포 분극과 관련된 인자의 발현 변화를 분석하였다. RAW 264.7 세포를 MSC^{DFO}와 공배양한 경우, 전처리 하지 않은 cAT-MSC와 공배양한 경우에 비해 M1 및 M2 마커의 발현이 각각 감소(iNOS, 1.32배, $p<0.01$; IL-6, 3.46배, $p<0.05$) 및 증가(CD206, 2.61배, $p<0.001$; Ym1, 4.92배, $p<0.01$)하였다. 따라서 DFO로 전처리한 cAT-MSC는 대식세포 분극을 더 효과적으로 항염증 상태인 M2 단계로 유도할 수 있다.

두 번째, EV^{DFO}가 STAT3의 인산화 활성화를 통해 대식세포를 조절한다는 것을 밝혔다. MSC^{DFO}에서는 HIF-1α가 축적되고 COX-2의 발현이 증가(16.77배, $p<0.001$)하였다. COX-2의 발현 변화는 MSC^{DFO}에서 유래한 세포외소포체에도 반영되었다. 개 대식세포주 DH82를 LPS로 자극한 뒤 EV^{non} 및 EV^{DFO}를 처리하여 그 변화를 중합효소 연쇄반응 기법 및 면역 형광 염색 분석을 통해 평가하였다. DH82를 EV^{DFO}로 처리한 경우, M1 관련된 지표의 발현은 감소(IL-1β, 2.45배, $p<0.001$; IL-6, 17.26배, $p<0.001$)하였으나, M2 관련된 지표의 발현은 EV^{non}으로 처리한 경우보다 향상(CD206, 7.24배, $p<0.001$)

되었다. 또한 DH82 세포를 EV^{DFO}로 처리했을 때 STAT3 발현의 인산화는 더 증가하였다(1.79배, $p<0.001$). si-COX2로 처리된 cAT-MSC에서 유래한 EV는 아무 처리하지 않은 EV와 유사한 효과를 보였으며, 대식세포 조절 효능은 EV^{DFO}보다 감소하였다(IL-1β, 2.21배, $p<0.001$; IL-6, 1.43배, $p<0.001$; CD206, 2.27배, $p<0.001$). 따라서 EV 내에 있는 COX-2는 STAT3를 조절하여 대식세포를 변화시킬 수 있는 핵심 인자 중 하나로 추정된다.

마지막으로, EV^{DFO} 치료가 전처리 하지 않은 EV보다 상대적으로 더 높은 항염증 효능을 가지며 EAE 모델에서 STAT3 조절을 통해 면역 체계를 조절할 수 있음을 밝혔다. 실험 비교를 위해 EAE 그룹과 EV 또는 EV^{DFO}를 비강 투여한 그룹으로 나누었다(C57BL/6, male, control=6, EAE=8, EAE+EV=8, EAE+EV^{DFO}=8, 10 μg/일/14회). 질환을 유도한지 25일 차에 쥐를 안락사 시키고 비장, 뇌, 척수를 조직병리학적, RNA 및 단백질의 발현 정도를 분석하였다. 조직학적으로 EV 및 EV^{DFO}군에서는 척수에서의 염증 세포의 침윤이 현저히 감소하였고(EV, 1.38배, $p<0.01$; EV^{DFO}, 1.72배, $p<0.01$) 탈수초화 현상이 완화되었다 (EV, 2.96배, $p<0.05$; EV^{DFO}, 5.28배, $p<0.05$). 면역형광 염색을 통해 M2 대식세포와 조절 T 세포(Treg)의 지표인 CD206과 Foxp3의 발현이 EAE와 EAE+EV 그룹에 비해 EV^{DFO} 그룹에서 증가하였다. EAE 그룹에서 비장의 CD4+CD25+Foxp3+ Treg 세포의 수는 naïve 그룹에 비해 유의하게 감소했다(2.74배, $p<0.001$). 반면, Treg 세포의 수는 EAE+EV 그룹보다 EAE+EV^{DFO}

그룹에서 더 큰 증가를 보였다(1.55배, p<0.05). STAT3와 pSTAT3의 단백질 발현은 naïve 그룹과 비교하였을 시 EAE 그룹의 비장에서 크게 증가하였다(STAT3, 2.02배, p<0.001; pSTAT3, 2.14배, p<0.001). 그러나 EV 처리한 그룹에서는 EAE 그룹에 비해 STAT3 발현이 감소하였으며(1.32배, p<0.001), 특히 EV 그룹에 비해 EV^{DFO}가 주입된 그룹에서 STAT3의 감소가 뚜렷하게 나타났다(1.90배, p<0.001). 따라서 EV는 STAT3 발현을 조절할 수 있는 것으로 추정되며, EV^{DFO}는 EV보다 그 효과가 크다고 종합할 수 있다.

결론적으로, cAT-MSC를 DFO로 전처리 하는 것은 MSC와 세포외소포체의 면역조절 효과를 향상시켜 치료능을 효율적으로 올릴 수 있는 방법이다. 또한, EV^{DFO}가 면역세포 내의 STAT3를 유동적으로 변화시키고 이를 통해서 면역 체계를 조절할 수 있다는 점에서, STAT3를 조절하는 것이 다발성 경화증의 치료법의 중요 원리로 제시될 수 있다. 이러한 발견은 다발성 경화증뿐만 아니라 다른 자가면역 질환에서의 새로운 무세포 치료법을 제시한다. 더 나아가 개의 질환 중 이와 유사한 질환인 원인 불명의 비감염성 뇌척수막염에도 EV^{DFO}가 새로운 치료제로 적용될 수 있음을 보여주는 주요한 첫 근거이며, 수의학에서의 자가 면역 질환 치료 발전의 토대가 되는 연구이다.

주요어: 다발성 경화증 / 중간엽줄기세포 / deferoxamine / 세포외소포체 / 항염증

학번: 2018-24679